THE INFLUENCE OF GEOLOGICAL STRUCTURE ON STRATIGRAPHIC DEVELOPMENT DURING MULTIPHASE RIFTING IN THE SONGKHLA BASIN, GULF OF THAILAND

Mrs. Jidapa Phoosongsee

A Dissertation Submitted in Partial Fulfilment of the Requirements
for the Degree of Doctor of Philosophy Program in Geology
Department of Geology
Faculty of Science
Chulalongkorn University
Academic Year 2018
Copyright of Chulalongkorn University

อิทธิพลของโครงสร้างทางธรณีวิทยาต่อการพัฒนาลำดับชั้นหินในช่วงการแยกตัวหลายครั้งในแอ่ง

สงขลา อ่าวไทย

นางจิดาภา ภูส่งสี

Thesis Title	THE INFLUENCE OF GEOLOGICAL STRUCTURE ON STRATIGRAPHIC DEVELOPMENT DURING MULTIPHASE RIFTING IN THE SONGKHLA BASIN, GULF OF THAILAND
By	Mrs. Jidapa Phoosongsee
Field of Study	Geology
Thesis Advisor	Associate Professor Thasinee Charoentitirat, Ph.D.
Thesis Co-Advisor	Christopher K. Morley, Ph. D.

Accepted by the Faculty of Science, Chulalongkorn University in Partial Fulfilment of the Requirements for the Doctoral Degree

……………………………………………. Dean of the Faculty of Science
(Professor Polkit Sangvanich, Ph.D.)

THESIS COMMITTEE

……………………………………………Chairman
(Professor Montri Choowong, Ph.D.)
……………………………………………Thesis Advisor
(Associate Professor Thasinee Charoentitirat, Ph.D.)
……………………………………………Thesis Co-Advisor
(Dr. Christopher K. Morley)
……………………………………………Examiner
(Associate Professor Pitsanupong Kanjanapayont, Dr.rer.nat.)
……………………………………………Examiner
(Dr. Sukonmeth Jitmahantakul)
……………………………………………External Examiner
(Dr. Stefan Back)

อิทธิพลของโครงสร้างทางธรณีวิทยาต่อการพัฒนาลำดับชั้นหินในช่วงการแยกตัวหลายครั้งในแอ่งสงขลา อ่าวไทย (THE INFLUENCE OF GEOLOGICAL STRUCTURE ON STRATIGRAPHIC DEVELOPMENT DURING MULTIPHASE RIFTING IN THE SONGKHLA BASIN, GULF OF THAILAND) อ. ที่ปรึกษาวิทยานิพนธ์หลัก: รศ. ดร. ฐาสิณีย์ เจริญฐิติรัตน์, อ. ที่ปรึกษาร่วม: Dr. Christopher Morley

แอ่งสงขลาเป็นแอ่งที่เกิดจากการแยกตัวของเปลือกโลก (rift basin) ในมหายุคซีโนโซอิค (Cenozoic Era) ตั้งอยู่ทางตะวันตกเฉียงใต้ของอ่าวไทย การวางตัวของแอ่งอยู่ในแนวเหนือใต้และมีลักษณะกึ่งกราเบน (half graben) โครงสร้างของรอยเลื่อนมีการพัฒนาเป็นแบบตั้งฉากกับแรงดึง ลักษณะกึ่งกราเบนของแอ่งถูกควบคุมโดยโครงสร้างรอยเลื่อนหลักที่มีการวางตัวในแนวเหนือใต้ถึงตะวันออกเฉียงเหนือและตะวันตกเฉียงใต้ และมีการเอียงเทไปทางทิศตะวันออก การแยกของรอยเลื่อนเกิดขึ้นสองครั้ง ครั้งที่หนึ่งในสมัยอีโอซีน (Eocene) ถึงสมัยโอลิโกซีนตอนต้น (Early Oligocene) ครั้งที่สองในสมัยโอลิโกซีนตอนปลาย (Late Oligocene) ถึงสมัยไมโอซีนตอนต้น (Early Miocene) การเปลี่ยนจากแอ่งรอยแยก (syn-rift) เป็นแอ่งยุบ (post-rift) เกิดขึ้นในช่วงตอนปลายของสมัยไมโอซีนตอนต้น (late Early Miocene) ถึงสมัยไมโอซีนตอนกลาง (Middle Miocene) หินกักเก็บปิโตรเลียมในแอ่งสงขลามีการสะสมตัวในช่วงของสมัยไมโอซีนตอนต้น จนถึงสมัยไมโอซีนตอนกลาง หินกักเก็บปิโตรเลียมส่วนใหญ่เกิดจากการสะสมตัวของตะกอนทางน้ำ โครงสร้างและการกระจายตัวของหินเหล่านี้มีความซับซ้อนทั้งในทางราบและทางลึก โดยเฉพาะบริเวณที่มีการสะสมตัวของสันดอนทราย (point bar), สิ่งทับถมน้ำล้นฝั่ง (overbank deposit) และตะกอนสะสมในแม่น้ำที่มีทั้งตะกอนทรายและตะกอนโคลน ในการศึกษานี้ได้มีการอธิบายลักษณะรูปแบบโครงสร้างและสภาพแวดล้อมการสะสมตัวของตะกอนของแอ่งสงขลาในช่วงส่วนแปรเปลี่ยนต่อเนื่องระหว่างแอ่งรอยแยกกับแอ่งยุบ โดยใช้วิธีการแปลข้อมูลคลื่นไหวสะเทือนแบบสะท้อนกลับ (seismic reflection data) การคำนวณคุณลักษณะคลื่นไหวสะเทือน (seismic attributes) ได้แก่ RMS similarity และ spectral decomposition รวมกับข้อมูลที่ได้จากหลุมสำรวจ และข้อมูลทางชีวภาพ จากการศึกษาพบว่าลักษณะเฉพาะของแม่น้ำที่กำเนิดขึ้นในแอ่งมีสองแบบ คือ 1. ธารน้ำโค้งตวัดในแนวเหนือใต้แบบซับซ้อน มีการวางตัวในแนวเดียวกันกับรอยเลื่อนหลัก เกิดขึ้นพร้อมกับแอ่งรอยแยกในช่วงตอนปลายของสมัยไมโอซีนตอนต้น 2. ธารน้ำที่มีลักษณะแคบและยาว มีการวางตัวในแนวตะวันออกเฉียงเหนือและตะวันตกเฉียงใต้ มีความสัมพันธ์กับสภาพแวดล้อมการสะสมตัวของตะกอนที่ได้รับอิทธิพลจากกระแสน้ำขึ้นน้ำลง (tidal depositional environment) และดินดอนสามเหลี่ยมปากแม่น้ำ (delta depositional environment) ในช่วงแอ่งยุบสมัยไมโอซีนตอนกลาง การวางตัวของธารน้ำทั้งสองแบบมีความสัมพันธ์กับการเปลี่ยนแปลงโครงสร้างของแอ่งสงขลาจากตอนปลายของการเกิดแอ่งรอยแยกจนถึงการเกิดแอ่งยุบตัว ในช่วงตอนปลายของแอ่งรอยแยก การวางตัวของธารน้ำมีทิศทางเดียวกับรอยเลื่อน ซึ่งควบคุมโดยการเคลื่อนตัวของรอยเลื่อนหลักอยู่ ในขณะที่การวางตัวของธารน้ำในช่วงแอ่งยุบถูกควบคุมด้วยรอยเลื่อนย้อนตามแนวของรอยเลื่อนหลักและการยุบตัวของแอ่งในตอนกลางของพื้นที่ ส่งผลให้ศูนย์กลางการสะสมตัวของตะกอนย้ายจากตรงกลางของกราเบนที่ติดกับรอยเลื่อนหลักไปยังตรงกลางของแอ่งสงขลา

ภาควิชา ธรณีวิทยา   ลายมือชื่อนิสิต...

สาขาวิชา ธรณีวิทยา   ลายมือชื่อ อ.ที่ปรึกษาหลัก..........................

ลายมือชื่อ อ.ที่ปรึกษาร่วม...........................

ปีการศึกษา 2561

5672886523 : MAJOR GEOLOGY

KEYWORD: structural geology, rift basin, reservoir characterization, seismic attributes, fluvial, depositional environments

Jidapa Phoosongsee: THE INFLUENCE OF GEOLOGICAL STRUCTURE ON STRATIGRAPHIC DEVELOPMENT DURING MULTIPHASE RIFTING IN THE SONGKHLA BASIN, GULF OF THAILAND: Advisor: Assoc. Prof. Thasinee Charoentitirat, Ph.D. Co-Advisor Christopher K. Morley, Ph.D.

The Cenozoic N-S trending Songkhla rift basin, located in the southwest Gulf of Thailand, was developed as a predominantly orthogonal extended half graben structure. The half graben is controlled by a boundary fault zone on the western side of the basin, which forms a series of N-S to NNE-SSW, east-dipping normal faults. The rift spans two phases of rifting; the Eocene-Oligocene and the Oligocene-Miocene phases, the late syn-rift to post-rift transition occurred from the late Early Miocene to Middle Miocene. The main clastic hydrocarbon reservoirs in the basin are located in the Early Miocene to Middle Miocene section. These reservoirs are predominantly fluvial channels with complex lateral and vertical geometries and distributions particularly as point bars, overbank deposits, and sand- or mud-filled channels. This study characterizes the reservoir architecture and depositional environment of the Songkhla Basin from the late syn-rift to post-rift by integrating the seismic attributes (RMS, similarity, and spectral decomposition), well log interpretations, and well biostratigraphic data. Two distinctive channel characteristics and patterns were interpreted: (A) N-S oriented meandering channel complexes, aligned sub-parallel to the western boundary faults, developed during the late syn-rift (upper Early Miocene) and (B) NE-SW oriented long, narrow fluvial channels with tidal and marine influence, developed in the post-rift phase I (Middle Miocene). These channel orientations reflect changes in the basin architecture passing from the late syn-rift stage to the post-rift. Syn-rift channel orientation was controlled by topography created by motion on the western boundary fault system, while the post-rift the channel orientations were affected by mild inversion on the boundary fault system and thermal subsidence, which resulted in an eastwards shift in the basin depocentre towards the flexural margin.

Department:	Geology	Student's Signature ………………………
Field of Study:	Geology	Advisor's Signature ………………………
		Co-advisor's Signature ………………………
Academic Year:	2018	

ACKNOWLEDGEMENTS

TABLE OF CONTENTS

Page

LIST OF TABLES

LIST OF FIGURES

CHAPTER I

INTRODUCTION

1.1 Thesis overview and structure

This thesis investigates the structural development and the reservoir distribution and deposition within the Songkhla intra continental rift basin, particularly from the late syn-rift to post-rift period (late Early Miocene to Middle Miocene), by using 2D and 3D seismic reflection data integrated with all available well log and biostratigraphic data. To unravel the tectono-stratigraphic evolution from the late syn-rift to post-rift period, several techniques have been applied, i.e., throw-length analysis, seismic attributes analysis, and the rock physics analysis.

This thesis is subdivided into six chapters. **Chapter 1** is an introduction to outline the rationale and specific research areas. **Chapter 2** describes the data and methodology being applied to analysis the 2D and 3D seismic reflection data of Songkhla Basin. **Chapter 3** presents the regional geology and stratigraphic framework of Songkhla Basin. The main body of original research and the results are presented in **Chapter 4** and **Chapter 5**, which have been published as two separate papers (Phoosongsee and Morley, 2018). The key conclusions and recommendation are being summarized in **Chapter 6**.

1.2 Background and motivation

The simplest depiction of the syn-rift to post-rift transition in failed rifts is the McKenzie model (1978), where the effecting of rifting (i.e. crustal stretching) were modelled as being instantaneous. Subsequent post-rift thermal subsidence, arising from the consequences of (exponential) thermal decay of the syn-rift lithospheric thermal anomaly, and sediment loading leads to broad, saucer-shaped thermal subsidence. In the flexural cantilever model of syn-rift and post-rift subsidence, a phase of erosion where the syn-rift topography is removed prior to subsidence is an option (e.g. Kusznir et al., 1995; Roberts et al., 2013). These early models of the syn-rift to post-rift transition describe the basic processes involved, and include an unconformity between

the rifting and the thermal subsidence phase. It is now recognized that the syn-rift to post-rift transition is highly varied in failed rifts and the variability in this transition is related to several different factors including: continental versus marine depositional environments, elevation of the basin (i.e. intermontane, coastal plain, shallow water to deep water), and duration of the transition (e.g. abrupt, slow, pulsed) (e.g. Nottvedt et al., 1995; Morley, 1999; 2002; Gabrielsen et al., 2001; Zachariah et al., 2009; Morley and Racey, 2011; Scherer et al., 2015; Marin et al., 2018). These factors in turn are controlled by different variables affecting rifts, such as their geographic and tectonic position (e.g. Morley, 2002; Basile et al., 2013), sediment supply, climate (e.g. McKenzie, 1978; Prosser, 1993; Scherer et al., 2015; Marin et al., 2018), the amount of stretching (McKenzie, 1978), whether tectonic inversion occurred at the end of rifting (Basile et al., 2013), and the driving mechanisms of extension (Morley, 2002).

In the rift basins of Thailand, examples of syn-rift to post-rift transition across all the basic elevation scenarios can be found, from the intermontane basins in the north of Thailand, to the coastal plains-shallow marine environments of the Central Basin, Gulf of Thailand (GOT) and Andaman Sea shelf, to the deep marine setting of the East Andaman Basin (see review in Morley et al., 2011). The variable timing of rifting events means that the end of rifting and onset of post-rift subsidence changes laterally within the Thailand Rift basins, but a general trend is for the syn-rift to post-rift transition to young northwards (Morley and Racey, 2011; Morley et al., 2011). Exposure in a sub-areal setting means that the syn-rift topography will be considerably eroded before post-rift subsidence occurs. Whereas a deep marine environment will preserve much of the syn-rift topography, which provides accommodation space for post-rift sediment to infill prior to the onset of thermal subsidence (e.g. North Sea) (Prosser, 1993; Gabrielsen et al., 2001; Zachariah et al., 2009; Marin et al., 2019). The coastal-shallow marine environment falls between extremes, and can exhibit continuity of deposition in the deeper parts of some basins, while undergoing considerable erosion of the syn-rift topography elsewhere. In this paper, we investigate the variations in the depositional environments between the syn-rift and post-rift sections in the Songkhla Basin, GOT. At the time of the transition, the basin lay in a coastal-transitional marine setting, and today the basin lies in water depths of less than 25 meters.

Fluvial reservoirs are the major hydrocarbon reservoirs in the GOT, which were deposited throughout the syn-rift and post-rift periods, ranging from Oligocene to Miocene sequences. These fluvial deposits interfinger with tidal and marine deposits, particularly in the Neogene section (see review in Morley and Racey, 2011). In general, the sands deposited in fluvial depositional systems have complex lateral and vertical geometries and distributions as they contain a series of point bars, overbank deposits, and sand- or mud-filled abandonment channels (Ahmad and Rowell, 2014; Jardine, 1997; Lockhart et al., 1997). Regarding this complexity, it is necessary to understand the factors controlling the reservoirs deposition and distribution.

To image the distribution of subsurface reservoirs within the Songkhla Basin, several seismic attributes could be applied. The analysis of seismic attributes such as root mean square (RMS), acoustic impedance, spectral decomposition, and similarity can delineate the subtle structural and stratigraphic from the ordinary seismic amplitude data which will allow the structure and depositional environment to be interpreted (Chopra and Marfurt, 2005). The reservoir distribution, depositional environment, and their relation to the structural evolution across the syn-rift to post-rift transition could be characterized.

Although there have been more research studies about the tectonics and sedimentations in the recent years, a wide variety of questions concerning the control of tectonic on sedimentary pattern and facies distributions still remain, especially within the syn- to post-rift transition in the GOT.

1.3   Aims and objectives

The present work aims to examine and expand the knowledge on the relationship between structural evolution and stratigraphic sequences in the syn – post rift transition in Songkhla Basin, Gulf of Thailand (GOT).

The study area is one of the least studied and least published on the tectono-stratigraphic processes in the GOT. Since the tectonic mechanisms are changing from syn- to post-rift, the corresponding channel morphology and characters are expected to change accordingly. The

broad, main aims of this thesis are as follows:

o   To investigate how faults/structures generated by tectonics control channel morphology and facies distribution, especially during the cessation of faulting activities

o   To improve the knowledge of fluvial depositional system in response to tectonic control, especially during the syn- to post-rift transition.

o   To use seismic attribute methods to reveal the channel size, shape and orientation in the syn- to post-rift transition period.

1.4   Study area

The Cenozoic N-S trending Songkhla rift basin, is located in the southwest GOT in water depths of less than 25 meters. The basin exhibits a half-graben geometry, basin with the boundary fault zone on the western side of the basin comprising a series of N-S to NNE-SSW, east-dipping normal faults.

The main study area within the Songkhla Basin is an area of 700 km^2 that is covered by 3D seismic reflection data (**Figure 1**). The area was chosen to better understand the tectono-stratigraphy of the syn- to post-rift transition between late Early Miocene to Middle Miocene.
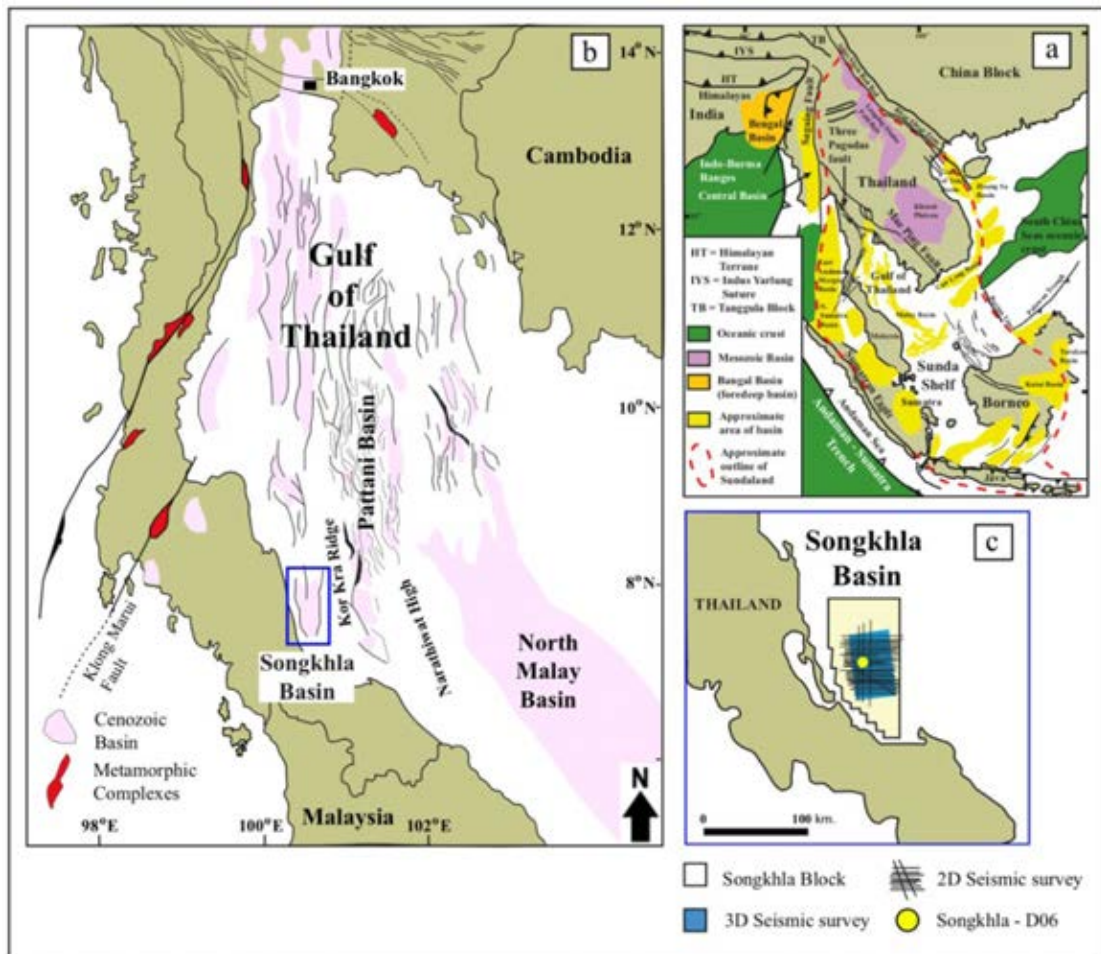
Figure 1 (a) Regional tectonic features within and around Sundaland (modified from Searle and Morley, 2011). (b) Location of Songkhla Basin in the Gulf of Thailand (blue square). (c) Songkhla concession block with the location of the 2D and 3D seismic reflection survey and Songkhla-D06, development well (modified from Morley et al., 2011).

1.5 Previous studies

In the Gulf of Thailand (GOT), the syn- to post-rift transition represents a gradual change from extensive fault activity to localized faulting, which is particularly complex because local structural development/tectonics is diminishing through regional subsidence. The evolution of these fault systems, including their nucleation, propagation and linkage, can be extracted from the sedimentary record. However,

within GOT, there is limited documentation regarding how channel morphology and facies distribution changes during the syn-rift to post-rift transition.

Major reservoirs in GOT are mainly fluvial sandstones deposited throughout the Miocene syn- to post-rift stages, and many of them are located in the transition from syn- (fault-controlled sedimentation) to post-rift (subsidence controlled depositional). A few research studies (Ahmad et al., 2014; Manh Do, 2013; Thi Tran, 2013; Praidee, 2013; and Inthana, 2013) have been published on mapping subsurface fluvial sandstones and detecting subtle faults in the GOT, using the seismic attributes to extract the reservoir architectures and extension.

Manh Do (2013) applied seismic attributes comprising Inversion, RMS, and Spectral decomposition to identity the depositional and architecture of the fluvial systems in the Southern Songkhla Basin. The results show that the inversion and spectral decomposition (at selected frequencies) provide better resolution of seismic imaging on channel morphology compared to the RMS in the deep, Early Miocene section. He concluded that the sedimentation in Songkhla Basin was controlled by syn-rift deformation from Oligocene to Early Miocene, while during the Middle Miocene the sedimentation was possibly controlled by the thermal subsidence due to the cessation of the main phase of rifting.

For the northern Songkhla Basin, Thi Tran (2013) concluded that the quantitative data of seismic geomorphology provided useful information for hydrocarbon reserve estimation. He also concluded that the RMS attributes provided the best seismic image of the fluvial channel morphology in the shallow part, which was well correlated with the wireline logging from the drilled wells.

Lawwongngam and Philip (1993) stated the tectonic and climate in Songkhla Basin controlled the changes of depositional environments, from lacustrine to mixed fluvial and perennial lake and transition to the low energy floodplain from Oligocene to Middle Miocene.

CHAPTER II
DATA AND METHODOLOGY

2.1   Introduction

The data used in this thesis comprises of 2D and 3D seismic reflection surveys, combined with borehole wireline log data, and information obtained from the industry unpublished reports, such as cuttings and sidewall core descriptions. All of these data sets were integrated and interpreted using Kingdom Suite (IHS), Petrel (Schlumberger Inc.), Traptester (Badley Geoscience Ltd.), and Hampson-Russel Suite (CGG). **Figure 2** illustrates a comprehensive workflow adopted for this research.
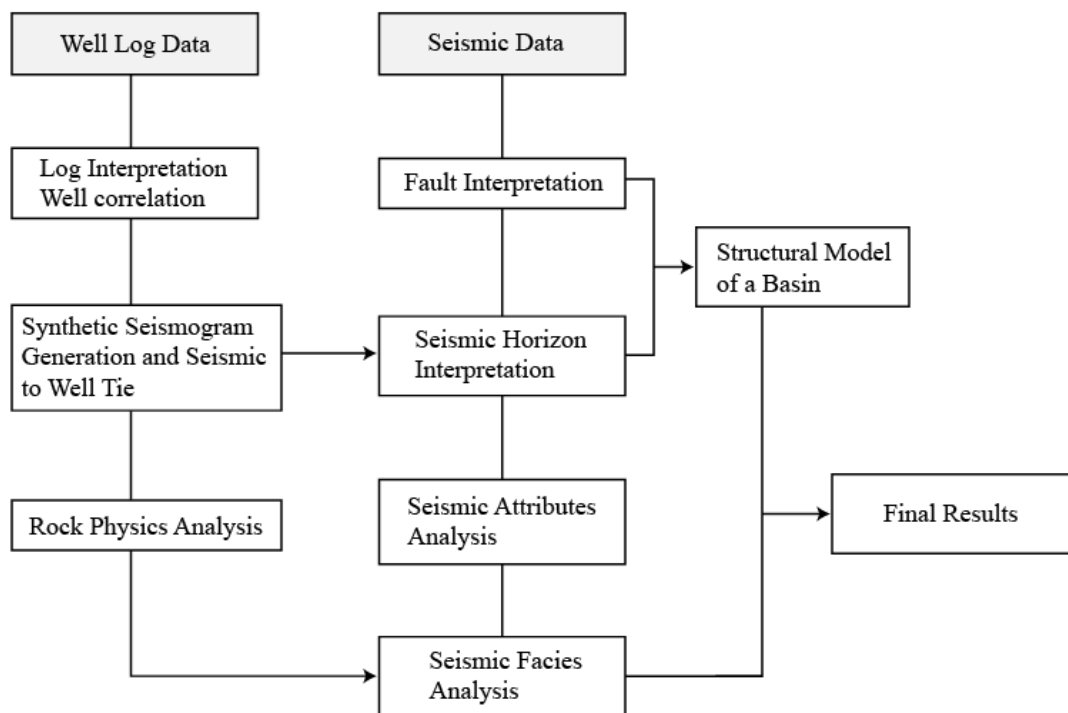
Figure 2 General workflow implemented for this thesis research.

2.2   Data set and software

2.2.1   Seismic survey data

The study focuses in an area of 700 km^2 within Songkhla Basin, which covered by 2D and 3D seismic reflection surveys (**Figure 1**; **Figure 3**). The SEG-Y format, 3D time-migrated seismic reflection survey consists of 1940 inlines and 3104 crosslines, with inline spacing of 12.5 meters (m) and a sampling interval of 4 millisecond (ms). The seismic data are zero phase and normal polarity (SEG convention), where an increase in acoustic impedance is displayed as a positive amplitude (black peaks) on the seismic cross section. The maximum frequency recorded is about 100 Hz, and the dominant frequency in the interval of interest ranging is about 40 Hz (**Figure 4**).
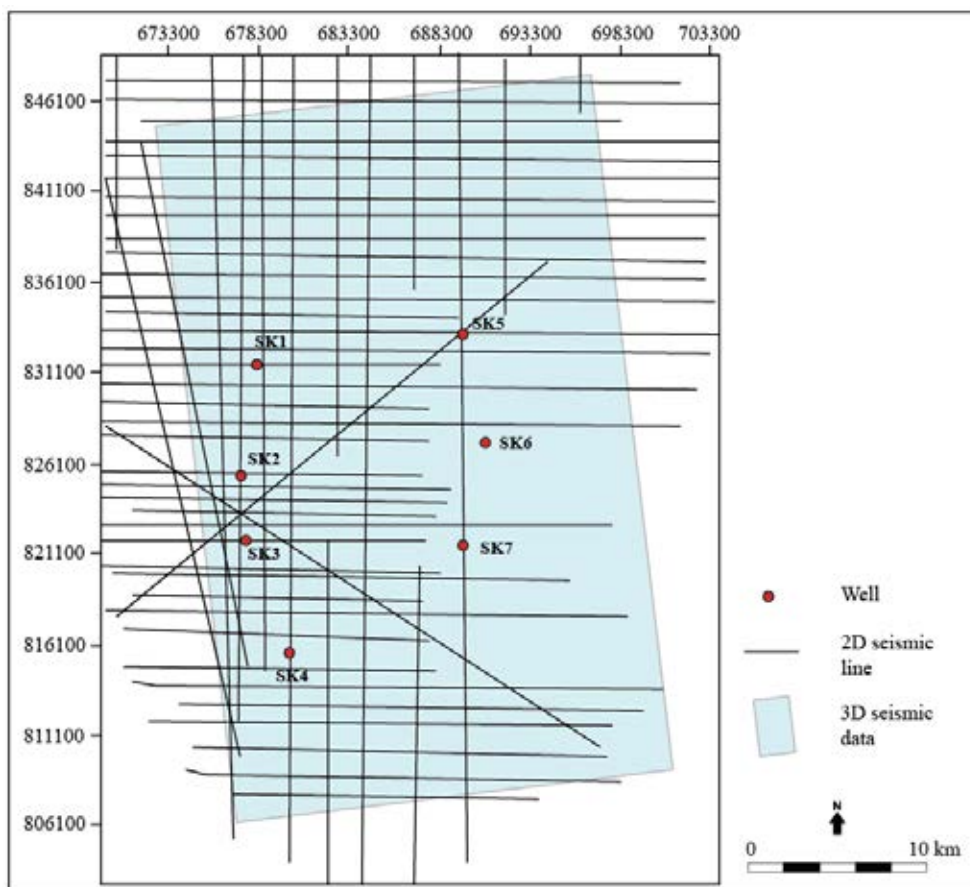
Figure 3 3D and 2D Seismic surveys and well locations.
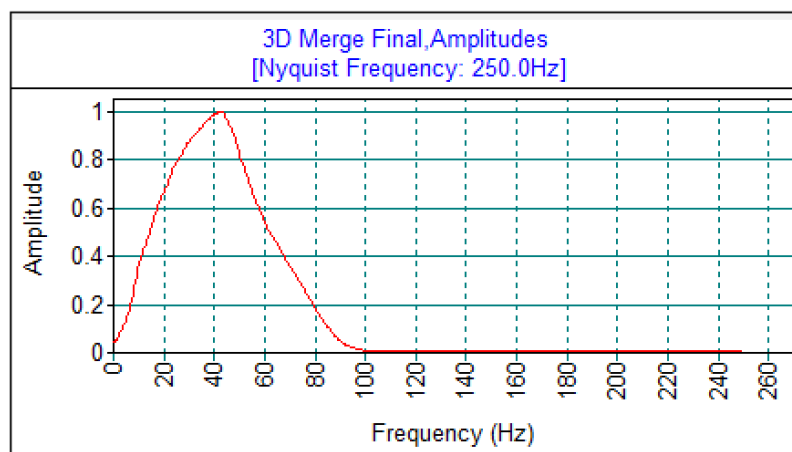
Figure 4 Frequency spectrum of seismic data within the interval of interest, 0-2 second.

Fault interpretation and horizon mapping are based on the 3D seismic volume, supplemented by a regional 2D reflection survey that covers a large area of the Songkhla Basin. The interpretation was conducted using 20 line spacing for the 3D seismic reflection data (250 meters' grid), sub-perpendicular and sub-parallel to average fault strike, as well as arbitrary lines oblique to fault strike.

2.2.2   Well data

In order to investigate the tectono-stratigraphic evolution of the Songkhla Basin, a total of seven wells covering the entire study area were selected, i.e., SK1, SK2, SK3, SK4, SK5, SK6, and SK7, in order to correlate the regional and local stratigraphy with seismic data covering the study area.

Table 1 shows all the Songkhla Basin well data being used, which comprises of final well reports, check shot, and composite logs.

Well	Gamma ray	sonic	Density	Neutron	checkshots	Bio data	Data available (meter)	
							From	Total depth (TD)
SK1	X	X	X	X	X	X	335	2005
SK2	X	X	X	X		X	335	2717
SK3	X		X	X	X	X	579	3011
SK4	X		X		X	X	1179	3188
SK5	X	X	X	X	X	X	396	2644
SK6	X	X	X	X	X	X	457	2790
SK7	X	X	X	X	X	X	1067	2816

Table 1 Well data being used for Songkhla Basin study.

2.3 Approaches and methodology

This study focuses on the application of various complementary data gathering techniques to better understand the impact of tectonics on the syn-rift to post-rift transition. An overview of the techniques used is briefly presented in this chapter. For more specific descriptions of the methodologies, the details can be found in **Chapter 3** and **Chapter 4**.

2.3.1 Seismic and well correlation

The purpose of the seismic and well correlation (seismic-well tie) is to have more accurate control on mapping subsurface stratigraphy. Synthetic seismograms are constructed to tie the well information in depth to seismic data in time (two-way time, TWT).

As shown in **Figure 5**, the acoustic impedance at the wells was calculated using the velocity data from sonic log and the density data from density log. After that, the reflection coefficients at each interface between contrasting velocities were calculated. The chosen synthetic wavelet, which has a frequency response and band width similar to the nearby seismic data is used to convolved with the reflection series for the entire well to generate the synthetic seismic trace. This synthetic trace closely approximates a trace from seismic lines that pass close to wells with the appropriate logs. The stratigraphic markers at intervals of interest can then be transferred from the well to seismic reflection data.
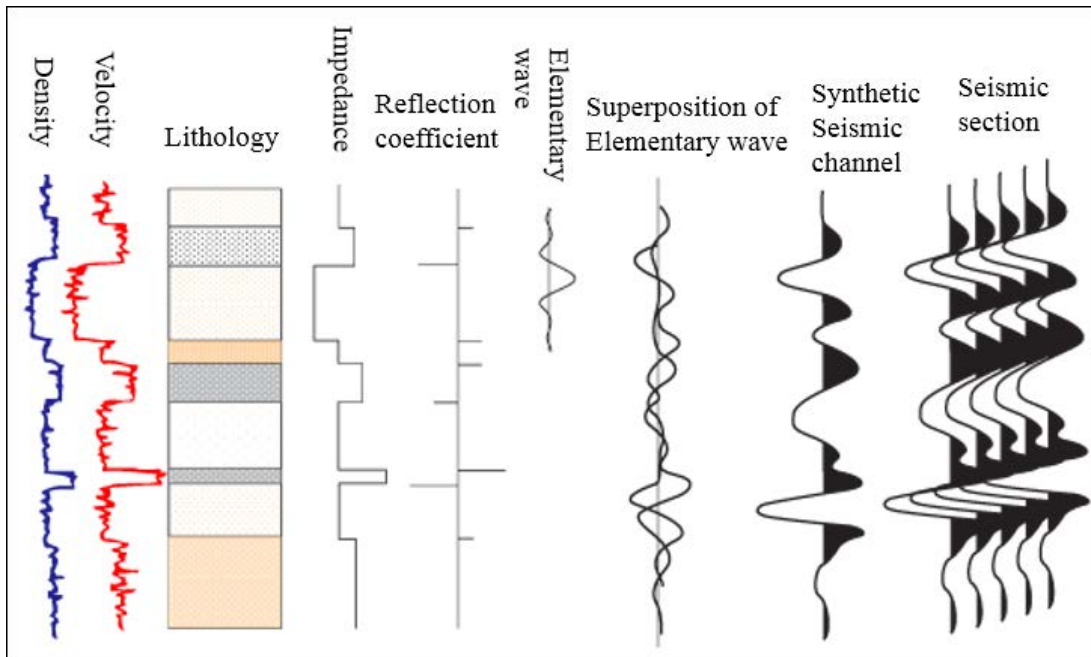
Figure 5 General seismic and well correlation process (Simm and Bacon, 2014).

2.3.2   Throw-length profiles

The geometry and evolution of faults have been study widely using displacement-length profiles to demonstrate the variations in displacement distribution on the fault plane along strike (e.g., Gawthorpe and Leeder, 2000; Kim and Sanderson, 2004; Morley, 2014). The variations in displacement can be used to analyze fault growth, propagation, interaction, and linkage.

Fault displacement (D) is the relative movement of two originally adjacent points on the fault surface, where displacement contours of the fault surface are ellipsoidal and bounded by zero displacement or tip line loop (**Figure 6**). Fault length is the distance between fault tips that is usually measured along the fault trace and in the horizontal plane (e.g., Scholz and Cowie, 1990; Peacock and Sanderson, 1991). For normal faults, the throw is usually obtained from well data.

The relationship between maximum displacement (Dmax) and maximum fault length (L or H) is generally written as a power law relationship:

$$D_{max} = cL^n,$$

Where the value of c is a constant, related to fault displacement at unit length. The value of the exponent n ranges between 0.5 to 2.0, where for normal faults, the range of n is between 1 to 2 (Watterson, 1986, Walsh and Watterson, 1988; Marrett and Allmendinger, 1991; Dawers et al., 1993, Cartwright et al.,1995; Dawers and Anders, 1995; Kim and Anderson, 2004). In tectonic environments with the uniform properties, the relationship of the maximum displacement to the fault length is linear scaling (i.e. n=1), making n a constant of the proportionality determined by the ratio of Dmax to L. Many factors affect the relationship including the mechanical stratigraphy and how overlapping faults interact (for example, Cowie and Scholz 1992).
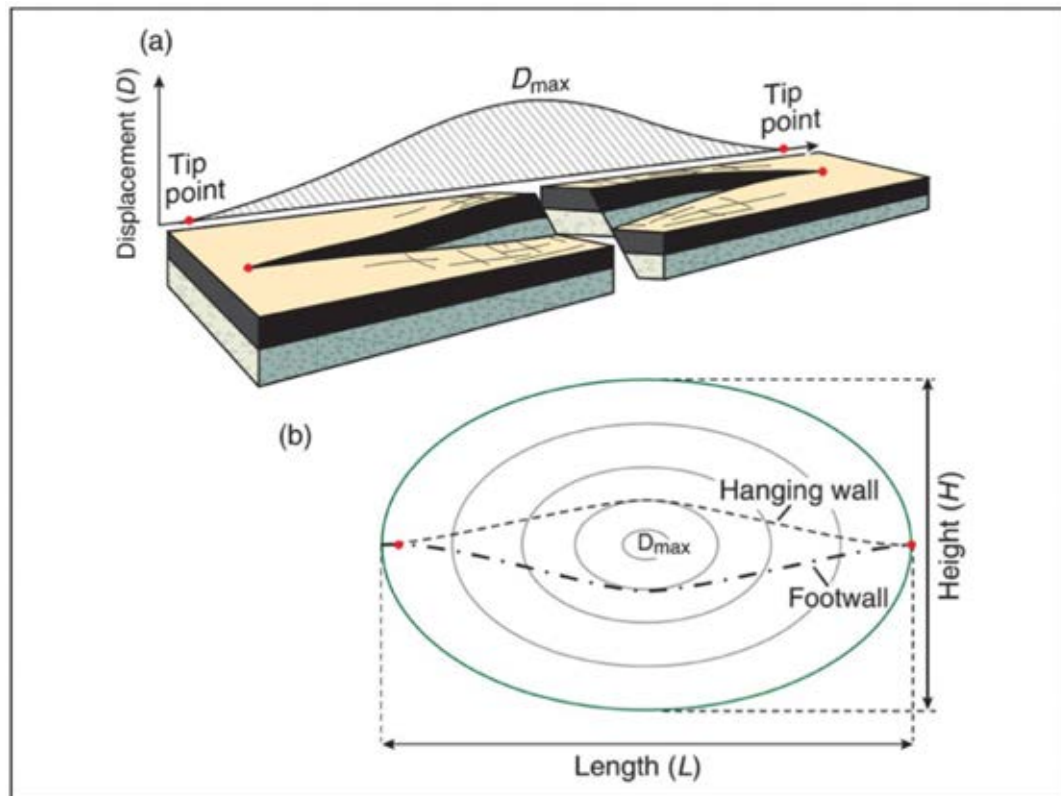
Figure 6 (a) Schematic illustration of an ideal, isolated fault. The displacement profile indicates maximum displacement near the center. (b) The fault plane with displacement contours. Stippled lines are the hanging-wall and footwall cutoff lines and the distance between them indicates the dip separation (Fossen, 2010).

In this study, throw versus fault length along the fault plane is used to demonstrate the fault geometry and the variations in throw distribution of five major western boundary faults in order to retrieve the fault growth history and their evolution. The throw-length profiles were constructed from five major horizons covering the syn- to post-rift interval. The fault throw values were measured based on the offset reference horizons in the hanging wall and footwall in seconds (s) two-way time, perpendicular to the strike of faults.

2.3.3   Rock physics analysis

Rock physics analysis is used to establish the link between seismic amplitudes and geological facies and reservoir properties based on the behaviour of seismic waves propagating through rocks. Different rock properties will directly control the stress-strain relationship and the corresponding seismic response. In a standard seismic interpretation workflow, rock physics analysis is usually used to correlate impedance and elastic parameters to specific rock properties.

P-wave velocity (Vp or primary wave), S-wave velocity (Vs or secondary wave), density (ρ), elastic impedance (EI) and acoustic impedance (AI) were derived from well log data at well locations to determine rock properties that can be used to discriminate lithology of sands and shales. The cluster separation of these parameters on cross plots was used to identify lithological facies. If the separation of facies using AI/EI cross-plots at well log scale is poor, then such facies discrimination at the seismic scale is also likely to be poor.

2.3.4   Seismic attributes analysis

Seismic attributes analysis plays an important role in unlocking hidden information from seismic amplitude data. It has been proven that seismic attributes are very useful tools and have been successfully applied to different geological setting (clastic, carbonate, and salt related basins) as well as different tectonic setting (extension, compression, and strike slip regimes). Nowadays, seismic attributes have been increasingly used in both exploration (basin scale stratigraphy and structural) and development (reservoir scale characterization for lithofacies and flow units) as one of the workflows to help identify prospects, determining depositional environments (e.g. fluvial or deep-water channels, carbonate build-ups, salt domes), detecting and enhancing faults and fractures for the structural evolution, and even provide direct hydrocarbon indication.

Seismic attributes are the components of the seismic data, which can be derived, extracted, and computed in order to visually enhance or quantify geological features of interest that might be subtler in a traditional seismic image, leading to a better geological or geophysical interpretation of the data. It was introduced as part of the seismic interpretation in the early 1970's. Now it has been widely used for geological and geophysical interpretations. Good seismic attributes are directly sensitive to the changes in seismic impedance and allow us to define the structure and depositional environment (Chopra and Marfurt, 2005).

In this research three types of seismic attributes have been applied following Brown (1996, 2004) classification: (1) the Time/horizon attributes of coherence and Curvature; (2) the amplitude attributes of Mean amplitude, RMS (root mean square) amplitude, Maximum amplitude; and (3) the frequency attribute which is normally called spectral decomposition. The seismic attributes that provide good results in this study are listed below.

2.3.4.1 Similarity

Similarity (known as a Lateral Continuity Attributes) is computed as semblance that is determined by considering a user-selected number of traces. The semblance is a measurement of coherent power existing between a number of traces versus the total power of all traces, as given by:

$$Semb(z) = \frac{\sum_{\tau=-N/2}^{\tau=N/2} \left\{ \sum_{m=1}^{M} f_m(z+\tau) \right\}^2 - \sum_{\tau=-N/2}^{\tau=N/2} \sum_{m=1}^{M} f_m^2(z+\tau)}{\sum_{\tau=-N/2}^{\tau=N/2} \sum_{m=1}^{M} f_m^2(z+\tau)}$$

where: fm (z) = the m'th trace of the gather; N = the length of the computational window in both time and depth domains and z = stands for either time or depth.

The number of traces depends on the signal to noise ratio (poor S/N, more traces), (more curvature, less traces), and higher lateral discontinuity resolution (better resolution, less traces) (IHS Kingdom, 2014).

It is an effective tool to determine the lateral changes along traces that might be associated with the geological features, i.e., faults and stratigraphic boundaries. In this study, the similarity volumes were generated from the full stacked seismic volume. The white colour represents the highest similarity, where black colour represents the lowest similarity (non-similarity).
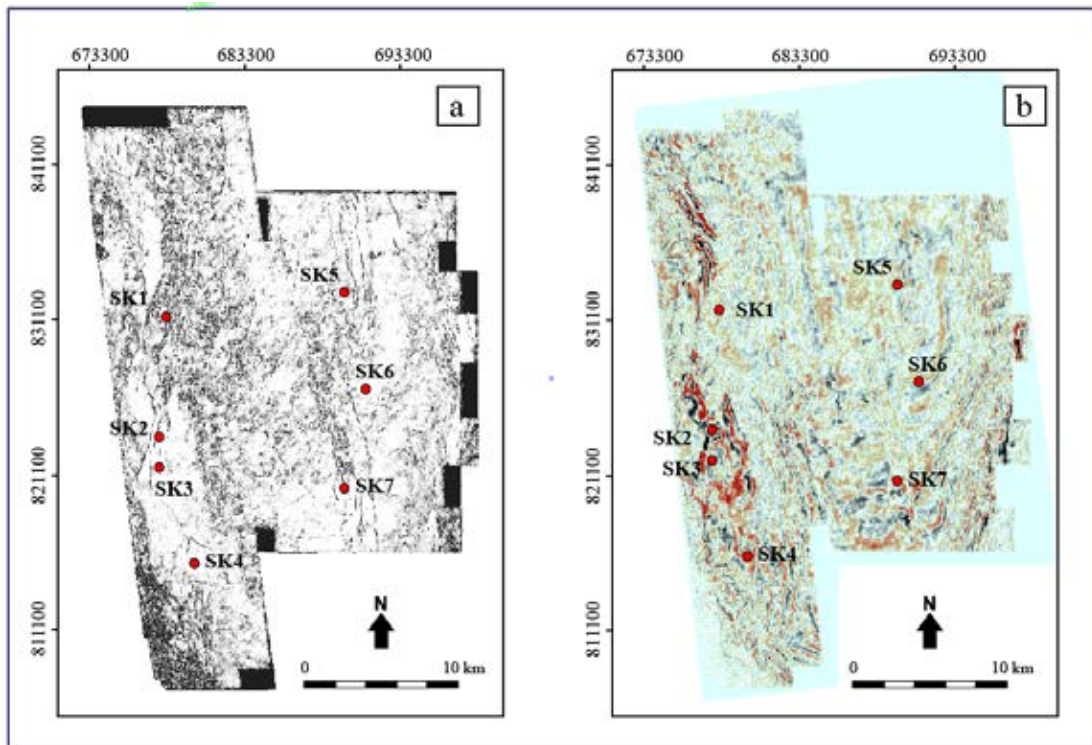
Figure 7 Comparison of similarity attributes (a) and seismic amplitude (b) on time slice
　　　0.78 second.

2.3.4.2　Root mean square (RMS)

The Root Mean Square (RMS) is a post-stack attribute, which computes the square root of the sum of squared amplitudes divided by the number of samples within the specified window being used following the equation of;

$$X_{rms} = \sqrt{\frac{(X_1^2 + X_2^2 + ... + X_n^2)}{n}}$$

Where X_i is the seismic amplitude of the ith sample, X_{rms} is the amplitude of RMS seismic attribute and n is the number of sample.

The RMS is very sensitive to changes in acoustic impedance. As a result, it emphasizes the variations in acoustic impedance in the selected window and provides information about the relative value of acoustic impedance of rocks. However, RMS is sensitive to noise as it squares every value within the window. Commonly, the higher

acoustic impedance variation, the higher RMS values will be. The high RMS in channels may cause by either high acoustic impedance contrast between channel fill with surrounding lithology or high acoustic impedance contrast between filled-sediments.
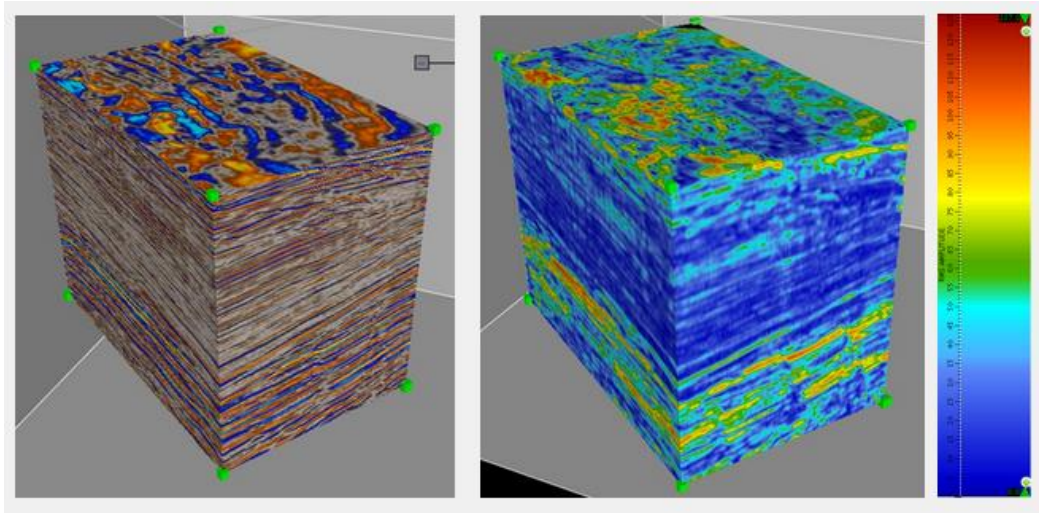
Figure 8 The Examples of original volume (left) and resultant RMS amplitude attribute volume (right) (after OpenWorks® software).

2.3.4.3   Spectral decomposition (SD)

Spectral decomposition attributes are the transformation of a seismogram (seismic signal) to a frequency domain of the seismic bandwidth, which provides a high detail for reservoir imaging and mapping of temporal bed thickness and geological discontinuities within the seismic survey by breaking down seismic signal into its' component frequencies. Many researchers have developed different methods to breakdown the seismogram to frequency for example; the conventional Fourier Transform, CWT (Continuous Wavelet Transform), MPD (Matching Pursuit Decomposition) and EPD (Exponential Pursuit Decomposition) methods for transformation of data to frequency domain. The latter two techniques offer more accurate analysis.

In this study, the conventional short window discrete Fourier Transform (SWDFT) has been applied using Kingdom Suite (IHS) software. The attribute computation algorithms have been developed by M. T. Taner and Associates at Rock Solid Images, where frequency/wavenumber decomposition splits seismic trace energy into spectral sub-bands based on Gabor-Morlet complex wavelet transform, followed by computations of the envelope of the complex trace in each sub-band (IHS Kingdom, 2014).
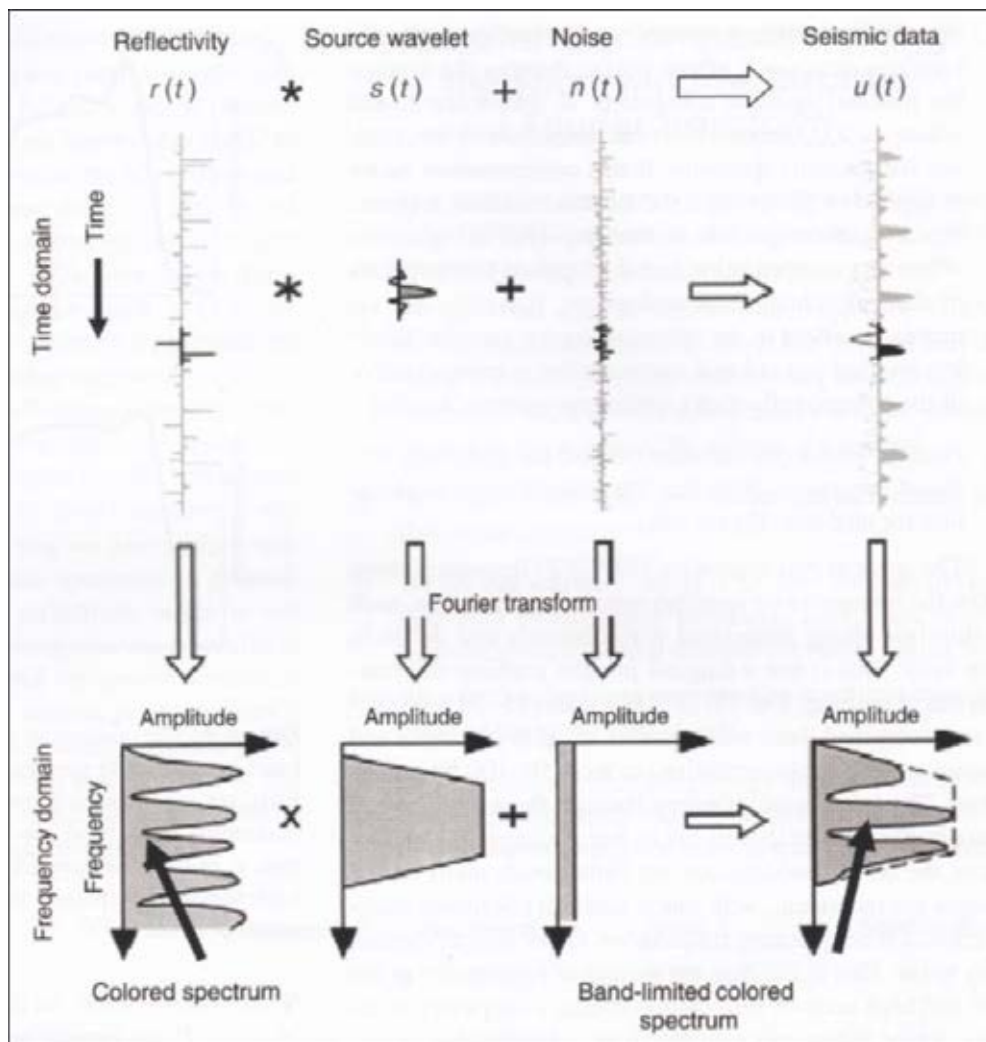
Figure 9 Short Windows analysis (Quoted from Partyka et. al.,1999).

CHAPTER III
GEOLOGICAL SETTINGS

3.1   Introduction

The regional development of Cenozoic rift basins in Thailand is complex, with older development of basins in the eastern and southern Gulf of Thailand (GOT) (Eocene-Oligocene), and younger development (Late Oligocene to Miocene) passing northwards and westwards (Travena and Clark, 1986; Searle and Morley, 2011; Racey, 2011; Morley, 2015). In the eastern GOT, major extension ended around the Oligocene-Miocene boundary. In the western GOT, rifting continued into the Miocene, and in northern Thailand, rifting ended in the Late Miocene. Some basins, particularly in central and northern Thailand, display evidence for inversion, which occurred in several phases during the Miocene and Early Pliocene (Morley et al., 2011; Morley, 2001; Morley, 2009). Other basins show evidence for rotation of the extension direction during the Miocene, which results in relatively complex fault patterns. In addition, the influence of pre-existing fabrics on rifting has produced varying degrees of faulting oblique to the extension direction (Morley et al., 2004; Morley, 2016).

3.2   Geological settings of Gulf of Thailand Cenozoic Basins

Thailand has a complex Cenozoic geological history of deformation and sedimentation and lies within the continental core of SE Asia called Sundaland, which covers a large part of present-day Southeast Asia (i.e., Cambodia, Laos, Vietnam, Thailand, Peninsular Malaysia, most of the Sumatra and Java, part of Borneo, and all their respective continental shelves). It is surrounded by active and complex tectonic boundaries: (a) Himalayan Orogeny belts in the northwest, (b) subduction of the Indian oceanic crust in the west-southwest-south (Andaman-Sunda-Java Trench), (c) collision of Australia continental crust with eastern Indonesia in the southeast (Timor Trough), (d) a number of marginal basins opening up during Cenozoic and the South China Sea in the east (Hall & Morley, 2004; Hall, 2008). Sundaland was built from continental

fragments that were separated from Gondwana and assembled in the end of Triassic during the Indosinian Orogeny, and then it was detached later to form the southern part by the continental fragments rifted from Australia during the Cretaceous (Hall and Morley, 2004; Hall, 2011; Hall, 2012; Charusiri, 2009). It lies on the thin hot, weak continental lithosphere with considerably high geothermal gradient ranging from 3.6-8 °C/100m (2.55 °C/100 m is considered as normal geothermal gradient) and high heat flow up to 110mWm^2 (Pigott and Sattayarak, 1993; Morley and Westaway, 2006). It was exposed as land during the Pleistocene lowstands and contains a large number of Cenozoic sedimentary basins, which formed between the Paleogene and the Middle Miocene (Morley and Racey, 2011).

Two principle tectonic blocks can be identified in Thailand; the Indochina Block in the east and the Sibumasu Block in the west (Racey, 2011; Hall and Morley, 2004; Metcalfe, 2010). The Indochina block comprises of Eastern Thailand, Cambodia, Laos, and Vietnam, while the Sibumasu block comprises of Myanmar, Western-Northwestern Thailand, and West Malaysia (Hall and Morley, 2004) (**Figure 10**). The opening of Cenozoic basins in Thailand have been widely discussed as strike-slip pull-apart basins (Tapponnier et al., 1986; Polachan and Sattayarak, 1989) or continental extension basins (Longley, 1997; Wheeler and White, 2002; Watcharanantakul and Morley, 2000). The collision of India with Asia began in the Eocene period about the same time as the development of Cenozoic basins, therefore the deformation in Indochina and SE Asia was interpreted as a result of the India-Asia collision (Tapponnier et al., 1986; Peltzer and Tapponnier, 1986). The recognition of the major strike-slip faults such as the Three Pagoda, Mae Ping and Red River Faults running cross the Indochina, South China, and disappear offshore was interpreted to cause the opening of Thailand Cenozoic basins as pull apart basins (Tapponnier et al., 1986; Polachan and Sattayarak, 1989). Some authors projected these faults to offshore and linked to Borneo Geology (Tapponnier et al., 1986; Briais et al., 1993; Lee and Lawver, 1995). However, these interpretations have been conducted base on the regional features without detailed analysis.

Cenozoic rift basins in Thailand formed a failed rift system, and they are intracratonic rift basins located in the central part of Sundaland. They were developed

in a complex tectonic setting significantly different from the other typical continental failed rift basins, e.g., East African Rift System, Central African Rift System, and the North Sea (Travena and Clark, 1986; Searle and Morley, 2011; Racey 2011; Morley, 2015). The key differences include: (a) widespread occurrence of low-angle normal faults found onshore Thailand; (b) basin inversion alternating with rifting; (c) diachronous initiation and cessation of rifting; (d) rapid subsidence with very thick Tertiary sediments; and, (e) extensive low-displacement post-rift faults (Morley, 2015).
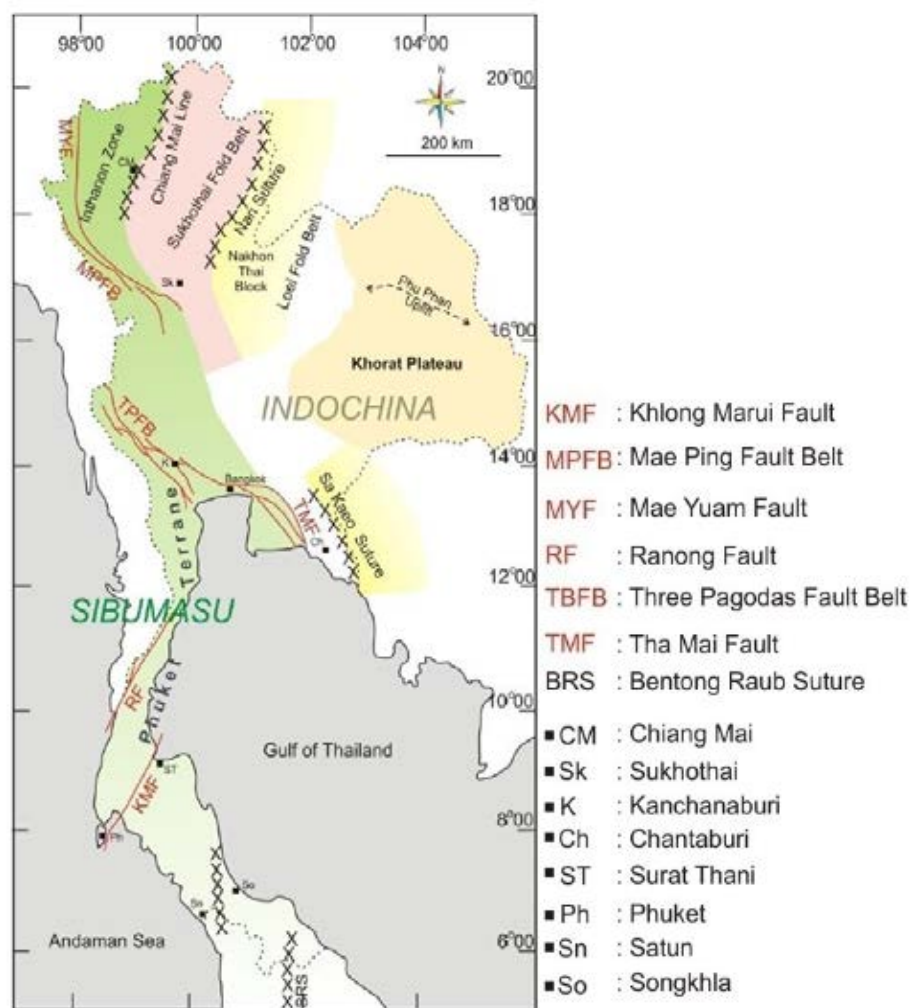
Figure 10 Thailand principle structural map, including two principle tectonic blocks, Sibumasu in the west (green) and Indochina in the east (yellow) (Ridd et al., 2011).

The timing of rifting and onset of post rift subsidence is diachronous, younging from east to west in the GOT. The end of rifting is also young in Central and Northern Thailand. The basins have also undergone the episodic inversion during Miocene, indicating the fluctuation in the stress stage with time (Morley et al, 2001; Morley 2001; Morley 2009). The timing and location of inversion in Thailand is highly variable. Some basins are not influenced by any inversion, while the others display multiple events and alternating with phases of extension over a period of 15-20 Ma (Morley et al, 2001; Morley 2001; Morley 2009). Inversion was well developed in the Malay Basin, but poorly developed in the GOT, while the intensity increasing northward to Central and Northern Thailand. The Central Thailand was affected by inversion during Early to Late Miocene, while basins in Northern Thailand were inverted at different times between the Late-Oligocene to Late Miocene and the Plio-Pleistocene (Morley, 2014).
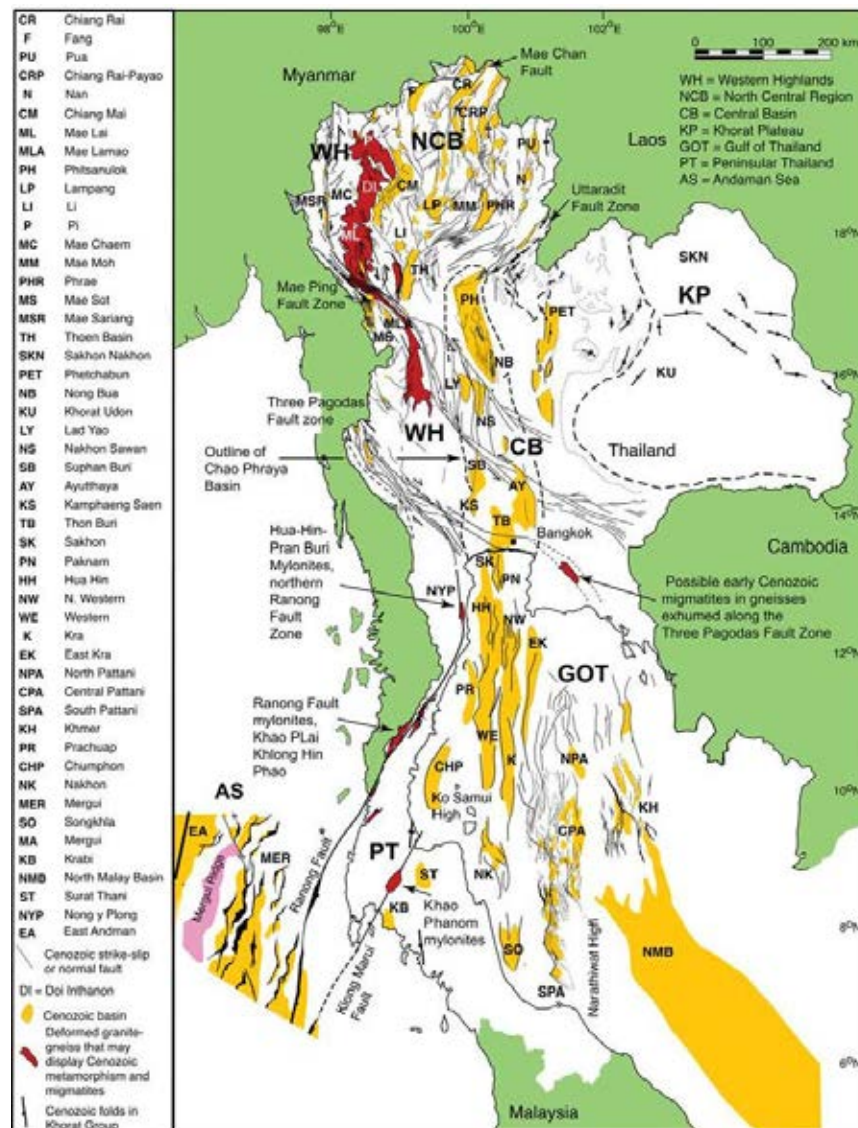
Figure 11 Location of the Cenozoic structure and basins in Thailand (Morley et al., 2011).

3.3 Gulf of Thailand structural framework

The Gulf of Thailand (GOT) is a shallow sea (water depth less than 100 meters) located on the southern edge of the Eurasian Plate covering an area of 270,000 km^2. It was dominated by the development of Cenozoic rift systems and post-rift basins with extensive sedimentation since the Eocene (Racey, 2011). It is divided by the north-south trending Ko Kra Ridge into two regions, east and west. The eastern GOT comprises the large Pattani, Khmer and North Malay Basins. On the other hand, the

western GOT comprises smaller, narrow, elongate basins: Western Basin, Kra Basin, and Chumphon Basin, which in turn are separated from each other by the north-south trending basement horsts (Racey, 2011) (**Figure 11**, **Figure 12**). The two major hydrocarbon producing basins are Pattani and North Malay Basins.
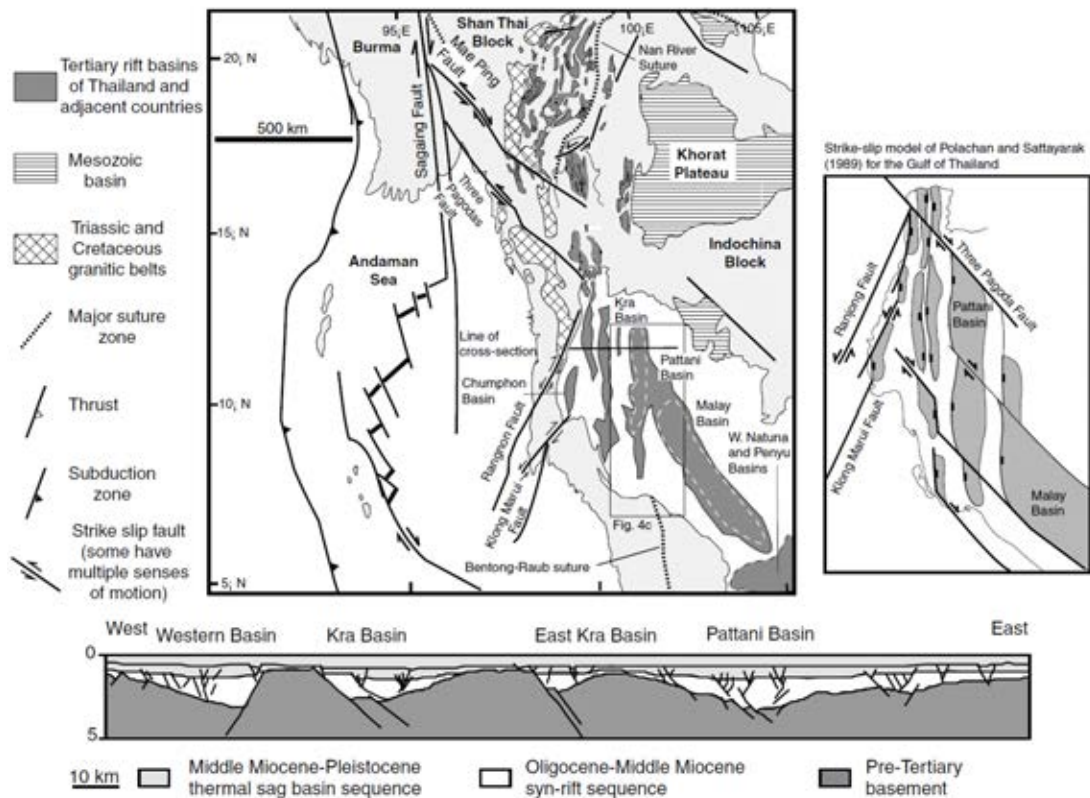
Figure 12 Regional tectonic map of western Southeast Asia modified from Packham (1996) and Leloup et al. (1995). The rift basins of Thailand are in dark grey. Cross-section through the northern Gulf of Thailand is from Oudom-Ugsorn et al. (1986). Strike-slip model for the Tertiary basin formation in the Gulf of Thailand is after Polchan and Sattayarak (1989) (after Morley et al. 2011).

The Cenozoic rift basins are extensively present in the Gulf of Thailand, and extend onshore into the central and the most northern parts of the country. They are a string of north-south trending basins filled by the continental deposits, predominantly of half graben geometry (Morley et al. 2011; **Figure 13**). 3D seismic reflection data

shows significant changes in syn-rift structural style of extensional faults between the half graben and the synformal geometries. Synformal geometry with low displacement on wedge shape boundary faults is found in the north and central part of Pattani Basin, while typical half graben geometries are well defined in south Pattani basin, the western GOT and North Malay Basin (northern part of Malay Basin). Watcharanantakul and Morley (2000) stated that the synformal geometry in the north and central part of Pattani, and the half graben bounded by east dipping boundary faults of the East Kra and Kra basins are compatible with a ramp-flat extensional detachment geometry.
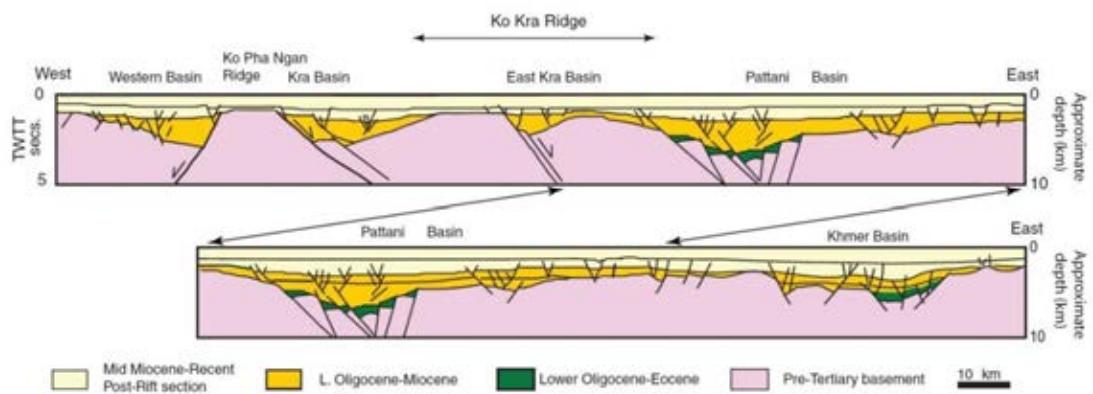
Figure 13 Cross-section through the Gulf of Thailand is from west – east showing half graben geometry of rift basins (after Morley et al. 2011).

Determining the location of syn to post rift transition in the eastern GOT, especially northern half of the Pattani basin, from the seismic reflection data is challenging for the synformal geometry basin. This is due to the thick post-rift sequences (leading to poor imaging seismic data on the syn-rift section) and the presence of numerous low-displacement conjugate normal fault sets. These conjugate fault systems were developed during the post rift subsidence with complex transferred zones or locally known as graben shift, where the opposite-dipping fault tips slightly overlap (Morley, 2015). The complex transfer zones are caused by the change in dip domain between fault sets propagating along the strike direction. Many of them are influenced by the pre-existing fabrics leading to the more oblique NE-SW and NW-SE trends (**Figure 12**). In contrast, in the southern part where the typical half graben

geometry is well developed, the location of the syn to post rift can be easily identified as the deepest depocenter is located near the major boundary faults (Kornsawan and Morley, 2002; Watcharanantakul and Morley, 2000; Morley and Westaway, 2006; Morley et al., 2011).

The Pattani and Malay Basins experienced considerably rapid post-rift subsidence during the Early – Mid-Miocene with up to 6-8 km of Miocene – Recent post rift section. The rapid subsidence rate contributed to thicker sediment succession if compared to the classic post-rift sequences such as the North Sea, East African Rift, and Anza Graben (Morley, 2015). Identifying the cause of rapid subsidence is complicated and cannot be explained by a simple subsidence mechanism. Besides the high subsidence rate, the basins have high heat flow (up to $110mWm^2$) and high geothermal gradient (up to 6 C/100 m) making it different from the other continental, failed rift basins (Morley and Westaway, 2006). The only comparison of high subsidence rate is the strike-slip pull-apart basins. However, the offshore seismic reflection data shows that the post-rift subsidence section formed as a synformal shape in broad area and was not controlled by any large-displacement faults (Morley and Westaway, 2006). Hence, the proposed pull-apart setting as the cause of thick sediments (Tapponnier et al., 1986) is not applicable in these basins. Instead Morley and Westaway (2006) proposed the rapid subsidence in the GOT was caused by the lower-crustal flow driven by sediment loading during the post-rift stage.

3.4   Stratigraphy of Thailand offshore basins

3.4.1   Kra and Western basins

Rifting was initiated in the Kra and Western Basins in the Late Oligocene (Pradidtan and Dook, 1992). Two Tertiary stratigraphic units were identified in the Kra and Western Basins by Pradidtan & Dook (1992): 1) post-rift Late Miocene – Recent Chao Phraya group; 2) Late Oligocene-Middle Miocene syn-rift section. Both units are separated by the Mid Miocene Unconformity (MMU) and are different from the Pattani Basin. The syn-rift section was divided into 2 groups, Kra A and Kra B, while the post-rift was defined as Kra C. Kra A and Kra B are dominated by alluvial and lacustrine

sediments, while Kra C is interpreted as alluvial sediments associated with braided and meandering river deposits, comprises of reddish-brown to grey claystone with sandstone and minor limestone (Morley and Racey, 2011). For the Western Basin, the syn-rift section is dominated by floodplain deposits, with poorer development of lacustrine sediments. The syn-rift section stratigraphy is divided in to three units, i.e., WA, WB, and WC. WA, the oldest unit, composed of alluvial fan deposit and some lacustrine episodes marked by the several hundred meters of limestone with thin claystone (Morley and Racey, 2011). The WB unit is dominated by low energy fluvial floodplain environment red silty clays and calcareous mudstones with thin limestones. The WC unit contains coarse, pebbly sandstones and a high percentage of sand. WC is interpreted as high energy fluvial floodplain that is different from the WB unit (Morley and Racey, 2011). The Chao Praya Group shows an influence of marine conditions, and ranges between estuarine, intertidal, and shallow marine (Morley and Racey, 2011; **Figure 14**).
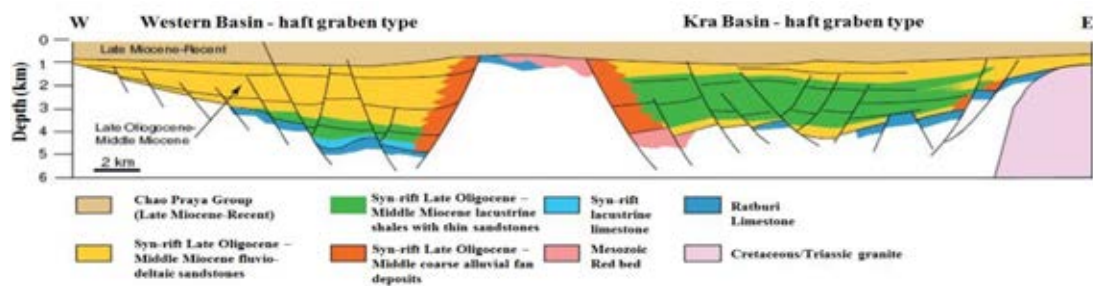
Figure 14 The western Gulf of Thailand (after Morley and Racey 2011).

3.4.2   Chumphon basin

Chumphon Basin stratigraphy was divided into three units: Unit I, Unit II and Unit III (Pradidtan, 1989; Heward et al., 2000). Unit I was deposited in the syn-rift sequence (probably of Late Eocene-Oligocene) comprises predominantly of alluvial plain and transgressive marine clays and shales with interbedded medium to coarse grain fluvial sands. Unit II was deposited in the Miocene syn-rift. It was divided into two groups: Unit IIa and Unit IIb. Unit IIa is the Lower Miocene age, overlying the erosional half graben of Unit I comprising of grey to dark grey shales and siltstones

with Minor sandstone and lignite. While Unit IIb was deposited in the Middle Miocene comprises of claystones and fine to coarse grain sandstones deposited in an alluvial floodplain environment (Morley and Racey 2011).

3.4.3 Nakorn basins

Songkhla and Nakorn Basins appear to have a long rift history similar to Chumphon Basin. There is little published stratigraphy for the Nakorn Basin.

3.4.4 Pattani basin

The Pattani and North Malay Basin-fill is predominantly fluvial-lacustrine facies from Oligocene to Mid-Miocene before becoming more marine or Marginal marine clastic-dominated facies in the Late-Miocene to Recent. Lockheart et al. (1997) published the stratigraphic sequences in the southern Pattani, while the central Pattani Basin stratigraphy is from Jardine (1997). Five stratigraphic sequences have been identified in the Pattani Basin; Sequence I, II, III, IV, and V. Morley and Racey (2011) provided the additional information to the Pattani stratigraphic descriptions based on the better seismic images from well-developed sections. From oldest to youngest, the five stratigraphic sequences are:

o   Sequence I sediments were deposited in the syn-rift section comprises of a mixture of the proximal alluvial fan/alluvial plain and lacustrine sediments in the Late Eocene to Oligocene, plus the Late Oligocene to Early Miocene post-rift lacustrine shale unit in the upper part of the unit. This sequence is the important petroleum source rocks, which contains organic matters both algal and terrestrial plant materials. The top of the sequence 1 is bounded by the Mid-Tertiary Unconformity (MTU), regional unconformity.

o   Sequence II was deposited during Early-Middle Miocene comprises fluvial floodplain and delta plain and intertidal deposits overlying the MTU. Seismic data shows Sequence II onlaps Sequence I and is conformably overlain by Sequence III. This sequence is the potential source-reservoir interval.

o Sequence III was deposited during the Middle Miocene. The sediment depositional environments are marginal marine to lagoonal delta plain. The sequence comprises sand and grey shales with some coals and carbonaceous shales. This sequence is believed to be the main source rocks in the Pattani and North Malay basins.

o Sequence IV or the Upper Red-beds was deposited during the Late Middle - Late Miocene. The sediments are fluvial red beds. This sequence is the major reservoir in the Pattani basin. The top of this sequence is the Mid-Miocene Unconformity (MMU).

o Sequence V was deposited above the MMU during the Upper Miocene to recent. It consists of delta plain to marine sediments.
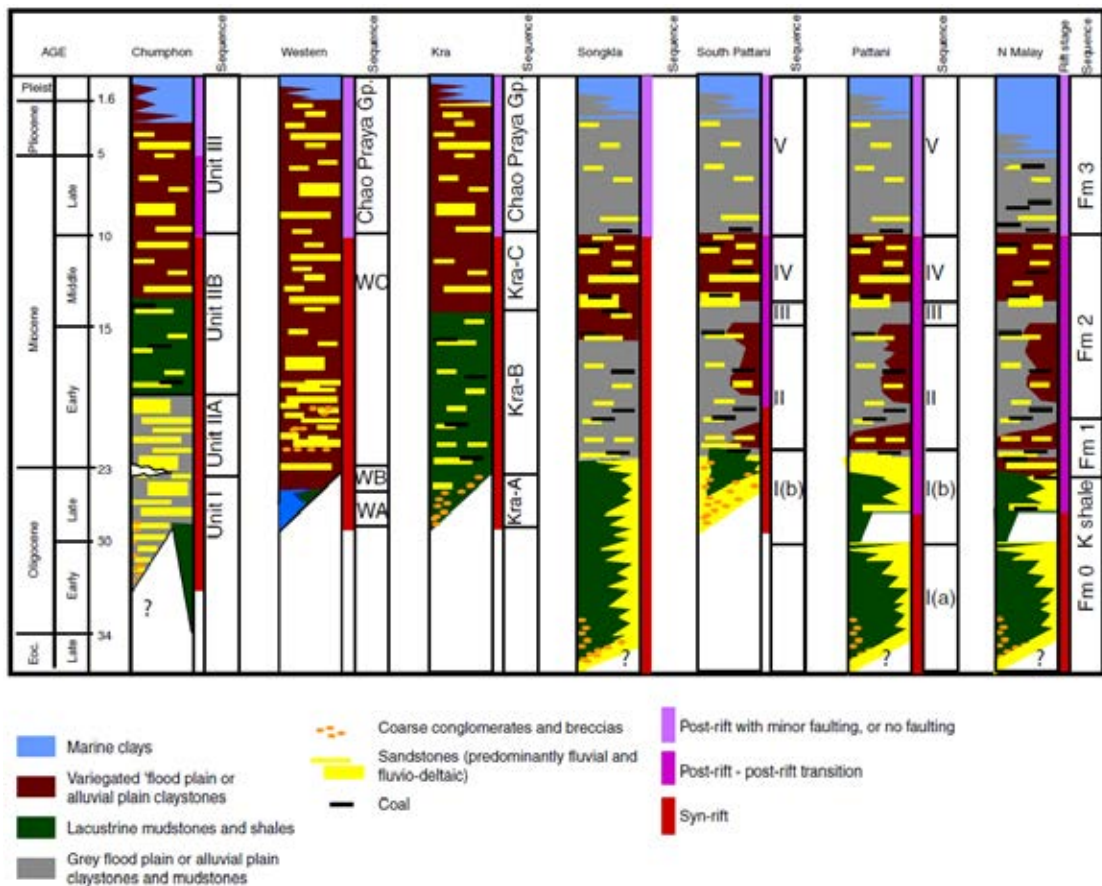
Figure 15 Stratigraphy comparison of the major Tertiary basin in the Gulf of Thailand (Morley and Racey 2011).

3.5   Geology of Songkhla Basin

The N-S trending Songkhla Basin is situated in the southwestern GOT, separated from the eastern GOT by the north-south trending Ko Kra Ridge (**Figure 1 (a)**). The basin has a half graben geometry, and is controlled by a set of large-scale, N-S to NNE-SSW, east-dipping normal faults that form the basin boundary fault system along the western margin (**Figure 16**). The basin is filled by up to 4 km (approximately 2.5 seconds) of Eocene to Middle-Late Miocene continental sequences (**Figure 17**).

The syn-rift strata in the study area comprises five stratigraphic sequences (**Figure 17**). The lowest sequence is the Eocene syn-rift package, represented by discontinuous weak to bright amplitude reflectors, well data indicates this sequence is dominated by mixed lacustrine shales and fluvial-alluvial sandstones (Morley and Racey, 2011; Kaewkor et al., 2015; Rivas et al., 2016). The overlying Lower Oligocene package is characterized by continuous high-amplitude reflectors across the basin. The well data indicates the Oligocene section is dominated by lacustrine deposits comprising organic rich shales (potential source rock) together with a few sandstones. The medium to high amplitude continuous reflectors observed in the 3D seismic data from Upper Oligocene to Early Miocene represent a basin that is dominated by lacustrine shale. The Middle to Late Miocene is characterized by low-amplitude discontinuous reflectors, and well data indicates a change to dominantly fluvial, sand-prone deposits.

The uppermost package of Pliocene age is represented by high amplitude continuous strong reflectors intercalated with discontinuous weak to bright amplitude reflectors and well data indicates the depositional systems during the Pliocene were predominantly in delta plain, marginal marine and shallow marine environments (**Figure 17**).
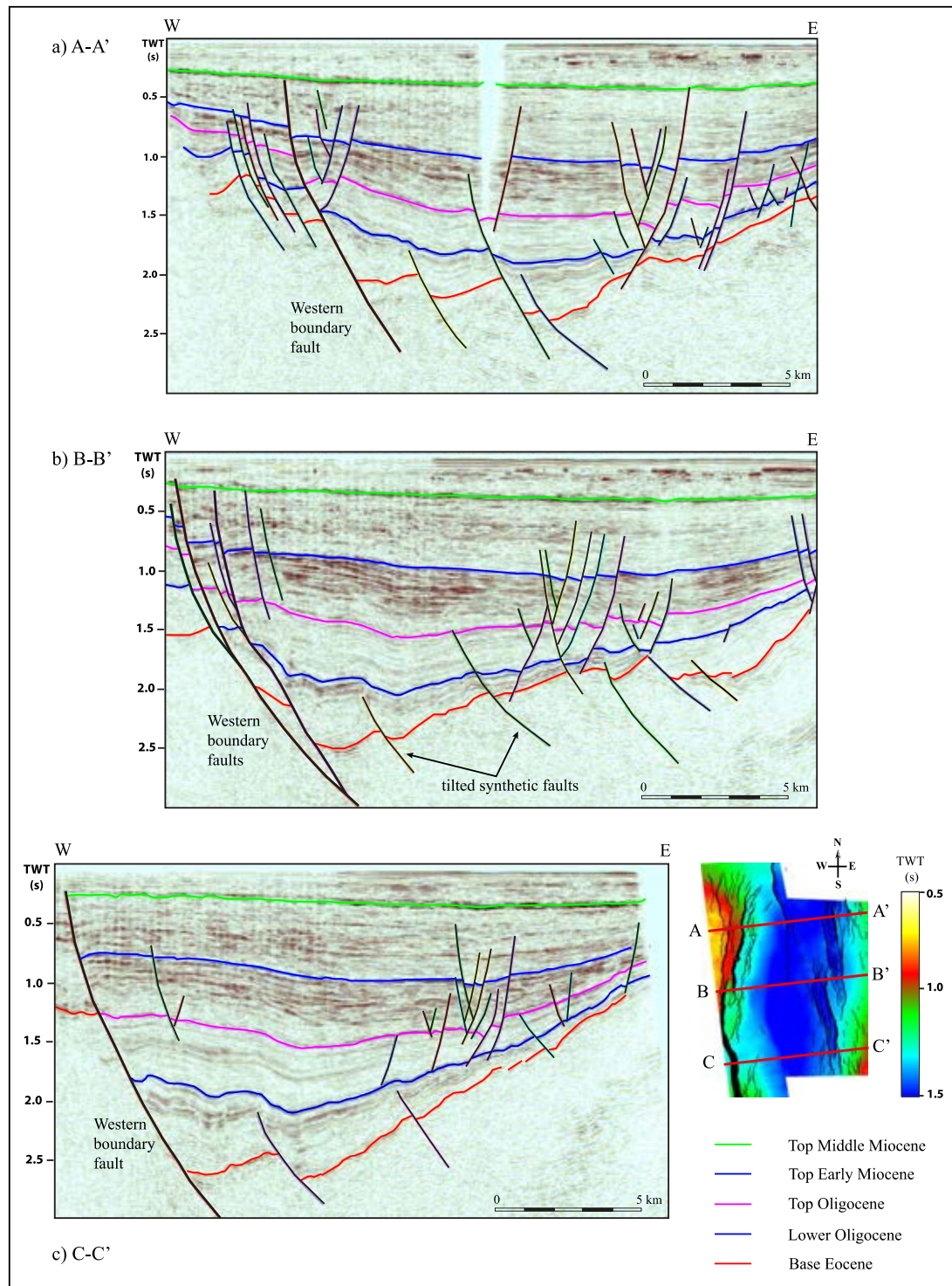
Figure 16 Interpreted full-stack seismic cross sections, in the east–west direction, of the Songkhla Basin showing the five major stratigraphic horizons, structural elements and lateral amplitude variations. (a) A-A' seismic cross section in

the northern part of a basin. (b) B-B' seismic cross section in the central part of a basin. (c) C-C' seismic cross section in the southern part of a basin.

Kaewkor et al. (2015) interpreted three main structural stages in the basin development: the initial syn-rift stage during the Eocene exhibits numerous low-displacement extensional faults; the second stage marks a switch to a half graben style, where many of the early domino faults became inactive; and the boundary fault becomes the dominant fault (Eocene-Lower Miocene). The final stage is post-rift subsidence that includes a phase of mild inversion during the Middle Miocene.

Seismic Reflection	Seismic Horizon	Depositional Environment	Rift Phase	Chrono-stratigraphy		Stratigraphic Sequences
	Top Middle Miocene	Delta plain Marginal marine Shallow marine	Regional subsidence	Pliocene-Recent	Quaternary	S5
	Top Early Miocene	Fluvial Fluvial-flood plain	Inversion early post-rift	Middle Miocene	Tertiary	S4
	Top Oligocene	Fluvial-flood plain Lacustrine	Syn-rift II	Early Miocene	Tertiary	S3
	Lower Oligocene	Lacustrine		Upper Oligocene	Tertiary	
	Top Eocene	Lacustrine		Lower Oligocene	Tertiary	S2
	Base Eocene	Alluvial Fluvial-flood plain	Syn-rift I	Eocene	Tertiary	S1
		Pre-Tertiary				

Figure 17 Stratigraphy in Songkhla Basin.

CHAPTER IV
EVOLUTION OF A MAJOR EXTENSION BOUNDARY FAULT SYSTEMS IN SONGKHLA BASIN

4.1   Introduction

In a rift basin, the deposition and distribution of the reservoirs are significantly influenced by the paleo-topography, which is largely controlled by the interaction and linkage of normal faults throughout the structural evolution. To understand the impact of structural elements towards the sedimentary successions, it is necessary to establish the basin structural evolution. Songkhla Basin 2D and 3D seismic reflection data calibrated by well data have been used to investigate the development of the boundary fault systems, including the deformation history, fault patterns, fault linkage history, and fault displacement patterns.

The main parts of this study have been published in the Journal of Asian Earth Sciences, Volume 130, 15 November 2016, Pages 239-255, under the title *"Evolution of a major extensional boundary fault system during multi-phase rifting in the Songkhla Basin, Gulf of Thailand".*

4.2   Methodology

This study focuses on an area of 700 km^2 within the Songkhla Basin, which is covered both by 2D and 3D time-migrated seismic reflection surveys (**Figure 1 (c)**). The seismic data is zero phase and normal polarity (SEG convention), where an increase in acoustic impedance is displayed as black peaks in the seismic cross section.

The seismic profiles are calibrated with synthetic seismograms generated from five wells (Songkhla-1, Songkhla South-1, Songkhla Southwest-1, C04, and D06). This calibration ties well information in depth to seismic data in time. The synthetic seismograms show good to fair correlation. D06 is an example of a good well-tie (**Figure 18**). In order to convert time to depth, a representative time-depth relationship

was used. The time-depth relationship was derived from synthetic seismograms, which were calibrated with check shot data where applicable. Five major marker horizons on seismic correspond with flooding surfaces in the wells. Key mapped horizons are: Top Middle Miocene, Top Early Miocene, Top Oligocene, Lower Oligocene, and Base Eocene (base syn-rift) (**Figure 16**; **Figure 17**).

The faults and key horizons were interpreted based on both 2D and 3D time-migrated seismic reflection surveys (**Figure 1 (c)**; **Figure 3**). The 3D seismic survey has a line spacing of 12.5 m for both the inlines and crosslines. A 250 m grid spacing was determined to be sufficient to study the east-dipping boundary faults (20 line spacing). 2D reflection surveys that cross, and extends further west than the 3D seismic data were used to determine the boundary fault zone geometry. The seismic data is of good quality and seismic inversion results provided excellent seismic features for stratigraphy analysis.
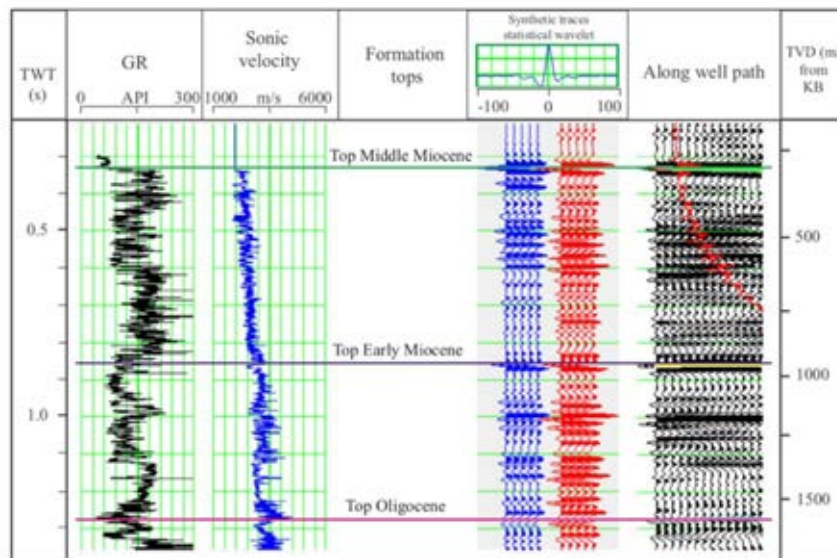
Fig. 4. Correlation of D06 well logs, 3D seismic profile along well path and the constructed synthetic seismogram used to generate a synthetic trace in the study area (wellbore location is shown in Figs. 1 and 5). The red seismic trace is a trace around the wellbore. The blue traces are synthetic traces calculated using sonic and density logs and the statistical wavelet from seismic profile. (For interpretation of the references to colour in this figure legend, the reader is referred to the web version of this article.)

Figure 18 Correlation of D06 well logs, 3D seismic profile along well path and the constructed synthetic seismogram used to generate a synthetic trace in the study area (wellbore location is shown in **Figure 1** and **Figure 19**). The red seismic trace is a trace around the wellbore. The blue traces are synthetic

traces calculated using sonic and density logs and the statistical wavelet from seismic profile. (For interpretation of the references to colour in this figure legend, the reader is referred to the web version of this article.)

The consistence dip attribute calculates dip between adjacent seismic traces in a 3D seismic volume and iteratively checks for continuity of traces. Where discontinuities in the data are encountered, they are marked with a quality attribute. Hence discontinuities such as faults are highlighted in a consistence attribute volume. **Figure 19** shows the structural contrast in the north and south areas from four selected horizons extracted from the consistence dip cube. The consistence dip attribute most clearly identifies low-displacement faults.

Structural maps and throw-length profiles were used for the structural interpretation and for determining fault growth history. Fault and horizon surfaces were imported into Badley Geosiences Ltd Trap Tester software, and were used to generate fault surfaces with throw contours plotted on them. Throw-length profiles of the major boundary faults are another way to demonstrate the variations in throw distribution on the fault plane along strike. The variations in throw can be used to make inferences about fault growth, propagation, interaction, and linkage. In this study, throw measurements are displayed in two-way time (TWT). The fault throw values were measured based on the offset reference horizons at the hanging wall and footwall in seconds (s). The deepest stratigraphic unit that shows expansion of section into the hanging wall of the fault indicates the initiation age of the fault.

Changes in the amount of accommodation space and the location of sedimentary input points throughout the development of normal faults will control the distribution and the architecture of the sedimentary strata. Therefore, the thickness variation of the strata across faults as a function of the sedimentary records on the hanging-wall of a fault plane can be used indirectly to identify tectonic history of segmented fault systems (e.g. Prosser, 1993; Morley, 1999; Young et al., 2001; Henstra et al., 2015). Isochron and isopach maps are typically used to demonstrate the variations of the sedimentary thickness associated with fault development. As shown in **Figure 16** and **Figure 17**, a total of five horizons have been mapped based on the ages of the reflectors from

Eocene-Miocene, which are tied to the exploration wells in the study area. Since these seismic horizons were used for basin structural description and fault throw analysis, detailed interpretation of the horizons around the footwalls and hanging walls was carried out. Isochron maps of four stratigraphic intervals have been generated to observe the stratigraphic thickness variation around the boundary faults (**Figure 20**).

a. Top Early Miocene

b. Top Oligocene

c. Lower Oligocene
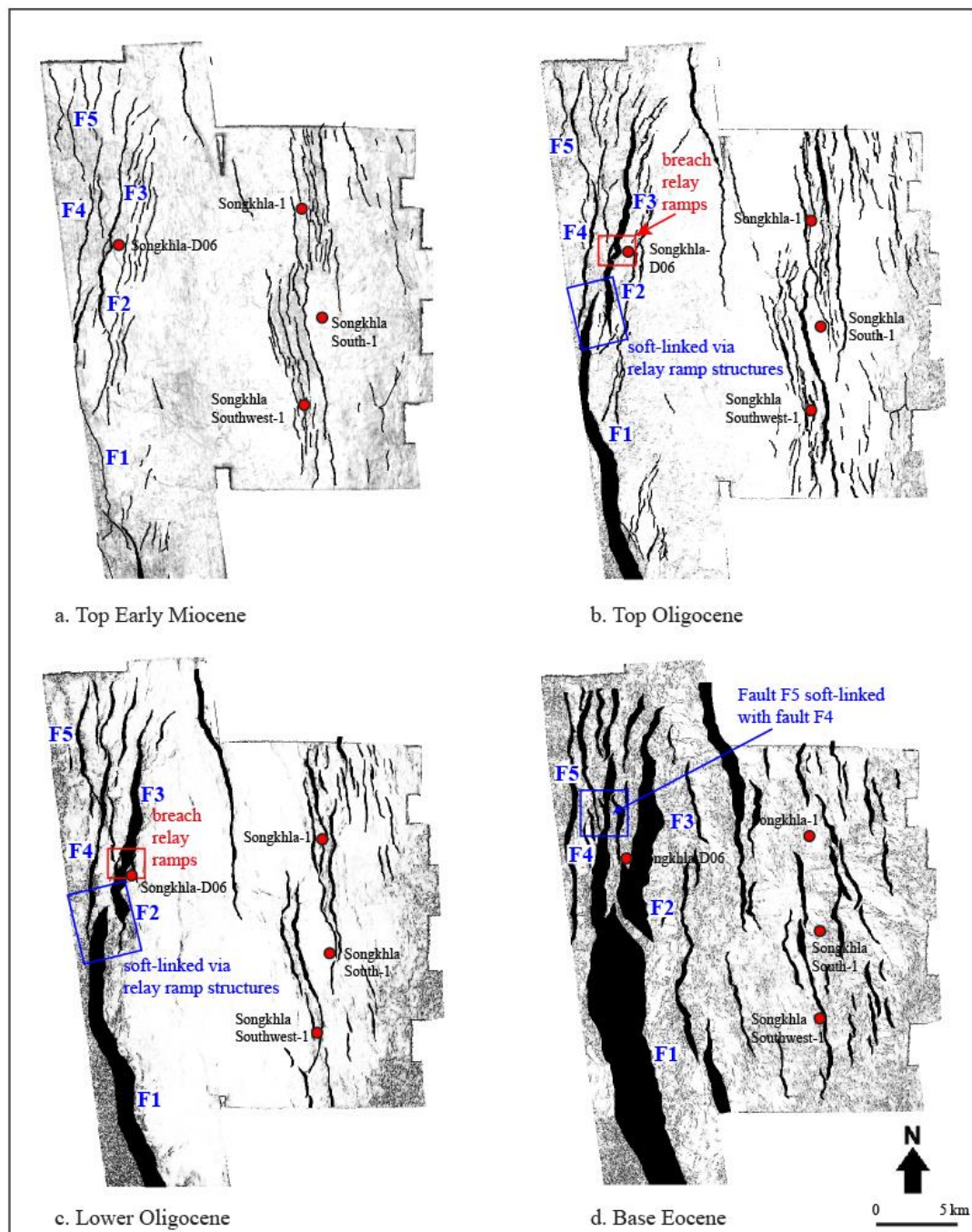
d. Base Eocene

Figure 19 Structural maps and location of five wells on the consistence dip attribute of the four major mapped horizons showing: soft linkage via relay ramps between F1-F2 and F4-F5 are shown on the (a) Base Eocene and (b) Lower Oligocene structural maps; hard linkage at breached relay ramps of F2-F3 are shown for the (c) Top Oligocene and the (d) Top Early Miocene structural maps.

d. Top Early-Miocene-Top Middle Miocene

c. Top Oligocene-Top Early-Miocene

b. Lower Oligocene-Top Oligocene

a. Base Eocene-Lower Oligocene
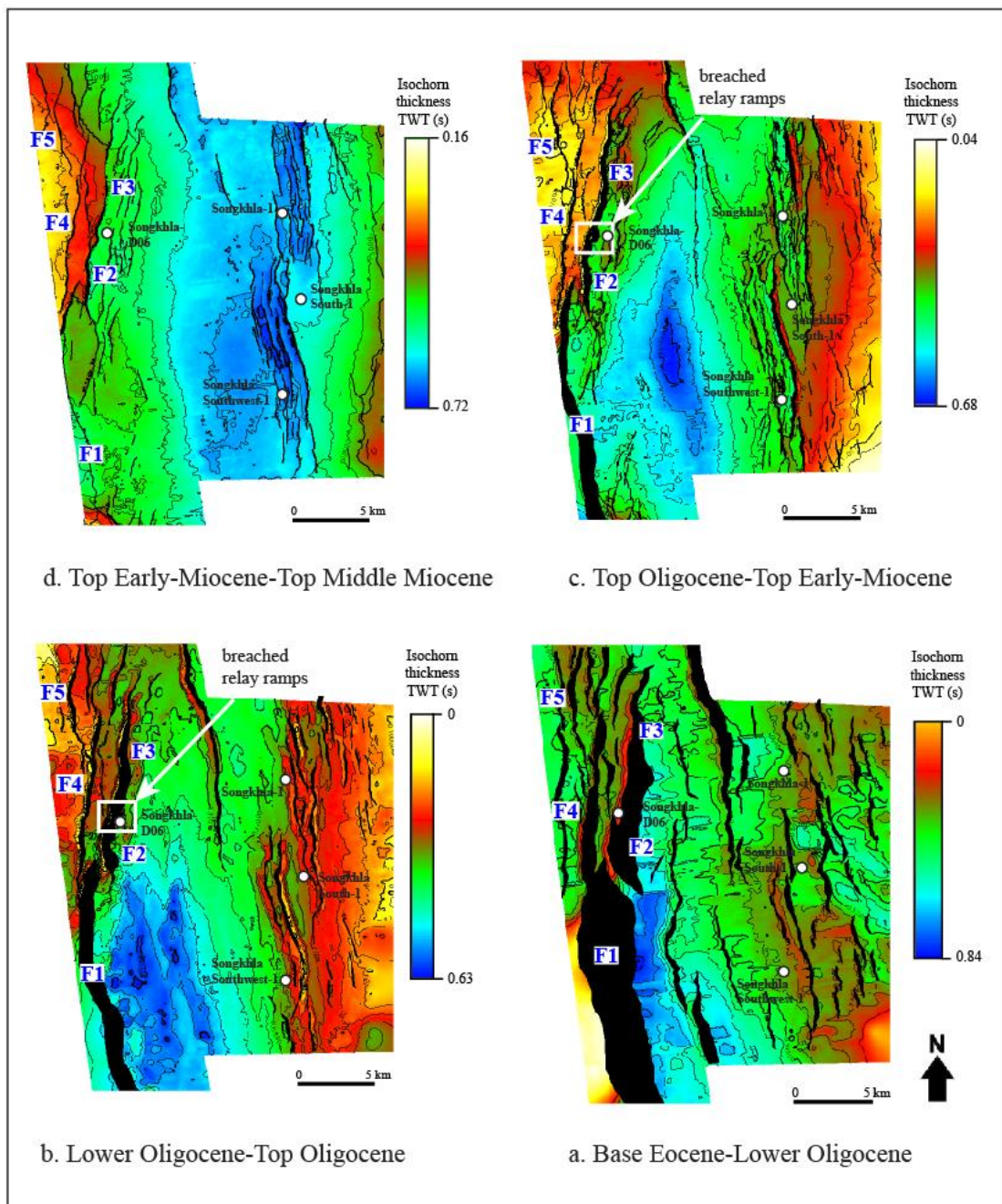
Figure 20 Isochron maps illustrate the vertical thickness changes for four intervals and the changing depocentre location from Eocene to Miocene times. (a) Base Eocene- Lower Oligocene isochron map shows the main depocenter of a basin is located adjacent to the major boundary faults. In (b) Lower Oligocene-Top Oligocene isochron map, (c) Top Oligocene-Top Early-Miocene isochron map and (d) Top Early Miocene-Top Middle Miocene isochron map, the depocentre shifts progressively towards the middle of the basin with time.

4.3   Fault Geometry and throw patterns

A series of normal faults, which form segments of the half graben bounding fault, are developed on the western basin margin. They dip eastwards and strike N-S to NNE-SSW (**Figure 16**). The boundary fault zone is predominantly extensional, but underwent weak inversion after extension ceased, in the Middle Miocene (Morley and Racey, 2011; Kaewkor et al., 2015). The major boundary fault segments are slightly listric in profile, and are steeper toward the northern part of Songkhla Basin. The highest observed throws occur at the Eocene horizon (base syn-rift) (**Figure 16**). There is syn-sedimentary thickening of the Eocene-Early Miocene sequences towards the bounding faults, and early-stage tilted fault blocks that affect the Eocene section (**Figure 16**; **Figure 17**). Smaller tilted synthetic faults are developed in the middle part of the basin.

The faults forming the major syn-sedimentary boundary fault zone (F1 to F5) in the study area were chosen for detailed analysis due to their coverage by 3D seismic data (**Figure 19** and **Figure 20**). These faults tend to converge downwards either within the lower part of the Cenozoic section or possibly in the pre-Cenozoic section (**Figure 16**), but commonly exhibit soft-linked geometries, in particular relay ramp structures, in the horizons mapped in this study (**Figure 19 (b)** and **(c)**). The east dipping, N-S trending F1 is the largest fault in the study area (**Figure 19** and **Figure 20**). It is located in the south and dominates the southern half of the basin. The southern tip of this fault lies outside of the study area, within the study area it is 19 km long. F1 is slightly listric in profile. The northern part of F1 overlaps via relay ramps with F4 in the west, and F2

in the east (**Figure 19**). Expansion of section towards F1 is clearest for the Base Eocene-Lower Oligocene and Lower Oligocene-Top Oligocene intervals (**Figure 16**). The Top Oligocene-Top Early Miocene section expands towards F1, but then starts to thin towards the boundary fault within about 5 km from the fault. This thinning towards the boundary fault is strongest in the Early Miocene interval. The thinning can in part be related to Miocene inversion, and in part to the post-rift subsidence depocentre shifting to a position eastwards of the earlier fault-controlled depocenter.

As shown in **Figure 21** and **Figure 22**, the throw-length plots for F1 show that the Eocene horizon (base syn-rift) has the highest throw, which is relatively uniform (about 1.2-1.5 s) for approximately 16 km of its length. Then, in the northern 3 km, the fault rapidly loses throw to zero. Throw is less in higher horizons, and for the Top Early Miocene maximum throw is around ~0.2 s.

The throw lost by F1 to the north passes predominately onto F2/F3 and F4 (**Figure 21** and **Figure 22**). F2/F3 are connected via a breached relay ramp (**Figure 19**). Their throw patterns for the Oligocene-Eocene intervals indicate that the throw decrease on segments F2 and F3 towards the linkage point but do not die out, whereas for the Top Early Miocene horizon, the throw goes to zero approaching the linkage point (**Figure 21**). In the overlap zone with F1, the throw at the Eocene horizon level decreases from around ~1 s to zero over 3 km. F4 displays a slightly asymmetric throw profile, with the throw dying out more rapidly towards the south, than towards the north (**Figure 22 (d)**). In about 2.5 km of overlap between F4 and F1, the throw at the Eocene horizon level for F4 decreases from around ~0.5 s TWT to zero.

As shown in **Figure 22 (e)**, F5 shows a gradual increase in throw towards the north, and there are four peaks in throw along the Eocene horizon, which suggests the fault probably was linked from four earlier faults that were initially separated in the Eocene. The throw is low compared with the other faults forming the boundary fault zone. For the Top Early Miocene horizon, the throw is very low.

a. Structural map on the Top Oligocene horizon

b. Throw distribution on the major boundary fault plane, F1-F5

c. Throw-length profile of Top Early Miocene horizon

d. Throw-length profile of Top Oligocene horizon

e. Throw-length profile of Lower Oligocene horizon

f. Throw-length profile of Base Eocene horizon
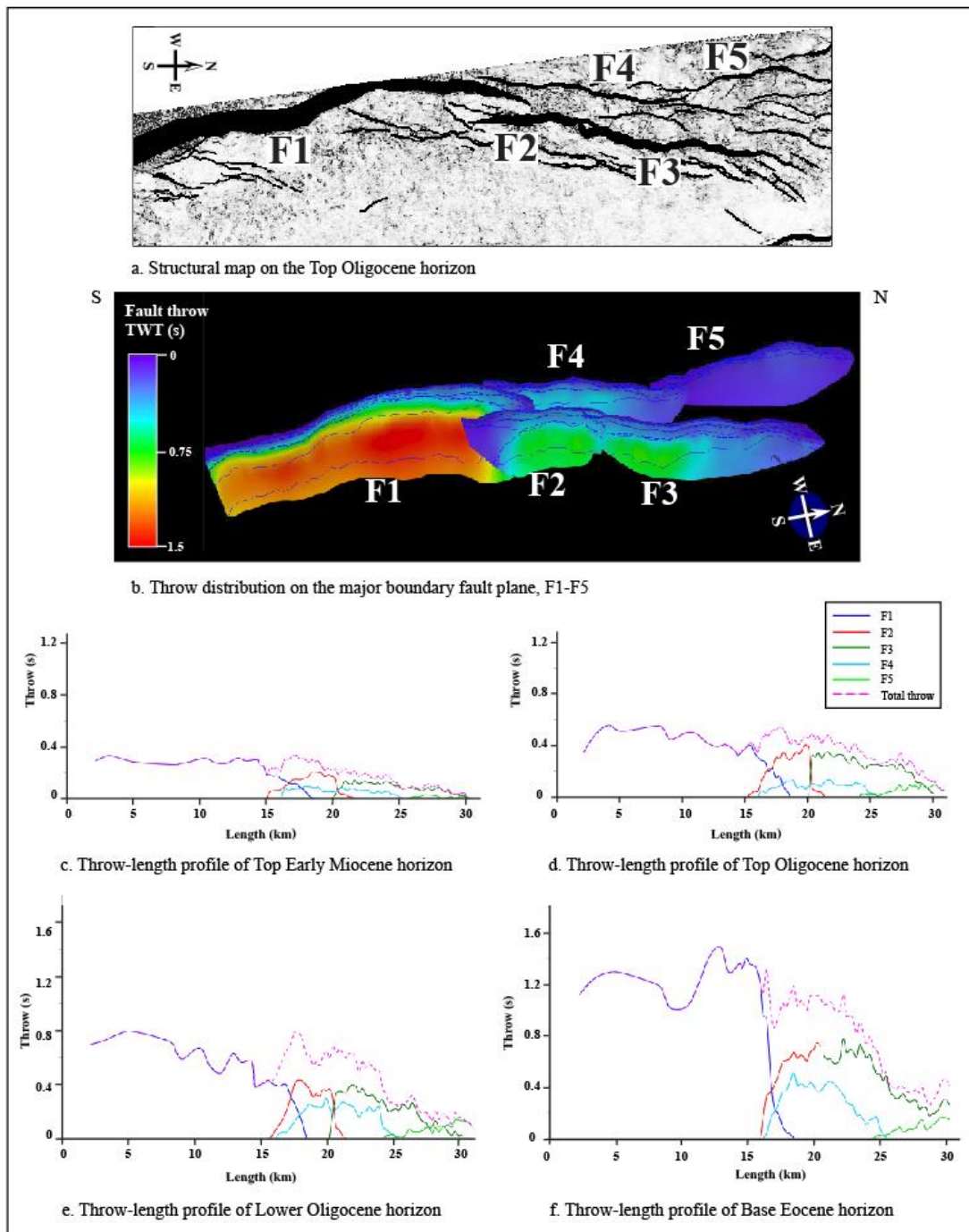
Figure 21 (a) Fault polygons for F1-F5 on the Top Oligocene horizon time structural map. (b) Three-dimensional view of the major boundary fault surface with the throw distribution on the fault planes. (c)–(f) Throw-length profiles of faults F1-F5 for four horizons from Eocene to Miocene.

a. F1

b. F2

c. F3

d. F4

e. F5

| Lower Oligocene horizon | Top Early Miocene horizon | Footwall Base Eocene horizon |
| Base Eocene horizon | Top Oligocene horizon | Hanging wall Base Eocene horizon |
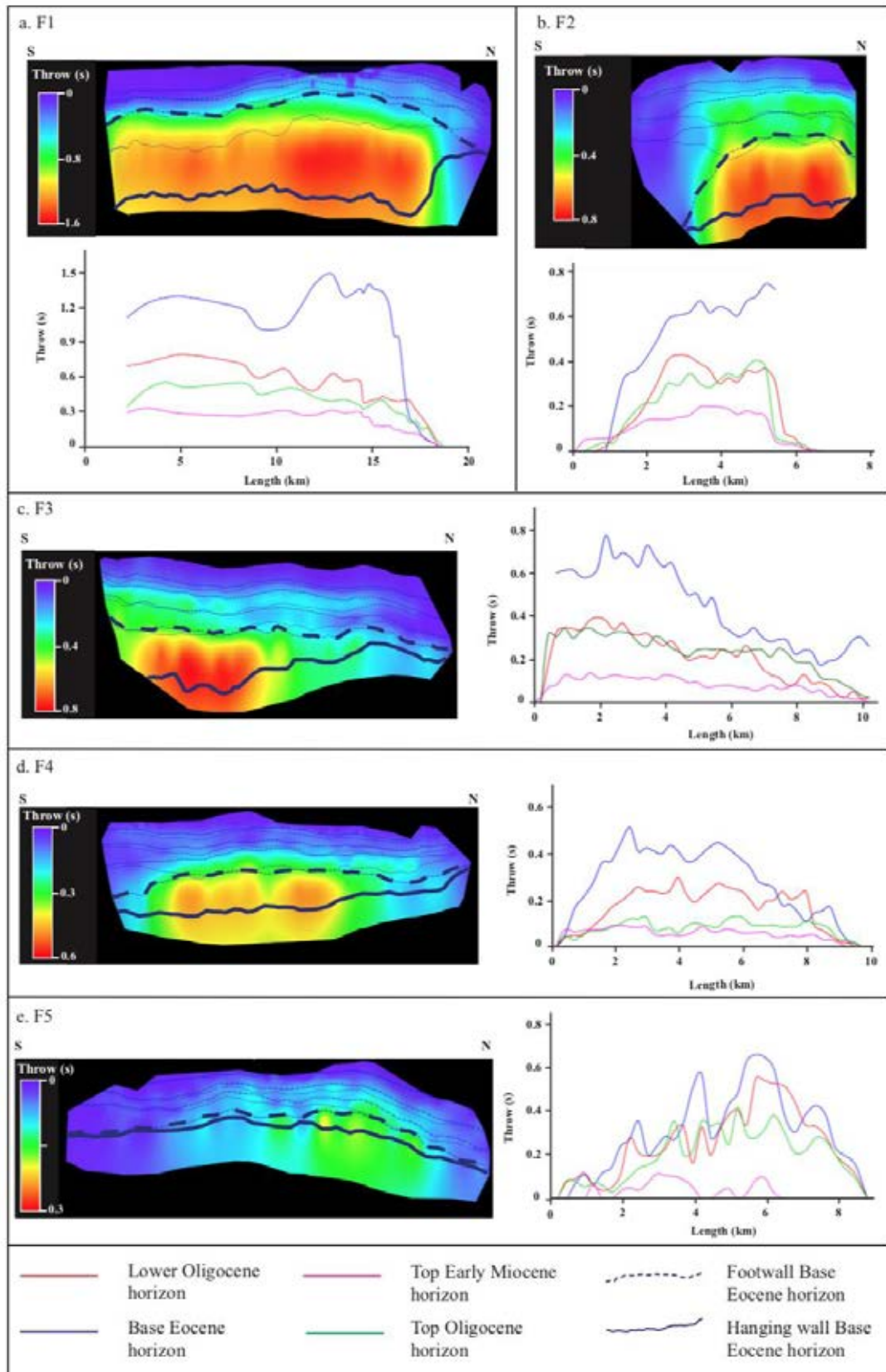
Figure 22 (a)–(e) Throw distribution on the fault surface, view towards the fault surface, and the throw-length profiles of F1-F5 showing variations in throw from the southern to northern tips.

4.4 Discussion

4.4.1 Songkhla Fault Model

Relatively large faults, whose growth can be measured from variations in sediment thickness (i.e. with displacements of 10's to 1000's of metres), have been shown in many studies to display a variety of displacement and linkage patterns (e.g. Walsh and Watterson, 1988; Cartwright et al., 1996; Morley, 1999; Morley, 2016; Mansfield and Cartwright, 2001; Walsh et al., 2002; Childs et al., 2003). The simplest model for fault growth is the isolated model, where with increasing displacement, the fault undergoes symmetric lateral propagation growth (e.g. Walsh and Watterson, 1988; Cartwright et al., 1996; Morley, 1999; Mansfield and Cartwright, 2001; Childs et al., 2003). There is a close relationship between fault displacement and fault length in the isolated model, where an increase in displacement is accompanied by a proportional increase in fault length (**Figure 23 (a)**). Commonly the ratio of the fault length to displacement ranges between 10:1 to 20:1 (e.g. Scholz and Cowie, 1990; Marrett and Allmendinger, 1991; Walsh and Watterson, 1991; Needham et al., 1996).

Another common pattern occurs when after linkage of several faults, and the displacement fails to relocate to the middle of the newly created fault zone. This can occur because the sites of linkage remain relatively strong regions and inhibit slip propagation into the linkage zones (e.g. Cartwright et al., 1996; Morley, 1999; **Figure 23 (b)**). When faults link, there is an abrupt jump in fault length, causing a decrease in the fault length to displacement ratio. The linkage development that most closely follows the isolated fault model occurs when two or more faults join and the displacement value for the newly joined fault is relatively low. Then as displacement builds, the lateral propagation of the fault is stalled. Upon the displacement value approaching typical length-displacement ratios for isolated faults, lateral fault propagation is likely to resume. Generally, faults are likely to develop through a number

of cycles of linkage until reaching their final length. In the isolated fault model, faults behave independently so where two faults overlap, and their displacement values are summed, displacement may decrease in the region of overlap. This displacement deficit is a characteristic of isolated fault arrays (Walsh et al., 2002).

As an alternative to the isolated fault model, a fault can approach its final length very early in its displacement history (constant length model) when linkage occurs on many small faults, hence typically little syn-kinematic sedimentary record is preserved (**Figure 23 (c)**). Then, most of the fault displacement is built after the fault length has been established (Morley, 1999; Walsh et al., 2002). Consequently, during much of the life of the fault it is relatively under-displaced with respect to length. Jackson et al. (2016) concluded that the constant length model is a common feature of large extensional faults. This type of development is part of the coherent fault model (Walsh et al., 2002). The coherent fault model typical displays low, or no displacement deficits in the areas of overlapping faults (Walsh et al., 2002).
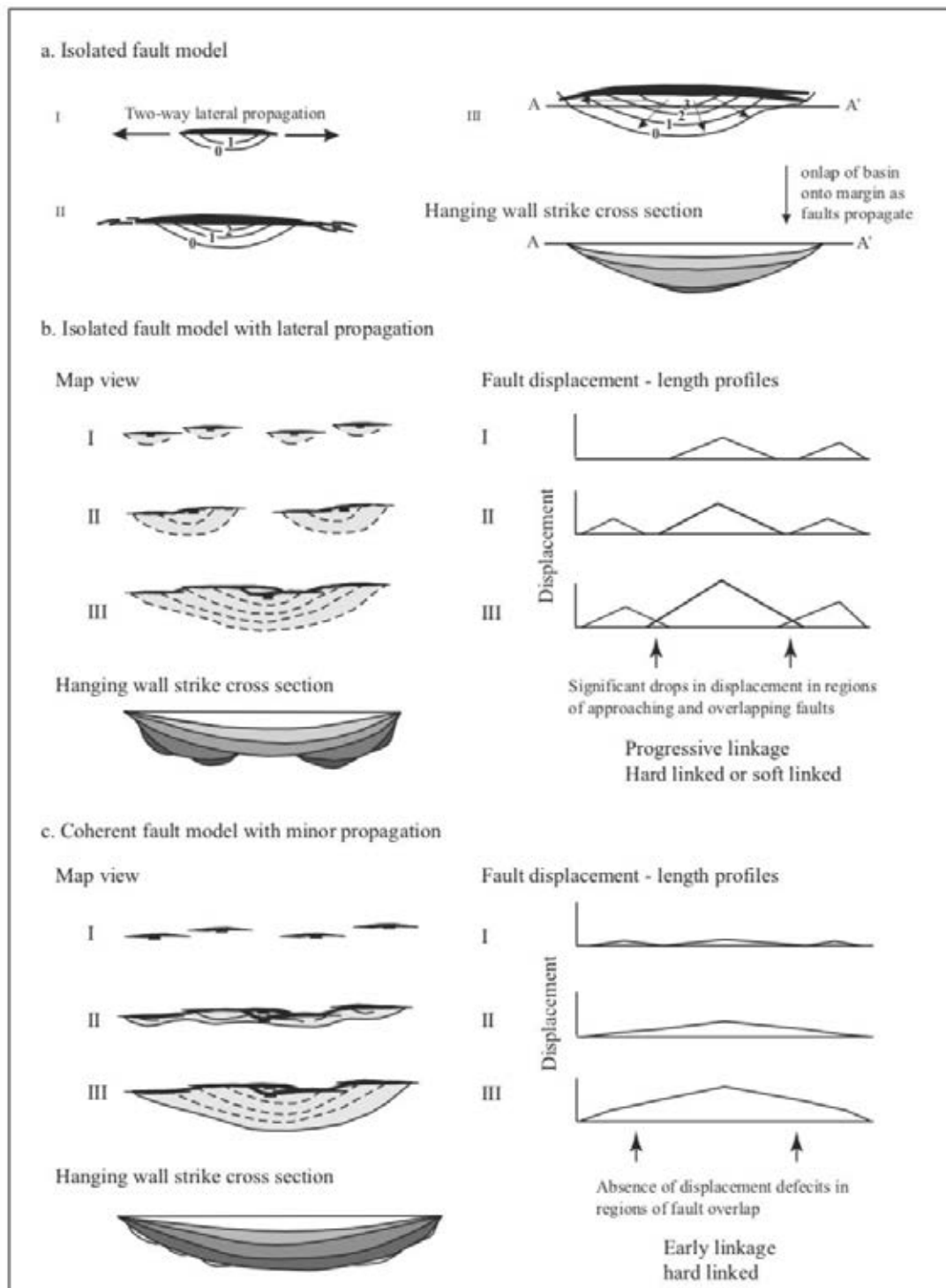
Figure 23 Schematic illustration of how fault systems may develop in relationship with the development of the fault displacement and fault length. (a) Isolated fault model. (b) Isolated fault model with lateral propagation. (c) Coherent fault model with early linkage (following Morley, 2016).

The Songkhla Basin bounding fault zone has remained segmented throughout its throw history with the four largest fault segments (F1, F2/F3, F4 and F5) plus other minor faults showing soft linkage geometries from the Oligocene to the Miocene horizons (**Figure 19**). The fault zone has been at least episodically active for around 25-30 My. At the level of the Base Eocene horizon, F1, F2/F3 and F4 are hard linked while F5 is soft linked (**Figure 19 (d)**). F1 shows strong asymmetry of throw-length plots into the transfer zone between F1, F2 and F4, with throw decreasing more rapidly with distance in the overlap zone to the north, compared with the loss of throw to the south (**Figure 21**). Throw patterns for the Eocene horizon show total throw across the five faults decreases towards the north, and they behave as a single fault (i.e. the throw pattern followed a coherent fault model, **Figure 23 (c)**). In the Songkhla Basin, the boundary fault system is a complex zone whose throw characteristics for the Eocene suggest rapid fault growth and linkage during the Eocene from numerous segments (**Figure 24 (a)**). During the later part of the Eocene, although many of the faults became hard linked, some soft linked segments remained, but overall the throw along these faults followed the coherent model.

For the Oligocene-Miocene horizons at around the 15-20 km and to lesser degree at the 22-26 km regions of fault length along strike (**Figure 21 (d)** and **(e)**) there is a decrease in throw indicating that when the fault was reactivated later in its history the throw patterns started to switch to an isolated fault model (**Figure 23 (b)**). Extension was accommodated on the existing faults without forcing further propagation and linkage. Probably this reflects the effects of lower strain rates during the waning stages of extensional activity in the region.
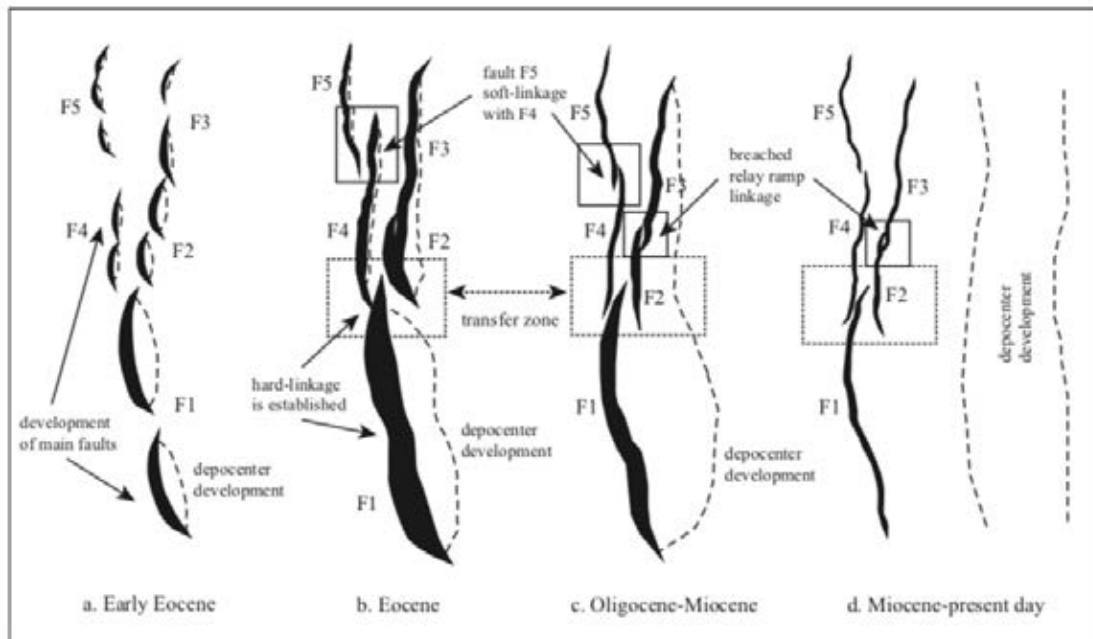
Figure 24 Schematic illustration of the evolution of major boundary faults in Songkhla
Basin. (a) The small fault segments developed and propagated during the
early rifting stage in the Early Eocene. (b) Fault segments propagated and
hard linked to form larger boundary faults (F1-F5) in the Eocene, except F5
and F4 and F2 and F1 show soft linkage. (c) The boundary faults continue
to grow by accumulating displacement with minimal lateral propagation due
to the relatively low extensional activity during the Oligocene-Miocene. (d)
Fault pattern near the top of the fault system, where extensional activity was
low. Extension ended in the Early Middle Miocene. Dashed line indicates
extent of main depocentre.

4.4.2 Structural Controls on Sedimentation in Songkhla Rift Basin

The timing and degree of fault interaction and linkage exert significant impact
on syn-rift stratigraphy as it controls the sedimentary input sites, types and distribution
of sediment transported to a basin throughout rift basin evolution (e.g. Cowie et al.,
2006). When an extensional basin is initiated, small isolated depressions are developed
(e.g. Cowie et al., 2000). These depressions with relatively little accommodation space
are typically initially dominated by predominantly coarse, immature, continental

deposits and marginal marine deposits (e.g. Lambiase and Bosworth, 1995; Gawthorpe and Leeder, 2000; Jackson, 2008), although they can transition upwards into more argillaceous- dominated sequences in a relatively short stratigraphic interval (< 100 m).

The throw-length analysis indicates most of the major boundary faults in Songkhla Basin have early linkage. The early linkage of the F1 boundary fault controlled the size and geometries of the main depocenter, especially during the Eocene – Oligocene. At this early stage of linkage, where faults are relatively short (< 15 km), modern geomorphology studies from the Basin and Range suggest that the majority of fluvial systems run down relay ramps parallel to fault strike, but the relationship seems to break down for longer fault lengths (Hopkins and Dawers, 2017). Greater accommodation space was created when isolated faults coalesced. Based on the stratigraphic interpretation of Songkhla Basin exploration wells, the depositional environment was mainly alluvial and fluvial. Once faults began to link, the drainage systems coming in from the hangingwall margin would have started to be re-arranged as a result of increased displacement, footwall uplift and hangingwall subsidence. This marks the time when the depositional environment in the hangingwall evolved from alluvial and fluvial environments to a lacustrine one. The way drainage adapts to changing boundary fault morphology depends on diverse factors such as fault spacing, orientation, segmentation and footwall lithology (Leeder and Jackson, 1993; Gawthorpe and Hurst, 1993; Duffy et al., 2015). The tectonostratigraphic development during this time of transition towards the establishment of a major boundary fault is generally complex compared to the rift climax as discussed by Jackson et al. (2006).

Regionally, the Cenozoic rift basins in Thailand display very different characteristics (see reviews in Morley et al., 2001; Morley 2015, 2016; Sautter et al., 2017): in northern Thailand, there was alternation of inversion with extension during the Miocene at least on three separate times, before strike-slip deformation becomes dominant in the Plio- Pleistocene). In central Thailand, there is evidence for rotation of the extension direction from E-W to NE-SW during the Miocene, as well as episodic inversion. In the Andaman Sea, rifting evolves from E-W extension to NNW-SSE transtension with time. While in the southern and eastern part of GOT, rifting begins in the Eocene and ends in the Oligocene- Miocene boundary. The rifting timing is earlier

than in the northern GOT and onshore areas. In the Andaman Sea, there is also northwards younging of the onset of rifting. There is also considerable influence of pre-existing fabrics on fault and basin morphology (Morley et al., 2004). Given this great diversity of behavior, the structural style and development of each sedimentary basin needs to be evaluated to understand the distribution of possible causes of these different effects.

The development of the Songkhla Basin is relatively straightforward in comparison with some rift basins in Thailand. However, in building the regional picture, this is significant information, and can serve as a near end member example (relatively simple extensional history), when comparing the behavior of different boundary fault zones within the rift system.

CHAPTER V

QUANTITATIVE INTERPRETATION OF SEISMIC ATTRIBUTES FOR RESERVOIR CHARACTERIZATION

5.1 Introduction

Fluvial reservoirs are the major hydrocarbon reservoirs in the GOT, which were deposited throughout the syn-rift and post-rift periods, ranging from Oligocene to Miocene sequences. In general, the sands deposited in fluvial depositional systems have complex lateral and vertical geometries and distributions as they contain a series of point bars, overbank deposits, and sand- or mud-filled abandonment channels (Ahmad and Rowell, 2014; Jardine, E., 1997; Lockheart et al., 1997). Regarding this complexity, it is necessary to understand the factors controlling the reservoirs deposition and distribution.

To image the distributions of subsurface reservoirs within the Songkhla Basin, several seismic attributes have been applied in this study. The analysis of seismic attributes such as root mean square (RMS), acoustic impedance, spectral decomposition, and similarity can delineate the subtle structural and stratigraphic from the ordinary seismic amplitude data allow us to define the structure and depositional environment (Chopra and Marfurt, 2005). The purposes of this study are to determining the reservoir distribution, depositional environment, and their relation to the structural evolution.

The main parts of this study have been accepted for publication by the Marine and Petroleum Geology Journal under the title *"Quantitative interpretation of seismic attributes for reservoir characterization of Early-Middle Miocene syn- and post-rift successions (Songkhla Basin, Gulf of Thailand)".*

5.2   Seismic database and methodology

The SEG-Y format 3D time-migrated seismic reflection survey consists of 1940 inlines and 3104 crosslines, with inline spacing of 12.5 meters (m) and crossline spacing of 12.5 meters covering a total area of 700 km2 within the Songkhla basin. The seismic data are zero phase and normal polarity (SEG convention), where an increase in acoustic impedance is displayed as a positive amplitude (black peaks) in the seismic cross section.

The focus of this 3D seismic study is from the late syn-rift in the Early Miocene to post rift phase one (I) in the Middle Miocene, 0.2-1.5 second two-way time (TWT) in Sequences 3 and 4 of **Figure 25**. The faults and three key horizons (S1-late Early Miocene, S2-top Early Miocene, and S8-top Late Miocene) were interpreted and mapped throughout the 3D full stack seismic reflection data. The results were used to extract various seismic attributes. In order to map the variations in vertical reservoir distribution and seismic geomorphology, additional strata slices were generated with reference to the three key horizons. The strata slices are proportional subdivisions of the interval between two horizons. Due to the low-amplitude discontinuous reflectors caused by low acoustic impedance contrast of sands and shales and the structural complexity of western boundary faults, it was extremely difficult to interpret chrono-stratigraphic surfaces, and phantom horizons were generated to aid the interpretation.
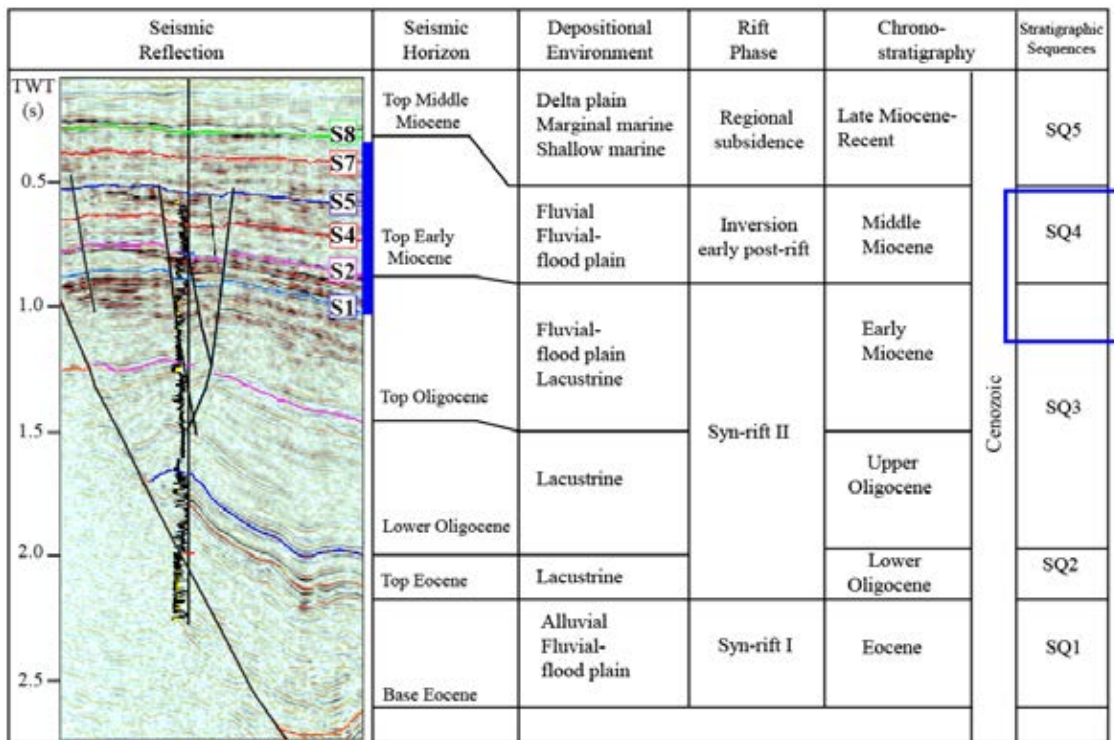
Figure 25 Stratigraphy of the Songkhla Basin tied to an example of 3D seismic reflection data and the gamma ray log of the representative well with the study interval in the blue block.
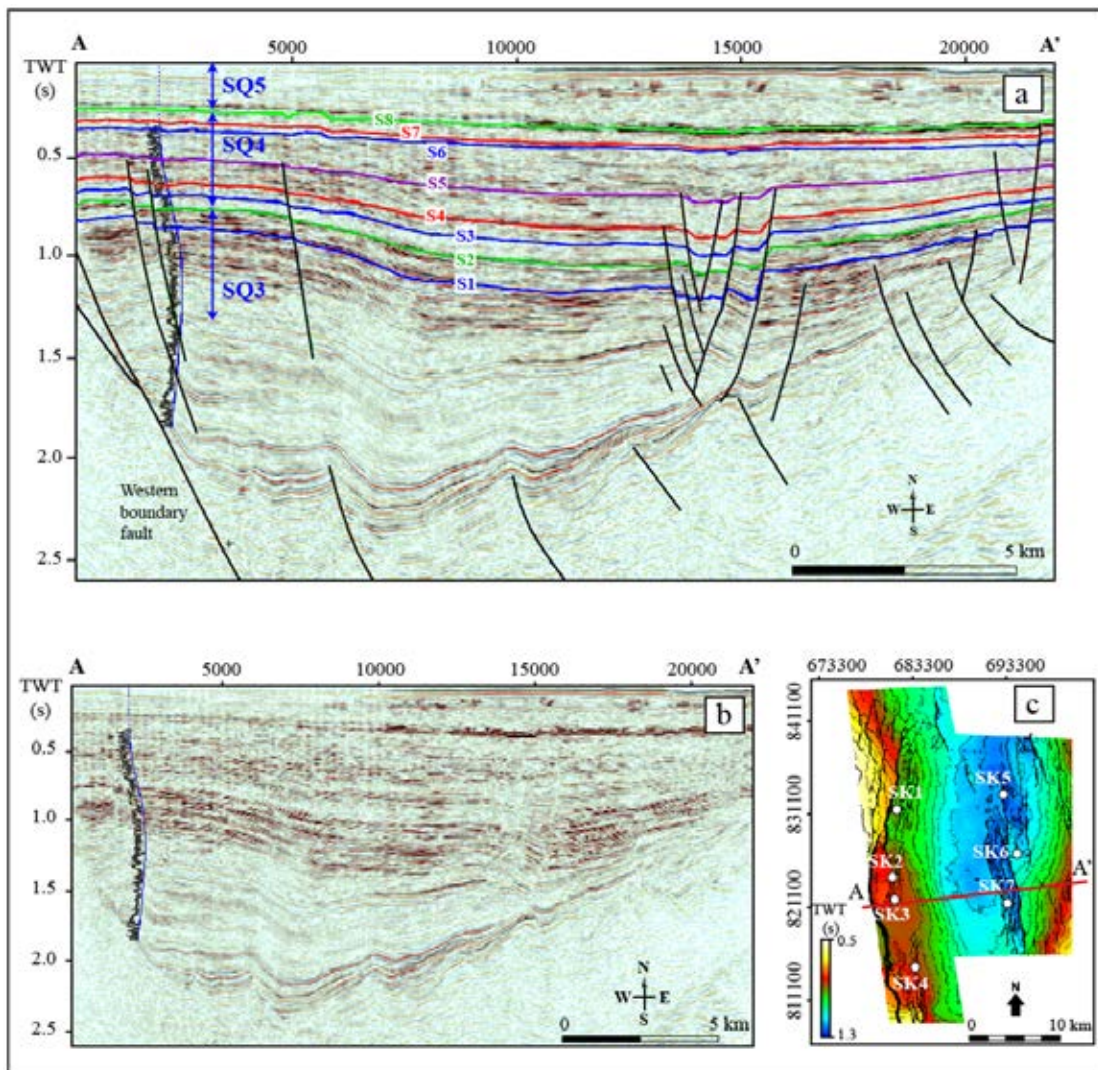
Figure 26 (a) Seismic cross section line AA' displays eight (8) selected horizons, S1-S8 in relation to the stratigraphic sequences of Songkhla Basin, sequence 3-5 (SQ3-SQ5) and the gamma ray log of the representative well. (b) Un-interpreted seismic cross section. (c) Time structural map on S1 horizon, late Early Miocene, displays seismic cross section line AA' location

Rock physics analysis and seismic attribute analysis are the two main techniques applied to this study after traditional seismic interpretation (structural and horizon mapping) was completed for the basin. Rock physics analysis was applied to establish the link between seismic amplitudes to geological facies and reservoir properties (e.g. Goodway et al., 1997; Connolly, 1999; see review in Bacon and Simm, 2014). P-wave

velocity (Vp or primary wave), S-wave velocity (Vs or secondary wave), density (□), and acoustic impedance (AI) were derived from well log data at well locations to determine rock properties that can be used to discriminate lithology, sands and shales. The cluster separation of these parameters on cross plots was used to identify lithological facies. If the separation of facies using AI cross-plots at well log scale is poor, then such facies discrimination at the seismic scale is also likely to be poor.

Seismic attributes are very useful for the structural interpretation and reservoir characterization apart from the traditional seismic interpretation. Good seismic attributes are directly sensitive to the changes in seismic impedance and allow structure and depositional environments to be defined (Brown, 2004; Chopra and Marfurt, 2005). In this study, a series of different seismic attributes were extracted along the interpreted horizons to aid the structural interpretation, reservoir distribution identification and their related meaningful geological features. The seismic attributes successfully used in this study were similarity, root mean square (RMS), and spectral decomposition. All these attributes were compared with the GR logs at blind test well locations to check the relationship between attributes and the reservoir zones.

Similarity and coherency, are computed based on changes in wave trace shape or both amplitude and shape, and are useful attributes for imaging subtle faults and the edges of fluvial channels and reefs (Bahorich, 1995; Marfurt et al., 1999; Ahmad and Rowell, 2012; Ahmad et al., 2014; Ghosh et al., 2014). In this study, the similarity attribute was extracted from horizons of interest in the syn-rift interval using IHS Kingdom 2014 (**Figure 27**). The attribute revealed low to moderate sinuosity, parallel, dark lines (non-similarity) set in broad white/light grey color zones of high similarity that mainly coincide with the main depocenter located in the south-western part of the study area (**Figure 27 (a)**). These sinuous features are associated with low amplitude channel-like features, surrounded by high amplitudes in vertical seismic sections, interpreted as mud filled channels (**Figure 27 (c)**). Therefore, the sinuous features are interpreted as channel edges. **Figure 27** shows the relationship of the similarity with the RMS attributes extracted from S1 horizon, and the seismic amplitudes in cross sections. Similarity maps can be integrated with the RMS and spectral decomposition attributes to provide more accuracy when mapping the reservoir distributions.

Root Mean Square (RMS) is a statistical measurement of the magnitude of amplitude variations over a data set by computing the square root of the sum of squared amplitudes divided by the number of samples within the specific window interval. RMS is very sensitive to amplitude variations, therefore, it emphasizes the variations in acoustic impedance in the selected window. A change of AI is assumed to be mainly due to a lithology change. Commonly, the higher the acoustic impedance variation, the higher the RMS values will be.
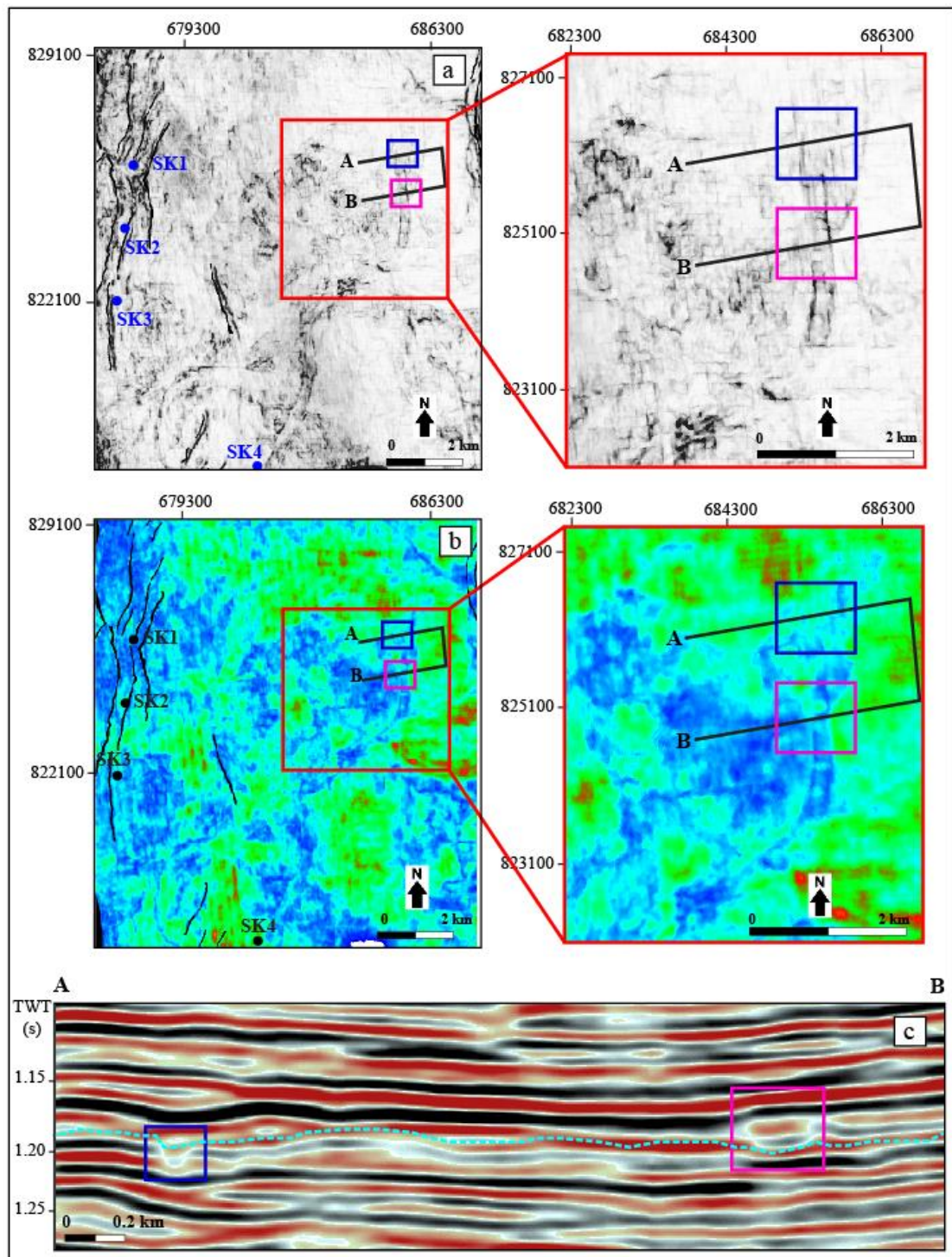
Figure 27 Examples of sinuous features associated with the S1 interval. (a) Similarity map shows channel-like boundaries. (b) RMS map displays sand distribution with channel-like features. (c) Vertical seismic amplitudes section along line AB shows low amplitudes channel features surrounded by high amplitudes that are interpreted as mud-filled channels. These

channels are located at A and B, their edges are well seen on the similarity map, (a).

The RMS attributes extracted from the interpreted major horizons in the study area displayed meaningful geological features, channel-liked patterns and reservoir distribution, throughout the interval of interest of the late syn-rift and post-rift phase I, where high amplitude contrasts are present. High RMS values on maps correspond to the sands at well locations, as confirmed by the blind test wells that penetrated high amplitude areas (**Figure 28 (a)**, **(b)**, **(c)**). The late syn-rift section exhibits good images of channel-like features in the southern part of the basin (**Figure 28 (a)**, **(b)**), while for post-rift phase I (**Figure 28 (c)**), good images of reservoir distribution are present in the middle and northeastern parts of the basin.

Spectral decomposition (SD) attributes are generated by the transformation of a seismogram (seismic signal) to a frequency domain of the seismic bandwidth (Partika et al., 1999; Brown, 2004). Spectral decomposition can provide highly detailed images of the reservoir related to subtle changes in bed thickness (Payton et al., 1998; Laughlin et al., 2002; Liu and Marfurt, 2007; Matos et al., 2005). Bed thickness can be mapped and geological discontinuities within the seismic survey are identified by breaking down the seismic signal into its' component frequencies (Partika et al., 1999; Marfurt and Kirlin, 2001; Sinha et al., 2005). In this study, 3D seismic data were transformed into iso-frequency domains using discrete fourier transforms (DFT) by applying the SD Trace Sub-band method (SD) in the short window range of 20-40 ms. The RMS amplitude spectra extracted from selected iso-frequency SD volumes display scattered anomalies along faults and unfaulted zones in the study area. Different sand thicknesses show the highest amplitude spectra at different frequencies ranging between 20 Hz – 80 Hz. The interval of interest has a tuning thickness of 25 meters at 25 Hz frequency. The 40 and 63 Hz frequencies offer the best imaging of channels (**Figure 29**). The RGB (red-green-blue) blending techniques were applied to the multiple frequencies to display different meaningful geological features detected by different frequencies. Frequencies of 20, 40, and 63 Hz were chosen for the RGB (red-green-blue) color blending.
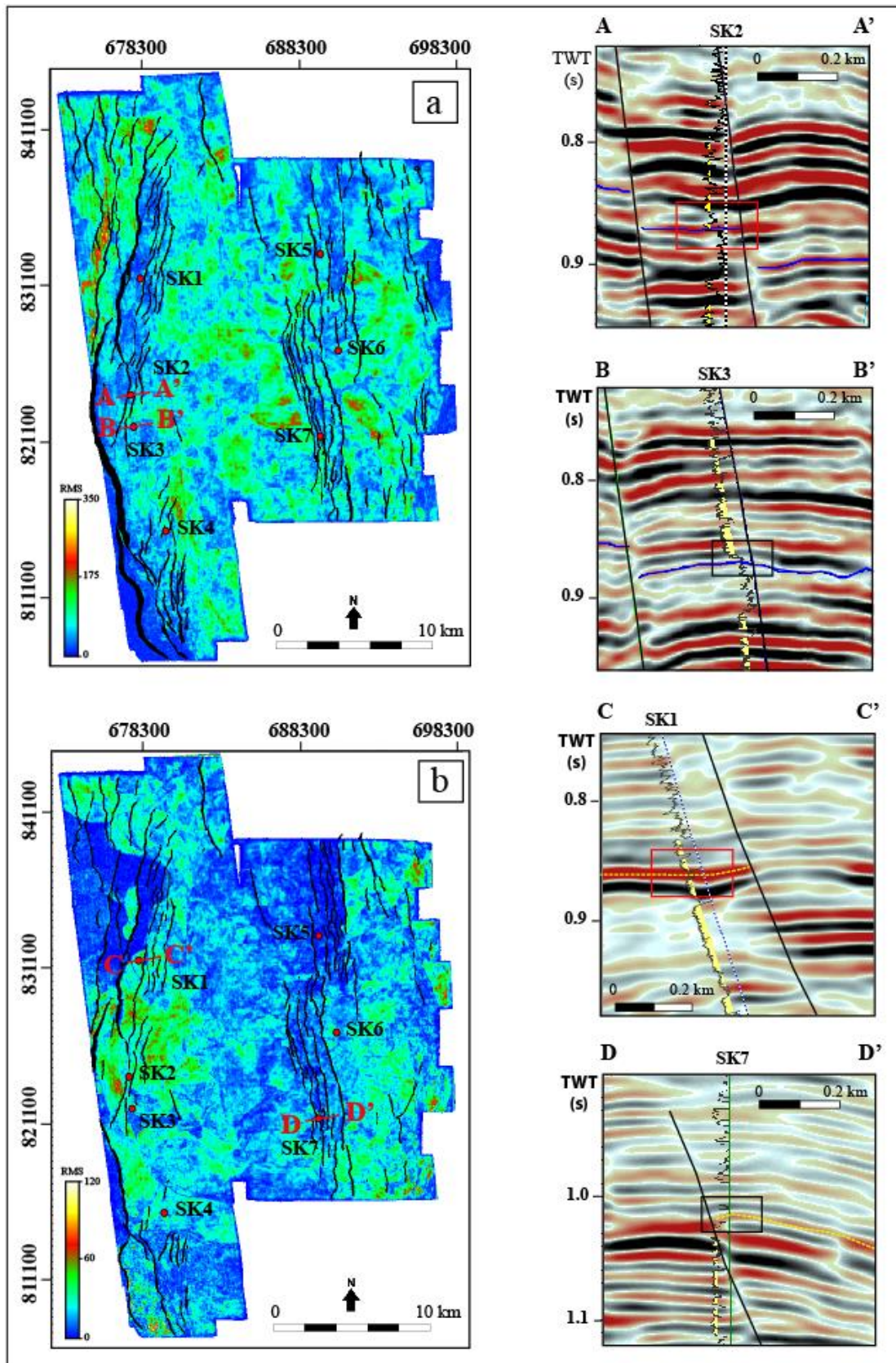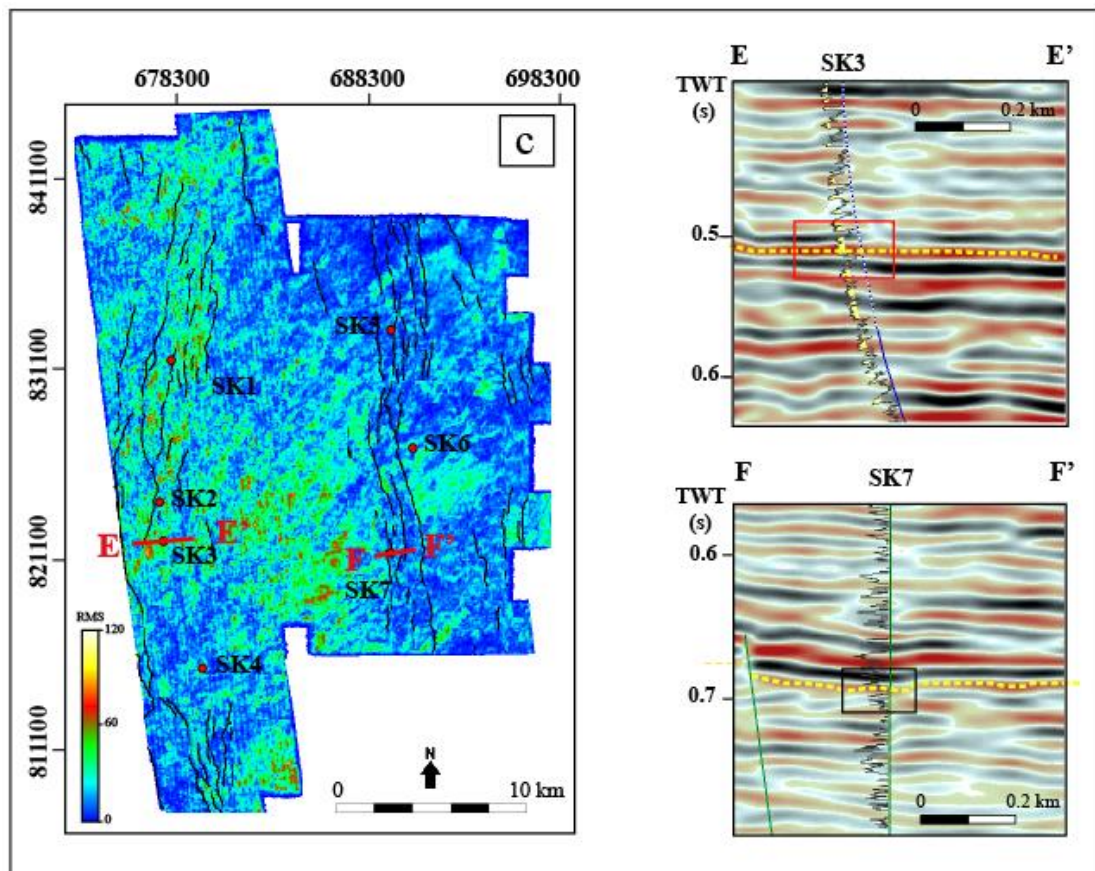
Figure 28 The relationship of the RMS maps, seismic amplitudes, and the lithology interpreted from gamma ray log characteristics at well locations on S1, S2, and S4 horizons (a) S1 RMS amplitude map (b) S2 RMS amplitude map (c) S4 RMS amplitude map: cross sections AA', CC', and EE' showing high RMS values, warm colors, correspond to sands at well locations and high amplitude contrasts in the seismic reflection data, where cross sections BB', DD', and FF' showing low RMS values, cold colors, correspond to shales at well locations with low amplitude contrasts in seismic reflection data. (add). SK1, SK2, SK3, SK7 are wells with gamma ray log with the GR scale of 0-300 API (left-right).
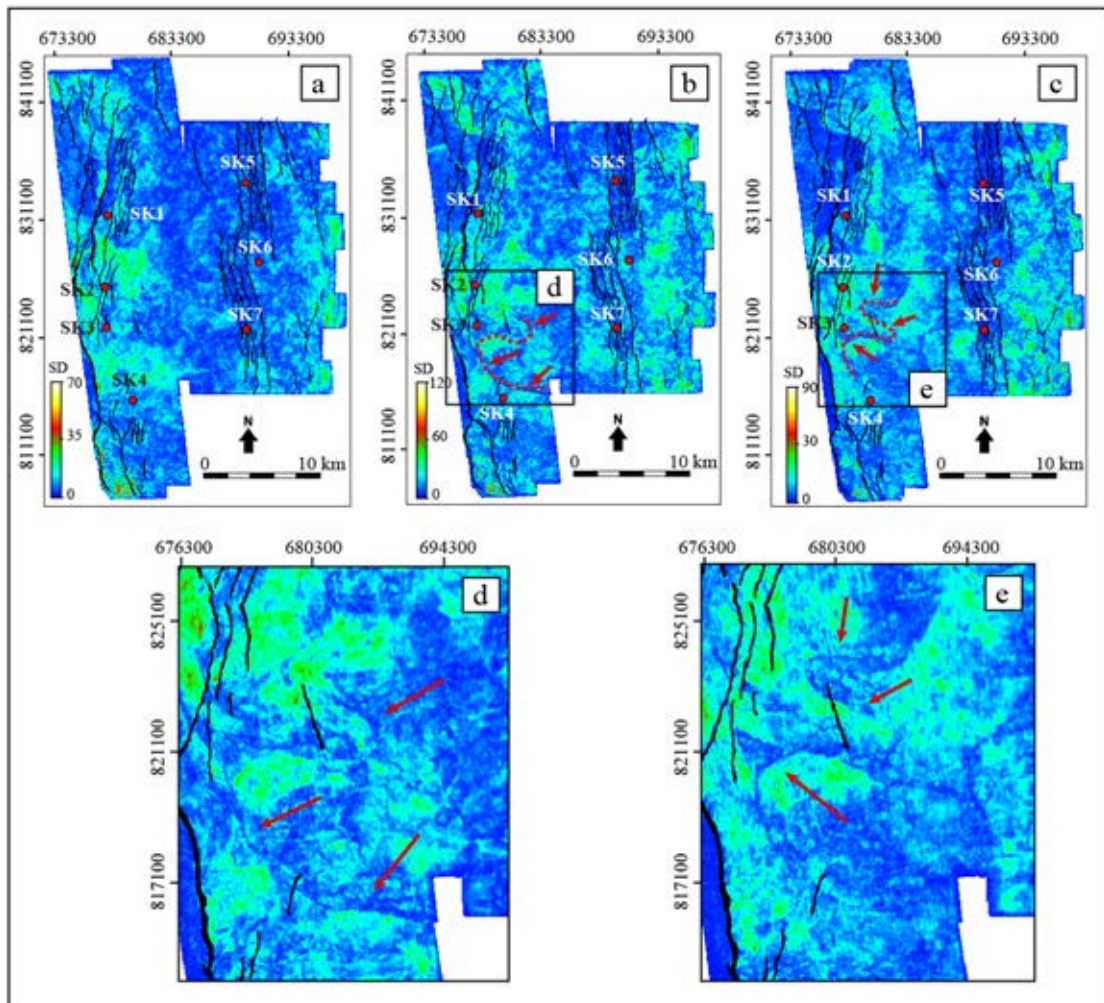
Figure 29 Example of SD Trace Sub-band of S2 horizon at 20 Hz (a), 40 Hz (b), and
63 Hz (c). These frequencies displayed the best channel images compare to
other frequencies. In (b) and (c) different parts of channels are highlighted
by the red dotted line with the red arrows. (d) and (e) displayed zoom-ins of
un-interpreted channel-liked features from b) and c).

5.3 Rock physics analysis

The cross-plots of rock physics parameters (density, P-wave velocity, P-
impedance) versus depth with respect to shale volume are shown in **Figure 30 (a)** to
(c). The results from a few key wells, where the data and the interpretation are most
integrated and reliable, indicate that generally the density trends of sand and shale
increases with depth, where overall sands are of lower density than shales in the both

late syn-rift (upper Early Miocene) and post-rift (Middle Miocene) sections. Density increases with depth and follows similar trends to velocity and acoustic impedance (**Figure 30 (a)**, **(b)**, **(c)**). However, a number of tight sands in the syn-rift section show high density, velocities, and acoustic impedance, similar to shale. Therefore, P-impedance can be used to discriminate sands and shale in the shallow post-rift sequence from 1000-2300 feet (0.3-0.5 s TWT). While in the syn-rift, impedance cannot be used to differentiate tight sands and shale.
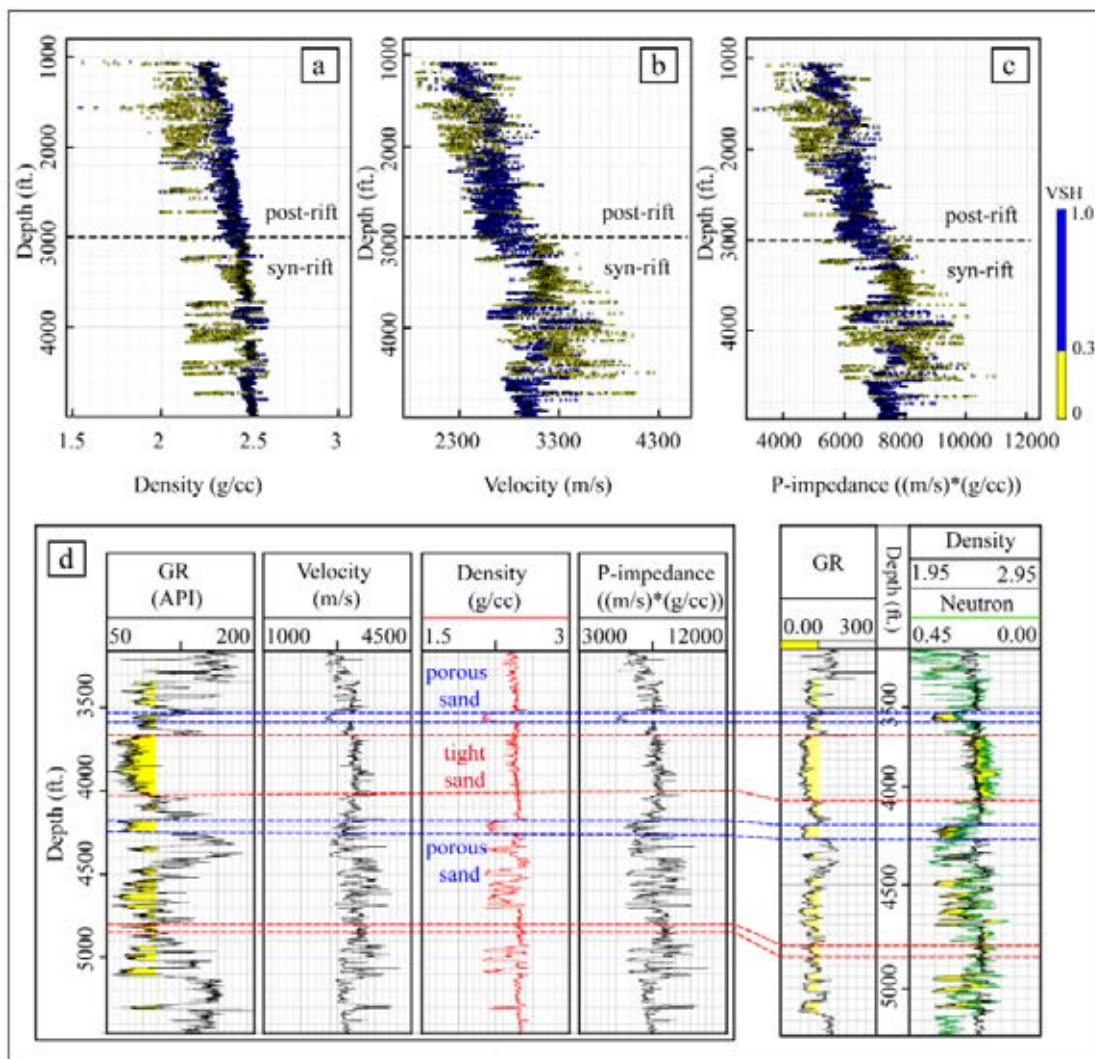
Figure 30 Cross-plots of (a) Density (b) Velocity (c) P-impedance against depth (ft. TVDSS) with respect to shale volume at well SK1. (d) Correlation analysis between gamma ray (GR), velocity, density, P-impedance and density and neutron crossover show the relationship of the tight and porous sand at well SK1 in the late syn-rift interval (S1-S2).

5.4   Seismic attributes analysis – Findings

5.5.1   S1 Horizon (Early Miocene)

S1 is the lowermost horizon of the upper Early Miocene syn-rift phase II interval (**Figure 26 (a)**), where meaningful geological features were readily imaged and analyzed (channel-liked features and reservoir distribution). The calculated RMS on the S1 horizon displays scattered high amplitude anomalies all over the study area, especially in the eastern and southern parts of the basin, with the overall N-S trend similar to that of the major western boundary fault zone. These high RMS anomalies are associated with sands, while low RMS values are associated with shale at well locations (**Figure 28 (a)**). The RMS map of the S1 horizon lacks clear images of channel-like features (**Figure 31 (a)**), but instead shows possible oxbow lake features in the southern part of the basin. Clearer images of channels and oxbow lakes were displayed on the SD volume at 40 Hz (**Figure 31 (b)**), while the channel boundaries are well-defined on the similarity volume (**Figure 31 (c)**), especially in the main depocenter, while the eastern and north-eastern areas display dim-images of channel edges.

Overlay of the RMS and similarity maps provides a good image of the channel shapes (**Figure 31 (d)**). While the RGB blending of three different frequencies (20, 40, and 63 Hz) from spectral decomposition provides better images of channel geometries compared to other attributes (**Figure 31 (e)**) as it combines together the different channels delineated in different frequencies. **Figure 31 (f)** illustrates the interpretation of channels and abandoned oxbow lakes. Integration of the RMS, similarity, and spectral decomposition shows that the channels in the S1 horizon have low to medium sinuosity, 1.2 sinuosity index (SI), especially in the main depocenter, where the channels follow NNW-SSE to N-S directions that correspond with the main fault strike directions. These channels are relatively wide (300-400 meters). The gamma ray (GR) log characteristics from the representative wells at this horizon show sands forming mainly blocky patterns, with some fining upwards patterns (**Figure 32**). Biostratigraphic data (pollen and spores, including Magnastriatites) from the delineation wells suggest the dominance of the fluvial depositional environment with

no evidence of lakes. Channels developed in this period are interpreted as meandering channels developed in a channel complex.
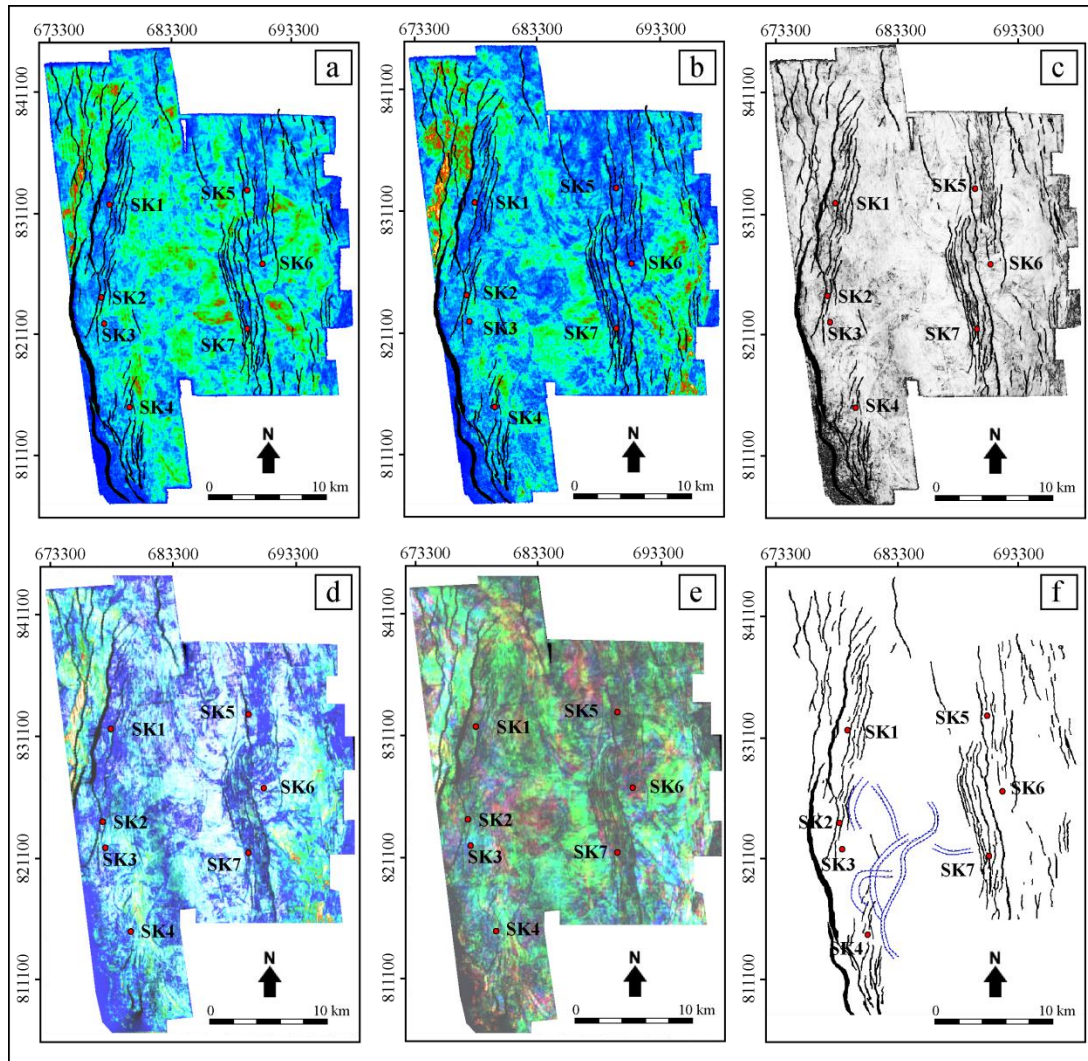
Figure 31 Comparison of extracted attributes for the S1 horizon (a) RMS amplitude map (b) SD Trace Sub-band at 40 Hz map (c) similarity map, which delineated different geological features. (d) The overlay of RMS and similarity helps confirm channel boundaries. (e) RGB blending of SD 20, 40, and 63 display better image of channels. (f) Interpretation of the channels and abandoned oxbow lakes.
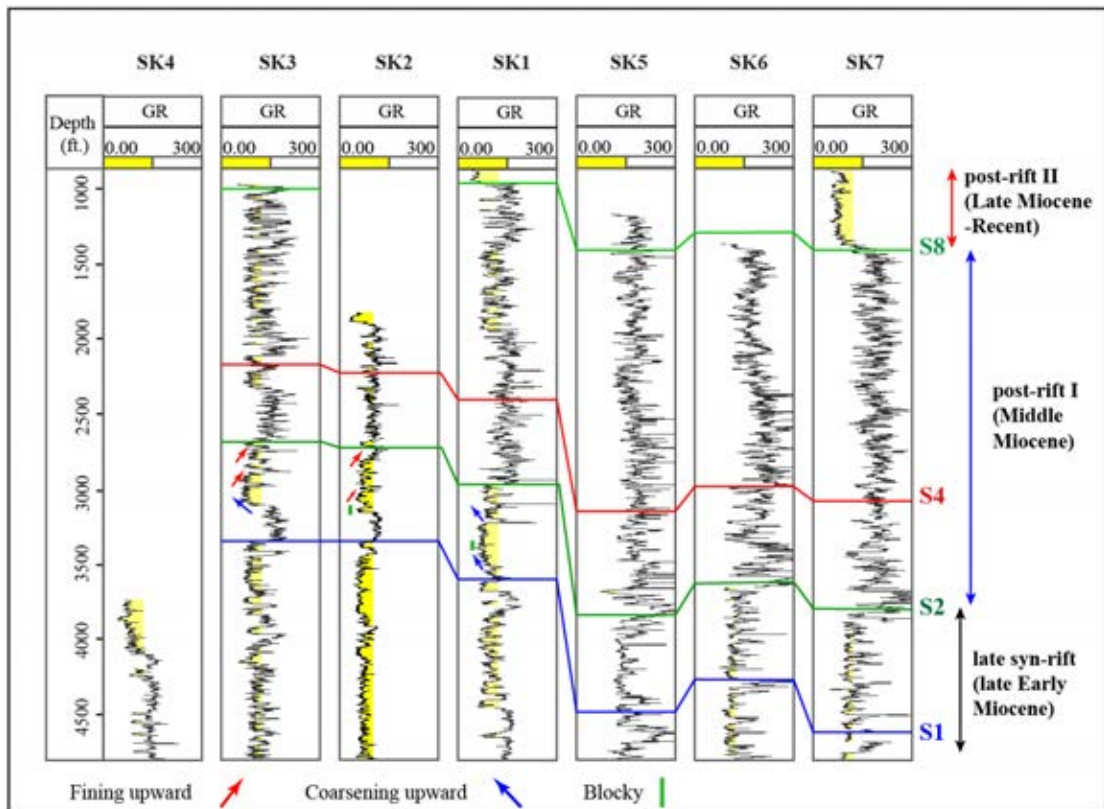
Figure 32 West to east well correlation panel during late syn-rift to post-rift. The overall gamma log pattern displays sand prone in syn-rift and more shalely lithology toward post-rift I and to the east of a basin.

5.5.2   S2 Horizon (Early Miocene)

S2 is the uppermost horizon of Early Miocene syn-rift phase II. High RMS amplitudes were observed in the western areas along the major boundary faults, especially in the main depocenter located in the southern half of a basin (**Figure 33 (a)**, **Figure 34 (a)**). The high RMS amplitude extractions are associated with sand deposits confirmed by the correlation of the high RMS values with the sandstone interval in representative wells (**Figure 28 (b)**). Although the channel-like features could not be imaged on RMS data, meaningful geological features, i.e. shape of pointbar accretion are presented (**Figure 34 (a)**). The integration with similarity data provides better images of channels as the channel edges are displayed as parallel, narrow black lines of low similarity (**Figure 34 (b)**). The correlated features on the vertical seismic sections

reveal channel-like patterns with both high amplitude sand filled-channel and low amplitude mud filled-channels (**Figure 34 (c)**).
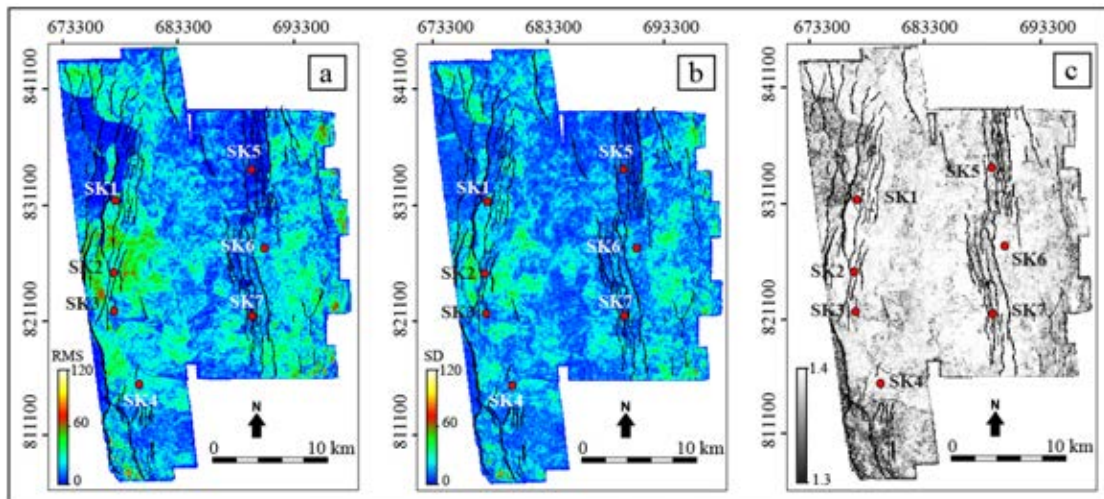
Figure 33 The extracted attribute maps for the S2 horizon displayed channel-like features in the main depocenter, south-western part, adjacent to major western boundary faults on the RMS map (a), SD 40 Hz map (b), and the channel edges on the similarity map (c).

The shapes of the channels were better imaged by high SD frequencies (iso-frequencies of 40 and 63 Hz). The observation shows that at 40 Hz frequency the southern channel is better displayed (**Figure 35 (a)**), while at 63 Hz frequency the northern channel is better displayed (**Figure 35 (b)**). The RGB visualization technique helped to combine these channels at different frequencies together (**Figure 35 (c)**).
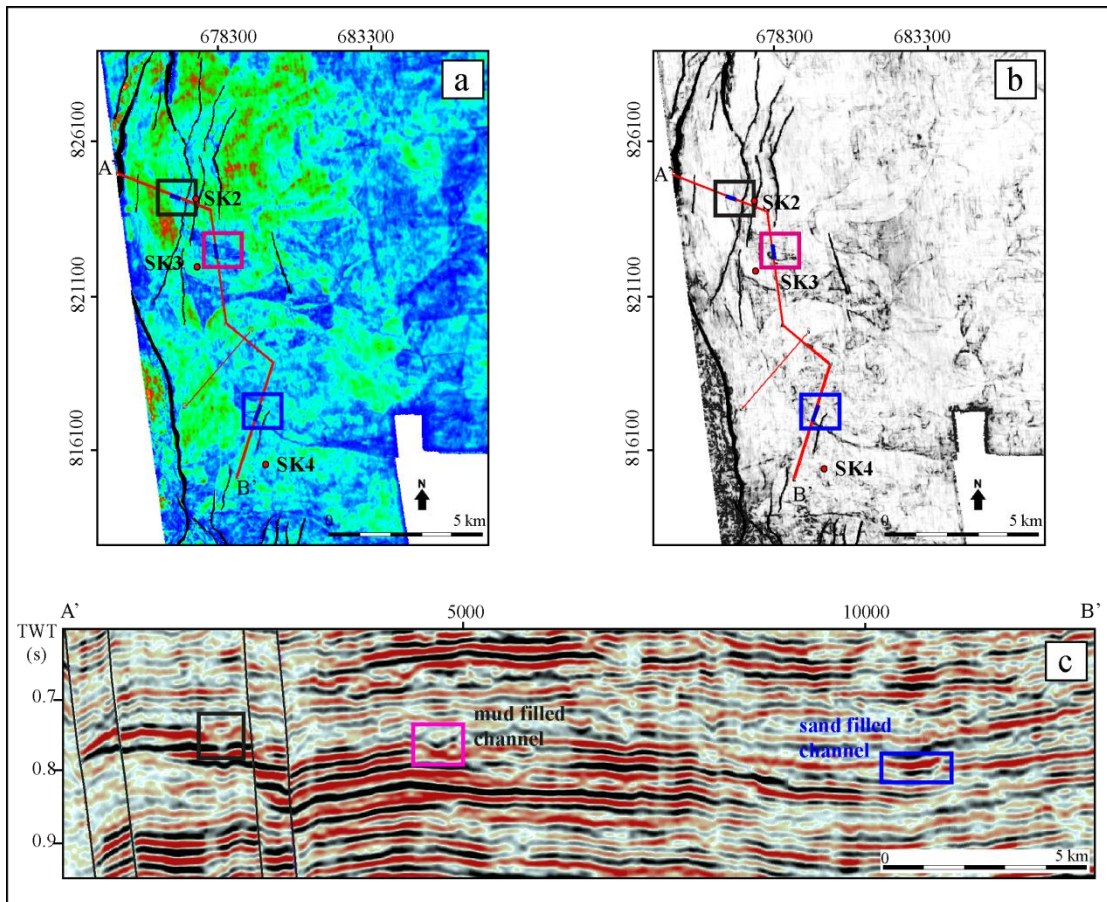
Figure 34 The relationship of the channel-like features on the RMS map (a), the channel edges on the similarity map (b), and the sand-and mud-filled channels in the seismic cross section (c).
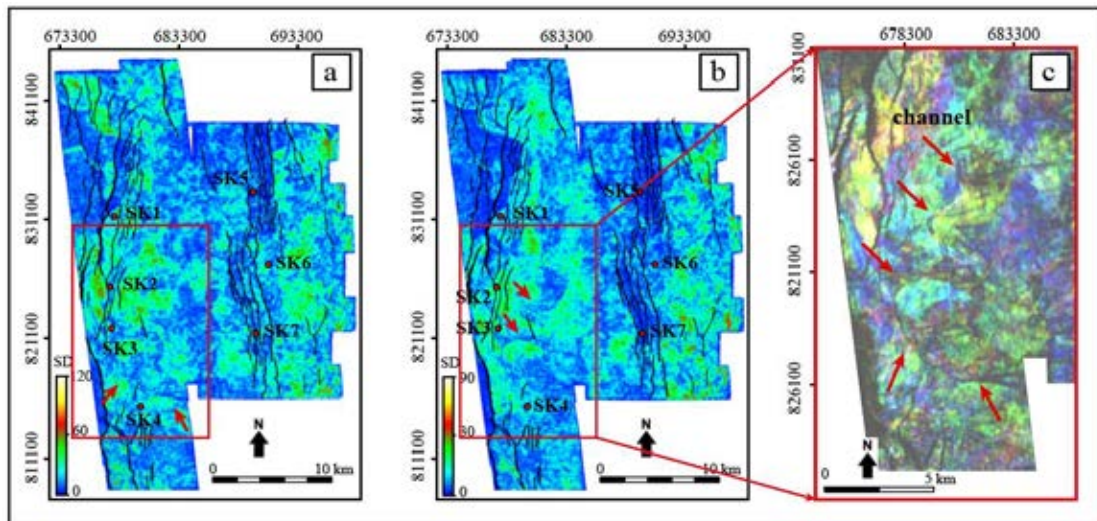
Figure 35 SD and RGB maps of S2 horizon (a) SD Trace Sub-band 40 Hz displays the southern part of a channel. (b) SD Trace Sub-band 63 Hz displays the northern part of channel. (c) The RGB blending of SD Trace Sub-band 20, 40, 63 Hz combines the two channels present in different frequencies.

S2 period channels are slightly wider (400-500 m) compared with the S1 period (300-400 m), with high sinuosity (SI = 1.8) and follow the N-S to NE-SW strike of the western boundary fault zone. The gamma ray log from well locations shows the horizon has mostly sandstone, but with more shale compared to horizon S1, with a variety of log patterns i.e. fining upward, blocky, and coarsening upward (**Figure 32**). Integration of all attributes indicates the channels are meandering.

5.5.3 S3-S4 Horizon (lower Middle Miocene: early post-rift phase I)

S3 is the deepest horizon of the Middle Miocene post-rift phase I. The RMS amplitude map displays scattered high RMS anomalies, mainly in the southwestern area (main depocenter-along major boundary faults), and in the eastern part of the basin (**Figure 36 (a)**). These high amplitude anomalies are associated with sands at well locations (**Figure 28 (c)**). Images of small, channel-liked features were observed in two areas: 1) the northwestern area along the western boundary faults, where channels with a N-S trend follow the strike of the western boundary fault zone, and 2) in the middle part of

the basin where channels trend NE-SW, slightly oblique to the boundary fault strike. Similarity on horizons S3 and S4 did not image the small channel edges probably due to resolution issues.

The geometries and orientations of the small channels are better imaged for the S4 horizon than S3 (**Figure 36 (b)**). The channels trend NE-SW, and are mainly developed in the middle part of the basin. The GR logs between horizons S3 and S4 show mainly high GR values, indicating sediments are mostly shale (**Figure 32**) compare to the higher sand content for the syn-rift phase II. Unpublished biostratigraphic data from the final well reports show the palynomorphs recovered (spores and pollen) were mainly fresh water at SK2 and SK4 wells and mangroves (Spinizonocolpites and Zonocostites) from the SK5-SK7 wells. These data indicate that during the early Middle Miocene (S3-S4 horizons), the basin was dominantly freshwater, especially in the southwestern area, while the eastern part experienced the onset of episodes of marine influence.
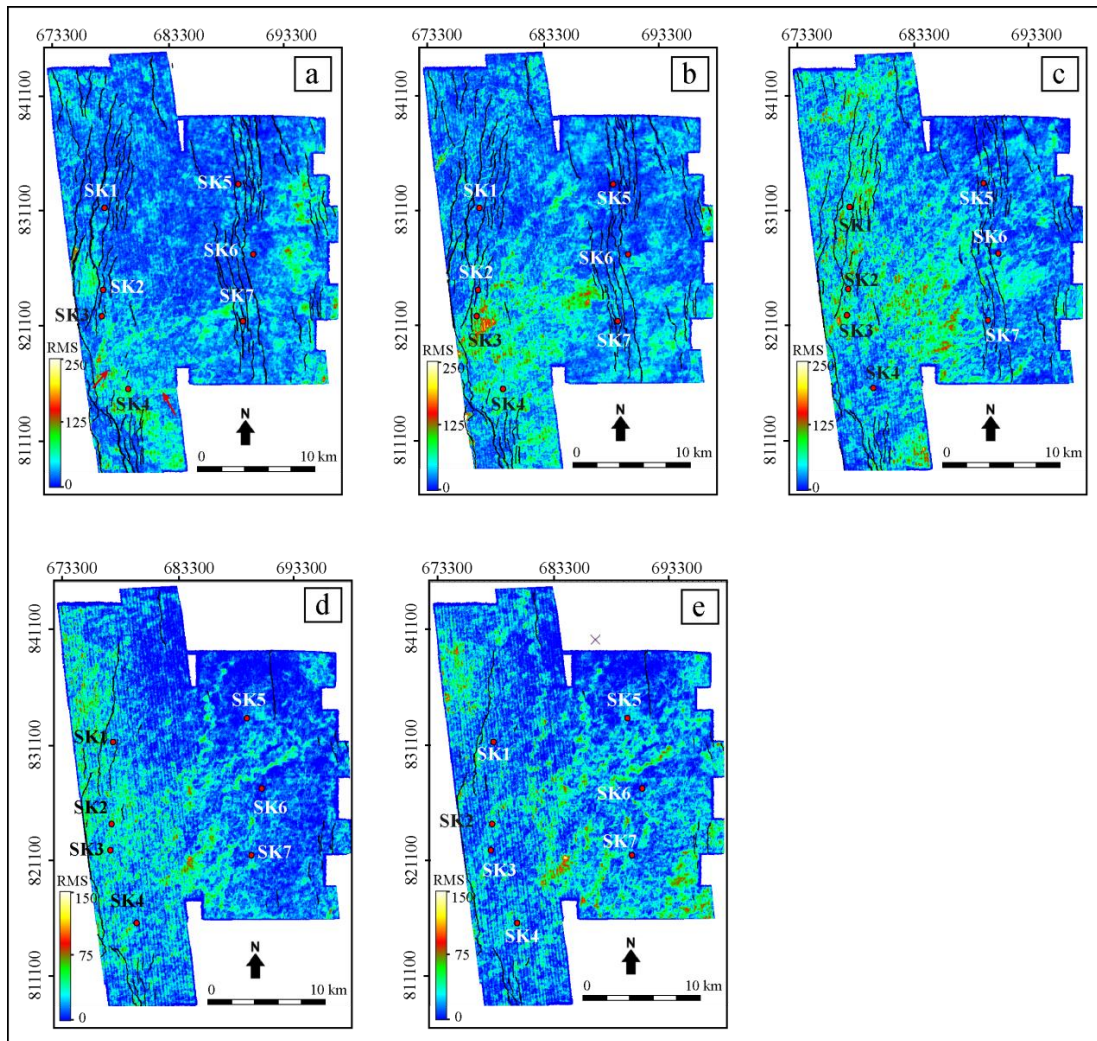
Figure 36 RMS maps showing development of channels in the post-rift section I (Middle Miocene), a) horizon S3, b) horizon S4, c) horizon S5, d) horizon S6, e) horizon S7.

5.5.4   S5-S7 Horizons (upper Middle Miocene: late post-rift phase I)

S5-S7 horizons are located in the upper interval of the Middle Miocene post-rift phase I. The RMS maps display a number of long, narrow bands of high amplitude anomalies in the middle part of a basin, which is the main depocenter during this period. These anomalies have low-medium sinuosity (SI= 1-1.15) and developed in a NE-SW direction (**Figure 36 (c)**, **(d)**, **(e)**). The similarity attribute shows parallel, narrow, low-medium sinuosity, non-similarity (black lines) features between a region of high

similarity (white area), especially for horizons S6 and S7 (**Figure 37 (c)**). These white features are interpreted as pointbar sands that can also be observed on vertical seismic sections (**Figure 37 (a)**).

High RMS values that correspond to high amplitude contrasts in the vertical seismic section, are interpreted as small point bars associated with a small shale-filled channel belt. Low amplitude, mud-filled material surrounded by high amplitudes, which exhibit differential compaction, were also observed in vertical seismic sections (**Figure 37 (a)**). The interpreted channels in this period have widths between 200-300 meters. Unpublished, oil industry biostratigraphic studies indicate marine conditions occupied almost the entire basin as indicated by all wells, except SK4. In SK4 mangrove palynomorphs (Spinizonocolpites, Zonocostites, Florschuetzia levipoli, and Florschuetzia meridionalis) are dominant, which indicate the southwestern part of the basin still had freshwater conditions, with degrees of tidal influence. Therefore, during this period the basin exhibits more marine influenced deposition compared to the lower horizons, and is accompanied by higher average GR log values.
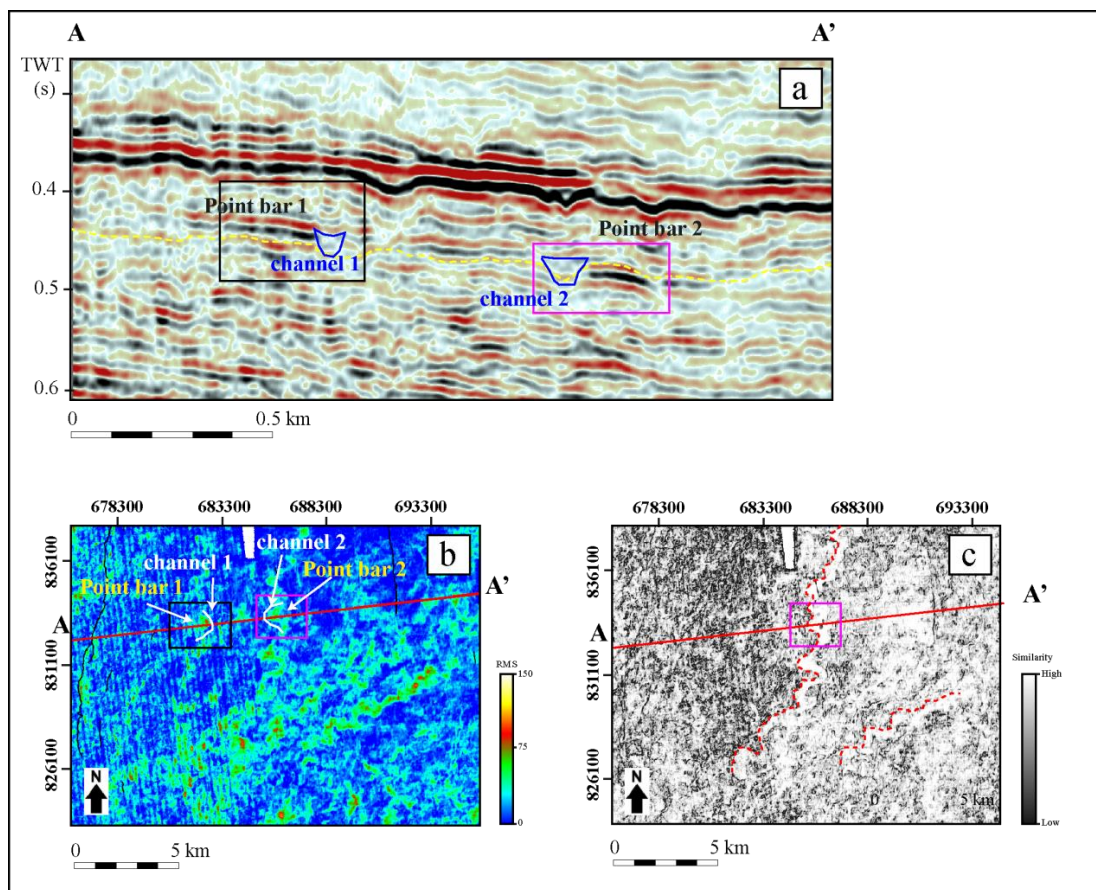
Figure 37 a) Cross section line A-A' showing locations of channels with pointbar development on the S7 horizon. b) RMS map showing high amplitudes that correlate with pointbar sands. c) Similarity map showing subtle indications of channel boundaries.

5.5   Discussion

5.6.1   Depositional environment

The results from integration of various seismic attributes (RMS, spectral decomposition and similarity), show that significant differences in channel characteristics and morphology exist between the late syn-rift and post-rift phase I. Therefore, it is interpreted that for these intervals the Songkhla Basin exhibits two fundamental depositional patterns (**Figure 38**). The first depositional pattern comprises fluvial channels developed in the late syn-rift, upper Early Miocene (S1 and S2 horizons) interval characterized by a dominance of sandstone on GR log data, while biostratigraphic data from sidewall cores indicates low energy fluvial conditions without marine influence (**Figure 38 (a)** and **(b)**). The integration of all seismic attributes indicate that the lower S1 horizon channels were developed in a meandering channel complex with low sinuosity as displayed by the oxbow lakes cut by channels, which suggests a process of channel straightening (**Figure 38 (a)**). Whereas, the upper S2 horizon displays higher sinuosity channels that are slightly wider compare to the S1 period (**Table 2**). There is thought to be a strong relationship between slope angle and sinuosity, with sinuosity increasing as slope angle decreases passing from straight channels to meandering channels, as slope decreases further and braided channels develop sinuosity decreases (Schumm and Khan, 1972). Although the channels in S1 and S2 have very different sinuosity index values, both are interpreted as having been deposited within a meandering fluvial system in a low relief area. The difference in sinuosity index value depends on which channel shapes are preserved in the geological record. When meandering channels are preserved prior to oxbow lake development, the sinuosity index (S2) is high. If the oxbow lakes have formed and the straighten channels are preserved in geological record, the sinuosity index will appear to be low (S1) although the depositional environment is also within the meandering fluvial system.

Horizon	Channel width (m)			Channel depth (m)			Width /Depth ratio	Meander belt width (km)	Sinuosity Index (SI=CL/ML)	Channel pattern
	min	mean	max	min	mean	max				
S1 - late syn-rift (lower Early Miocene)	150	360	500	18	27	34	15	5	1.2	low sinuous
S2 - late syn-rift (upper Early Miocene)	210	450	600	23	28	39	17	7.5	1.85	meandering
S3-S7 - post-rift I (Middle Miocene)	110	230	350	15	22	31	11	1.5-2	1-1.1	low sinuous

Table 2 Comparison of channel width, depth, width/depth ratio, meander belt width, sinuosity, and patterns during late syn-rift and post-rift phase I.

The second depositional pattern found in the Songkhla Basin comprises fluvial channels associated with deltaic and tidal depositional environments in the post-rift phase I section (**Figure 38 (c)** and **(d)**). The results of seismic attributes integrated with well data and biostratigraphy reveals fluvial channels developed close to the major boundary faults in the southwestern part of the basin during the beginning of the post-rift stage. During the early Middle Miocene (S3-S4 horizons), the basin was dominantly freshwater, especially in the southwestern part, while biostratigraphy indicates the eastern area started to experience episodes of marine influence. Later, in the upper Middle Miocene (S6-S7 horizons) the channel geometries evolved to higher sinuosity with more marine influence across almost the entire basin indicating by mangrove palynomorphs in all wells, except SK4.
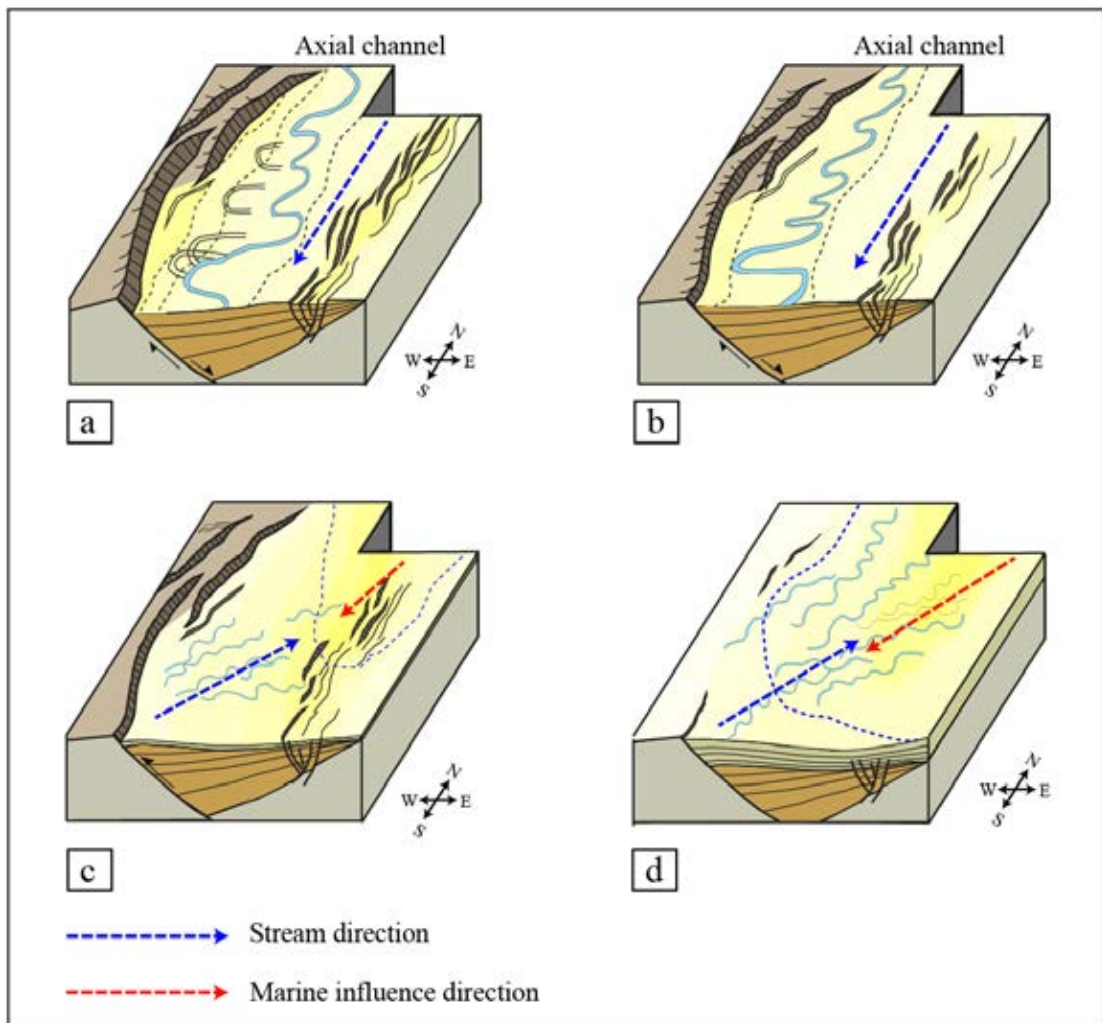
Figure 38 Conceptual model of depositional environment development in the Songkhla
Basin from the late syn-rift (late Early Miocene) to post-rift I (Middle
Miocene). (a) S1-lower late syn-rift horizon. Fault controlled western
boundary fault margin, with axial fluvial channel-dominated depocentre in
boundary fault hangingwall. Minor conjugate fault sets near flexural margin
(b) S2-upper late syn-rift horizon. Declining boundary fault activity, with
axial channel fluvial system in similar position to a). (c) S4-lower post-rift I
horizon. Mild inversion of the boundary fault forces depocentre to the east.
Smaller channels compared with a, and b are developed that trend NE-SW to
NNE-S. Marine incursions enter from the NE part of the basin. SW (d) S7-
upper post-rift I horizon. Post-rift subsidence depocentre focused in eastern-
central part of basin, boundary fault morphology largely covered. Small N-S

to NNE-SSW trending channels developed with widespread marine incursions.

5.6.2   Tectonic influence on channel morphology

Tectonic processes in rift basins exert an important role in controlling rift geometries and stratigraphic successions throughout their evolution from rift initiation to post-rift subsidence (Bosworth and McClay, 2001; Baudon et al., 2009; Bridge and Leeder, 1979; Gupta and Cowie, 2000; Karp et al., 2012; Lambiase, 1990; Lambiase and Bosworth, 1995; Lambiase and Morley, 1999; Leeder and Gawthorpe, 1987; Leeder and Jackson, 1993; McClay and Khalil, 2009; Olsen, 1990; Prosser, 1993, Williams and Dobb, 1993; Withjack et al., 2002). The Songkhla basin is part of a rift system whose period of transition from the syn-rift to the post-rift stage does not coincide with a neighboring region undergoing continental breakup. Instead, the syn-rift to post-rift transition, which is regionally diachronous (Morley et al., 2011), is probably related to 1) the varied and complex combination of factors causing extensional stresses (Pubellier and Morley, 2014), and 2) the mechanics of the lithosphere evolution during rifting that can cause some rifts to cease activity (strain hardening) while others can continue to extend (e.g. Kusznir and Park, Corti et al., 2019). In general sedimentation rates in the Gulf of Thailand remained high through the Early-Middle Miocene, and declined during the Late Miocene-Recent as the climate became dryer and the winter monsoon became stronger across Asia (Clift, 2006). Overall there is remarkably little variation in water depth throughout the Miocene-Recent in the GOT (near sea level, maximum of 80 m water depth today), which reflects sedimentation rates and subsidence rates being locked in tandem, and is highly suggestive of subsidence being largely controlled by sedimentation rates (Morley and Westaway, 2006). The upper Early Miocene stratigraphic successions in Songkhla basin is considered to represent the last stage of the rift cessation due to the subaerial depositional environment of fluvial channels (that replaced earlier shale-prone lacustrine-lagoonal deposition) prior to the transition to the fluvio-deltaic deposits of the Middle Miocene post-rift section.

Sedimentary deposits, which were developed in the late syn-rift, upper Early Miocene (S1 and S2 horizons), are characterized by basinwide channel systems with low to high sinuosity large-scale channel belts with individual channels stacked together. These channels are concentrated in the main depocenter in the hangingwall of active major extensional boundary faults with the main flow directions along the strike of the faults. These relationships indicate boundary fault-controlled sedimentation and minor river avulsion with downslope cut-off, resulting in wide channel belt sand-bodies, which in other basins have been interpreted as a gradual response to slow tectonic subsidence (e.g. Alexander and Leeder 1987; Leeder and Gawthorpe, 1987; Leeder and Jackson, 1993). During this waning stage of extensional activity in the region, the decreasing extensional strain was mostly accommodated on the major western boundary fault system (Phoosongsee and Morley, 2018) indicating that tectonics still controlled basin subsidence during this time. For the North Sea, McLeod et al. (2002) discuss how differential tectonic subsidence has a strong control on the facies distribution and depositional patterns during the syn-rift period. In the Songkhla Basin meandering channels become wider and exhibit higher sinuosity from S1 to S2 reflecting the decrease in accommodation space and decrease of the slope from the eastern flexural margin toward the footwall uplift on the boundary fault margin as a result of slow tectonic subsidence rate before extension ended.

The regional syn-rift paleogeography (**Figure 39 (a)**) shows that north of the Songkhla Basin a branch of the Ko Kra Ridge runs between the Ko Kra Basin and the Nakhon Basin, and this ridge could be a source of sediment from the north into the Songkhla Basin, as well as from the east into the flexural margin. While the existing high area today, Peninsular Thailand, could have supplied sediment from the west and south. Probably the footwall high area along the western boundary fault margin of the basin would have prevented most of the sediment from the west from entering the basin, and instead have deflected that sediment northwards to the Nakhon Basin. The NNW-SSE to N-S channel orientations following major western boundary faults strike indicate these drainage systems could arise either from paleohighs to the north of the basin, or from Peninsular Thailand to the south.
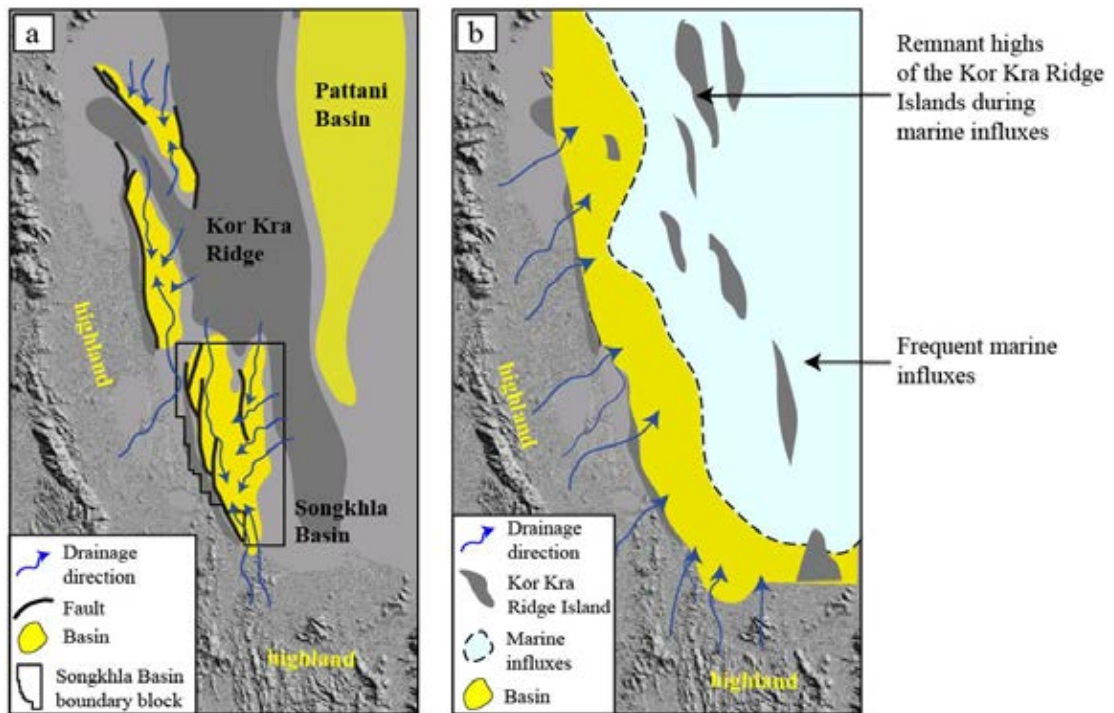
Figure 39 The regional syn-rift paleogeography map illustrating potential directions of river flow, as indicated by the blue arrows, from highlands to basin lows.

The second depositional pattern found in the Songkhla Basin is related to fluvial channels associated with deltaic and tidal depositional environments during post-rift phase I. During the beginning of the post-rift stage, channels are observed in the southwestern part of the area close to the western boundary faults (S3). These channels were relatively small, but can be seen on the seismic attributes (Fig. 12) as having NE-SW orientations. The change in channel directions to a NE-SW trend was probably caused by the changes of slope accompanying migration of depocenters away from the western boundary faults toward the east of a basin that probably resulted from mild inversion that occurred after the termination of extension (Phoosogsee and Morley, 2018). It is uncertain whether these channels were sourced from the western boundary fault margin or from the eastern, flexural margin. We favor a source from the west, assuming that as displacement declined on the western boundary fault margin topography became lower, enabling river systems to enter from the west. Additionally, with marine incursions entering the NE part of the basin it can be concluded that the topography to the north and east of the basin had become degraded and lowered to permit such incursions, making a sediment source from that direction unlikely (**Figure**

39 (b)). A higher density of small narrow channel belts is present during the later post-rift period and they trend NNE-SSW (S4-S7) flowing away from western boundary faults to the new depocenter that migrated from west to east in the basin during post-rift thermal subsidence. Biostratigraphy for the early Middle Miocene indicates the southwestern part of the basin was dominantly freshwater with varying degrees of sub-areal exposure and intertidal episodes defined by the spores and pollen and mangrove elements. Subsequently, in the late Middle Miocene (S6-S7) the eastern basin had transitioned to intertidal, upper estuarine and lower coastal plain margin depositional environments.

Climate change is another important factor that could potentially influence channel morphology as it controls the river discharge and sediment delivery, which affects the fluvial response (Miall, 2002). Based on Morley (2012), the period from Early Miocene to Middle Miocene (i.e., syn- to post-rift transition period of Songkhla Basin) experienced the same moist monsoonal climate regime covering much of the Sunda and East Asian region (**Figure 40**). This East Asian monsoon for wetter climates was initiated by the closure of the Indonesian Throughflow following the collision of Australian Plate with Sunda at the end of Oligocene (Morley, 2012). Zachos et al., 2001, stated the earliest Early Miocene is characterized by an abundance of sands that resulted from erosion at the time of the sea level fall from the J1000 horizon of the Malay Basin (Morley, 2012). This sequence may be equivalent to the late Early Miocene in Songkhla Basin as it also contains abundant of sands (**Figure 32**) reflecting the high sediment charge during the everwet climate. However, in the Middle Miocene, the region experienced the Middle Miocene thermal maximum (Morley, 2012) with the continuation of the everwet climate. Yet sand input to the Songkhla Basin decreased, coincident with post-rift subsidence and the development of lower-relief regionally, accompanied by an increase in the frequency of marine incursions into the basin. With a consistent wet climate throughout the Early to Middle Miocene, there is no clear link between the paleoclimate and channel morphology variations in the Songkhla Basin, the variations observed are more closely linked with tectonics during the syn-rift to post-rift transition.
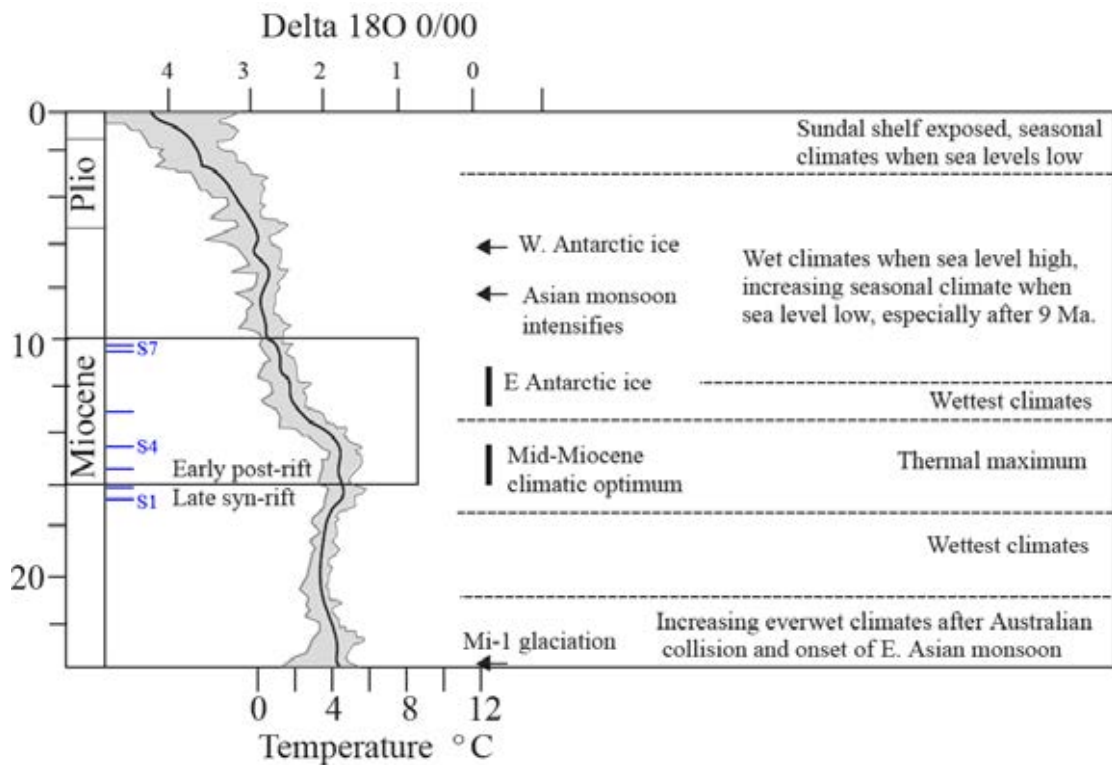
Figure 40 Oxygen isotope curve of Zachos et al. (2001) compared to the major tectonic and climate, including the study interval from S1 (late Early Miocene) to S7 (Middle Miocene).

The syn-rift post-rift transition in the Songkhla basin is characterized by a very gradual transition, both in the decrease in activity along the boundary faults (Phoosongsee and Morley, 2018) and in the change in depositional environments. Some of the changes, in particular channel orientation are related to reorganization of topography within the basin (particular due to inversion of the boundary fault zone hanging wall), while others, such as increasing frequency of marine incursions are related to eustatic events and tectonic subsidence which operated beyond the confines of the Songkhla basin.

With a better reservoir characterization of the fluvial to tidal deposits, the orientation of the thin reservoirs (channelized and point bars) within the depocenter versus the faulting structure will allow a better positioning of the exploration, appraisal and development wells within the Songkhla Basin for this petroleum play.

Identification of channels and point bars will allow the potential for stratigraphic traps or combination structure-stratigraphic traps within the Songkhla Basin to be tested.

CHAPTER VI
CONCLUSIONS AND RECOMMENDATIONS

6.1   Conclusions

Detail analysis of the reservoir characterization and distribution, and the depositional history in relation to the tectonostratigraphic evolution of Songkhla Basin significantly contribute our understanding of how tectonics controls sedimentation, especially during syn-rift to post-rift transition period.

Study of the major boundary fault displacement characteristics and evolution shows that the Songkhla Basin appears to represent an example of a predominantly orthogonal extension half graben, little affected by pre-existing fabrics, that developed in phases between the Late Eocene and the Early Miocene. The rift spans two phases of rifting, the Eocene-Oligocene phase that is present in the eastern GOT, and the Oligocene-Miocene phase that is present in the western GOT and onshore area. The tectonic phases that can be distinguished within the Songkhla basin are slightly different and comprise: (1) an early rift stage in the Eocene; (2) a late rift stage from Oligocene to Early Miocene; (3) post-rift Middle Miocene possibly with minor inversion; and, (4) post-rift Pliocene to recent.

The boundary fault is composed of five large segments (F1-F5). During the Eocene, the segments, except for F5, became hard linked, and generally by the end of the Eocene, throw conformed to the constant length, and coherent fault models. This observation adds to the growing body of literature that indicates the importance of these models in fault development (as reviewed by Jackson et al., 2016). During subsequent reactivation of the boundary fault system, the linkage points become more apparent in the throw-length profiles, and the later throw patterns during waning extensional activity tend to follow an isolated fault model as shown in **Figure 24**.

Two distinctive channel characteristics and patterns developed in two different periods: meandering channels developed in channel complexes during the late syn-rift (upper Early Miocene) and long narrow channel belts developed during post-rift phase I (Middle Miocene) indicating different mechanisms controlling sedimentation.

Tectonic is a major control on the channel development and reservoir distribution throughout rift evolution in Songkhla Basin. Channel development during the late syn-rift stage was mainly located in the depocenter adjacent to the major boundary faults and shows the same trend or slightly oblique trends to the fault strikes, suggesting that faults were still active at this stage, while during the post-rift stage, channels flowed to the new depocenter that had migrated eastwards from being adjacent to the western boundary faults in the syn-rift phase to the middle part of the basin in the post-rift phase. This shift is both a consequence of mild inversion along the boundary fault margin, and the location of maximum thermal subsidence.

By integrating seismic attributes and well interpretations to study subsurface preserved stratigraphy, it has been found that the Songkhla basin represents a very gradual syn- to post-rift transition in a coastal-transitional marine setting. The stratigraphy is controlled by both the decrease in activity along the boundary faults and the change in depositional environments. Although coastal-shallow marine depositional environments are complex due to the sub-aerial exposure involving erosion of the syn-rift topography, the stratigraphic succession throughout the transition in Songkhla basin was still be preserved. Based on literature review, this is a rare published example for the coastal-shallow marine transition period that are preserved in subsurface.

Meaningful geological features were successfully extracted from 3D seismic data using the RMS, similarity, and spectral decomposition i.e. sand distribution, channel boundaries, oxbow lakes, point bars. The integration of all seismic attributes helped to identify channel geometries. This approach is more efficient for identifying depositional patterns than conventional seismic reflection data. This methodology can be applied to other basins for both exploration and production purposes.

6.2 Recommendation for future research

This study has achieved the main purposed of establishing the tectono-stratigraphic evolution of Songkhla Basin. The influence of geological structure to the channel morphology and distribution during syn- to post-rift transition on a basin scale is now well understood in the study area. However, at the local sub-basin scales, especially in the vicinity of the conjugate fault sets in the middle part of a basin the sedimentary development could be more complicated.

The present investigation helped identify the types of the seismic attributes that provide good images of the subsurface geomorphology i.e. RMS, similarity and spectral decomposition (SD), where the SD provides better images using the RGB blending technique of different frequencies. Due to the software limitation, the SD being used in this study is the traditional discrete Fourier transform (DFT) that has fixed time-frequency resolution over the entire time frequency plane. Therefore, it is recommended to use the continuous wavelet transform (CWT) to produce better time-frequency maps as theoretically it has the ability to adjust window length and does not have fixed time-frequency resolution.

REFERENCES

Ahmad, M. N., Rowell, P., 2012. Application of spectral decomposition and seismic attributes to understand the structure and distribution of sand reservoirs within Tertiary rift basins of the Gulf of Thailand. The Leading Edge, 31, 630-634.

Ahmad, M. N., Rowell, P., Sriburee, S., 2014. Detection of fluvial sand systems using seismic attributes and continuous wavelet transform spectral decomposition: case study from the Gulf of Thailand. Marine Geophysics Research, 35, 105-123.

Alexander, J. A., Leeder, M. R., 1987. Active tectonic control of alluvial architecture. In: Ethridge, F. G., et al., eds. Recent Developments in Fluvial. Sedimentology Society of Economic Paleontologists and Mineralogists, Special Publications, 39, 243-252.

Bacon, M. and Simm, R., 2014. Seismic Amplitude: An Interpreter's Handbook. Cambridge University Press, doi.org/10.1017/CBO9780511984501.

Bahorich, M., 1995. 3-D seismic discontinuity for faults and stratigraphic features: The coherence cube. The Leading Edge, 14, 1053–1058

Basile, C., Maillard, A., Gaullier, V., Loncke, L., Roest, W., Mercier de Lepinay, M., and Pattier, F., 2013. Structure and evolution of the Demerara Plateau, offshore French Guiana : Rifting, tectonic inversion and post-rift tilting at transform-divergent margins intersection. Tectonophysics, 591, 16-29.

Baudon, C., Fabuel-Perez, I., Redfern, J., 2009. Structural style and evolution of a LateTriassic rift basin in the Central High Atlas, Morocco: controls on sediment deposition. Geological Journal, Special Issue, 44 (6), 677–691.

Bosworth, W., McClay, K.R., 2001, Structural and stratigraphic evolution of the Neogene Gulf of Suez, Egypt: In: Ziegler P.A., Cavazza W., Robertson A.H.F. and Crasquin-Soleau S. (Eds), 2001. Peri-Tethys memoir 6: Peri-Tethyan Rift/Wrench Basins and Passive Margins. Memoirs du Meuseum National d'HistoireNaturelle de Paris, 186, 567-606.

Bridge, J. S., Leeder, M. R., 1979. A simulation model of alluvial stratigraphy. Sedimentology, 26, 617–644.

Brown, A. R., 2004, Interpretation of three-dimension seismic data, 6th edition). American Association of Petroleum Geologists, Tulsa, Oklahoma, Memoir 42, 295-308.

Cartwright, J.A., Mansfield, C., Trudgill, B., 1996. The growth of faults by segment linkage. In: Buchanan, P.G., Nieuwland, D.A. (eds.), Modern Developments in Structural Interpretation, Validation and Modelling. Geological Society, London, Special Publication, 99, 163–177.

Childs, C., Nicol, A., Walsh, J.J., Watterson, J., 2003. The growth and propagation of synsedimentary faults. J. Struct. Geol. 25, 633–648.

Chopra, S., Marfurt K. J., 2005. Seismic attributes-a history perspective. Attribute Review Paper, 1-71.

Connolly, P., 1999. Elastic Impedance. The Leading Edge, 18, 438-452.

Cowie, P.A., Gupta, S., Dawers, N.H., 2000. Implications of fault array evolution for synrift depocentre development: insights from a numerical fault growth model. Basin Res. 12, 241–261.

Cowie, P.A., Attal, M., Tucker, G.E., Whittaker, A.C., Naylor, M., Ganas, A., Roberts, G.P., 2006. Investigating the surface process response to fault interaction and linkage using a numerical modelling approach. Basin Res. 18, 231–266.

Duffy, O.B., Brocklehurst, S.H., Gawthorpe, R.L., Leeder, M.R., Finch, E., 2015. Controls on landscape and drainage evolution in regions of distributed normal faulting: Perachora Peninsula, Corinth Rift, Central Greece. Basin Res. 27, 473–493.

Gabrielsen, R.H., Kyrkjebo, R., Faleide, J.I., Fjeldskaar, W., and Kjennerud, T., 2001. The Cretaceous post-rift basin configuration of the Northern North Sea. Petroleum Geoscience, 7, 137-154.

Gawthorpe, R.L., Leeder, M.R., 2000. Tectono-sedimentary evolution of active extensional basins. Basin Res. 12, 195–218.

Gawthorpe, R.L., Hurst, J.M., 1993. Transfer zones in extensional basins - their structural style and influence on drainage development and stratigraphy. J. Geol. Soc. London 150, 1137–1152.

Ghosh, D., Sajid, M., Ibrahim, N. A., Viratno, B., 2014. Seismic attributes add a new dimension to prospect evaluation and geomorphology offshore Malaysia. The Leading Edge, 33 (5), 536-545.

Goodway, W., Chen, T., Downton, J., 1997. Improved AVO fluid detection and lithology discrimination using Lame petrophysical parameters: $\lambda\rho$", "$\mu\rho$", & "λ/μ fluid stacks from P and S inversions. SEG Technical Program expanded abstracts 1997, 183-186. Doi: 10.1190/1/1885795.

Gupta, S., Cowie, P. A., 2000. Processes and controls in the stratigraphic development of extensional basins. Basin Research, 12, 185-194.

Hall, R., 2012. Late Jurassic-Cenozoic reconstructions of the Indonesian region and the Indian Ocean. Tectonophysics 570, 1–41.

Hall, R., Morley, C.K., 2004. Sundaland Basins, In: Clift, P., Wang, P., Kuhnt, W., Hayes, D. (eds). Continental-ocean interactions within East Asian Marginal Seas. AGU Special Publication, 149, 55–87.

Hall, R., Van Hattum, M.W.A., Spakman, W., 2008. Impact of India-Asia collision on SE Asia: the record in Borneo. Tectonophysics 251, 229–250.

Henstra, G.A., Rotevatn, A., Gawthorpe, R.L., Ravnås, R., 2015. Evolution of a major segmented normal fault during multiphase rifting: the origin of plan-view zigzag geometry. J. Struct. Geol. 74, 45–63.

IHS Global Inc., 2014. IHSTM Kingdom, User manual. Houston, Texas: Author.

Hopkins, M.C., Dawers, N.H., 2017. The role of fault length, overlap and spacing in controlling extensional relay ramp fluvial system geometry. Basin Res. 30, 20–34.

Inthana, C., 2013. Mapping of Middle Miocene reservoir sands and subtle faults to understand reservoir compartmentalization in Erawan Field of Pattani Basin, Gulf of Thailand. BEST, 6, 2, 17-28.

Jackson, C.A.L., 2008. Sedimentology and significance of an early-syn-rift paleovalley, Wadi Tayiba, Suez Rift, Egypt. J. Afr. Earth Sci. 52, 62–68.

Jackson, C.A.L., Gawthorpe, R.L., Leppard, C.W., Sharp, I.R., 2006. Rift-initiation development of normal fault blocks: insights from the Hammam Faraun fault block, Suez rift, Egypt. J. Geol. Soc. London 163, 165–183.

Jackson, C.A.L., Bell, R.E., Rotevatn, A., Tvedt, A.B.M., 2016. Techniques to determine the kinematics of synsedimentary normal faults and implications for fault growth models. Geol. Soc. London, Special Publ. 439, 187–217.

Jardine, E., 1997. Dual petroleum systems governing the prolific Pattani Basin, Offshore Thailand. Indonesian Petroleum Association, Proceedings of the Petroleum Systems of SE Asia and Australia Conference, 351-363.

Kaewkor, C., Watkinson, I. M., Burgess, P., 2015. Structural Style and Evolution of the Songkhla Basin, western Gulf of Thailand. GEOINDO, Conference Proceeding, November 23-24, 2015.

Karp, T., Scholz, C.A., McGlue, M.M., 2012. Structure and stratigraphy of the Lake Albert Rift, East Africa: Observations from seismic reflection and gravity data: In Bartov, Y., and Nummedal, D. (Eds.), Lacustrine Sandstone Reservoirs and Hydrocarbon Systems. AAPG Memoir 95, 299-318.

Kim, Y., Sanderson, D. J., 2004. The relationship between displacement and length of faults. A review, Earth-Science Reviews, 68, 317-334.

Kornsawan, A., Morley, C. K., 2002. The origin and evolution of complex transfer zones (graben shifts) in conjugate fault systems around the Funan Field, Pattani Basin, Gulf of Thailand. Journal of Structural Geology, 24, 235-499.

Kusznir, N. J., Roberts, A.M., Morley, C. K., 1995. Forward and reverse modelling of rift basin formation. In: Lambiase, J. (ed.), Hydrocarbon Habitat in Rift Basins. Geological Society, London, Special Publications, 80, 33-56.

Lambiase, J. J., 1990, A model for tectonic control of lacustrine stratigraphic sequences in continental rift basins. In Lacustrine basin exploration-case studies and modern analogs (ed. B. J. Katz): American Association of Petroleum Geologists Memoir, 50, 265-286.

Lambiase, J., Bosworth, W., 1995. Structural controls on sedimentation in continental rifts. Geological Society of London, Special Publication, 80, 117-144.

Lambiase, J. J., Morley C.K., 1999. Hydrocarbon habitat in rift basins: the role of stratigraphy. Philosophical Transactions of the Royal Society of London., 357, 877-899.

Laughlin, K., Garossino, P., Partyka, G., 2002. Spectral decomp applied to 3D. AAPG Explorer, 23, 5, 28-31.

Lawwongngnam, K., Philip, R. P., 1993. Preliminary investigation of oil and source rock organic geochemistry from selected Tertiary basins of Thailand. Journal of Southeast Asia, 8, 433-448.

Leeder, M., Gawthorpe, R. L., 1987. Sedimentary models for extensional tilt/half-graben basins. In Continental extensional tectonics (ed. M. P. Coward, J. F. Dewey & P. L. Hancock): Geological Society Special Publication, 28, 139-152.

Leeder, M.R., Jackson, J.A., 1993. The interaction between normal faulting and drainage in active extensional basins, with examples from the western United States and central Greece. Basin Res. 5, 79–102.

Lockhart, B.E., Chinoroje, O., Enomoto, C. B., Hollomon, G. A. 1997. Early Tertiary deposition in the southern Pattani Trough, Gulf of Thailand. In Proceedings of the International conference on Stratigraphy and Tectonic Evolution of Southeast Asia and the South Pacific (Geothai'97), 19-24 August 1997, Bangkok, 476-489.

Liu, J., Marfurt K., 2007. Instantaneous spectral attributes to detect channels. Geophysics,72, 2, P23–P31.

Manh Do, T., 2013. Architecture and Depositional Environment of Fluvial Systems of Southern Songkhla Basin, Gulf of Thailand. BEST, 6, 2, 131-141.

Mansfield, C., Cartwright, J.A., 2001. Fault growth by linkage: observations and implications from analogue models. J. Struct. Geol. 23, 745–763.

Marfurt, K. J., Kirlin R. L., 2001. Narrow-band spectral analysis and thin-bed tuning. Geophysics, 66, no. 4, 1274–1283.

Marfurt, K. J., Sudhaker, V., Gersztenkorn, A., Crawford, K. D., Nissen, S. E., 1999. Coherency calculations in the presence of structural dip. Geophysics, 64, 104–111.

Marin, D., Escalona, A., and Grundvåg, S.-A., Olaussen, S., Sandvik, S., Śliwińska, K.K., 2018. Unravelling key controls on the rift climax to post-rift fill of marine rift basins: insights from 3D seismic analysis of the Lower Cretaceous of the Hammerfest Basin, SW Barents Sea. Basin Research, 30, 587-612,

Marrett, R., Allmendinger, R.W., 1991. Estimates of strain due to brittle faulting: sampling of fault populations. J. Struct. Geol. 13, 735–738.

Matos, M. C., Osorio, P. L. M., Mundim, E. C., Moraes, M. A. S., 2005. Characterization of thin beds through joint time-frequency analysis applied to a turbidite reservoir in Campos basin, Brazil. 75th Annual International Meeting, SEG, Expanded Abstracts, 1429–1432.

Metcalfe, I., 2013. Tectonic evolution of the Malay Peninsula. J. Asian Earth Sci. 76, 195–213.

McClay, K.R., Khalil, S.M., 2009. Structural control on syn-rift sedimentation, northwestern Red Sea margin, Egypt. Marine and Petroleum Geology, 26, 1018-1034.

McKenzie, D.P., 1978. Some remarks on the development of sedimentary basins. Earth and Planetary Science Letters, 40, 25-32.

McLeod, A. E., Underhill, J. R., Davies, S. J., Dawers, N. H. (2002). The influence of fault array evolution on synrift sedimentation patterns: Controls on deposition in the Strathspey-Brent-Statfjord half graben, northern North Sea. AAPG Bulletin, 86(6), 1061-1094.

Miall, A. D., 2002, Architecture and sequence stratigraphy of Pleistocene fluvial systems in the Malay basin, based on seismic time-slice analysis. AAPG Bulletin, 86, 1201–1216.

Morley, C.K., 1995. Developments in the structural geology of rifts over the last decade and their impact on hydrocarbon exploration. In: Lambiase, J.J. (ed.) Hydrocarbon Habitats in Rift Basins. Geological Society of London, Special Publication, 80, 1–32.

Morley, C.K., 1999. Comparison of hydrocarbon prospectivity in rift basins. In: Morley C.K. (ed.), Geoscience of Rift Systems - Evolution of East Africa. AAPG Studies in Geology, 44, 233-231.

Morley, C.K., 2001. Combined escape tectonics and subduction rollback back arc extension: a model for the evolution of Tertiary rift basins in Thailand, Malaysia and Laos. J. Geol. Soc. London 158, 461–474.

Morley, C.K., 2002. Tectonic settings of continental extensional provinces and their impact on sedimentation and hydrocarbon prospectivity. SEPM special publication, 73, 25-56.

Morley, C.K., 2009. Evolution from an oblique subduction back-arc mobile belt to a highly oblique collisional margin; the Cenozoic tectonic development of Thailand and eastern Myanmar. In: Cawood, P.A., Kröner, A. (eds.), Earth Accretionary Systems in Space and Time. The geological Society, London, Special Publications, 318, 373–403.

Morley, C. K., 2015. Five anomalous structural aspects of rift basins in Thailand and their impact on petroleum systems. In: Richards, F. L., Richardson, N. J., Rippington, S. J., Wilson, R.W. & Bond, C. E. (eds), Industrial Structural Geology: Principles, Techniques and Integration. Geological Society, London, Special Publications, 421(1), 143-168.

Morley, C.K., 2016. The impact of multiple extension events, stress rotation and inherited fabrics on normal fault geometries and evolution in the Cenozoic rift basins of Thailand. In: Childs, C., Holdsworth, R.E., Jackson, C.A.-L., Manzocchi, T., Walsh, J. J., Yielding, G. (eds.), The Geometry and Growth of

Normal Faults. Geological Society, London, Special Publications, 439, 413–445.

Morley, C. K., Racey, A., 2011. Tertiary stratigraphy. In: Ridd, M. F., Barber, A. J. & Crow, M. J., The Geology of Thailand. Geological Society, London, 223–271.

Morley, C.K., Westaway, R., 2006. Subsidence in the super-deep Pattani and Malay basins of Southeast Asia: a coupled model incorporating lower-crustal flow in response to post-rift sediment loading. Basin Res. 18 (1), 51–84.

Morley, C.K., Nelson, R.A., Patton, T.L., Munn, S.G., 1990. Transfer zones in the East African rift system and their relevance to hydrocarbon exploration in rifts. AAPG Bull. 74, 1234–1253.

Morley, C.K., Woganan, N., Sankumarn, N., Hoon, T.B., Alife, A., Simmons, M., 2001. Late Oligocene-Recent stress evolution in rift basins of northern and central Thailand: implications for escape tectonics. Tectonophysics 334, 115–150.

Morley, C.K., Woganan, N., Kornsawan, A., Phoosongsee, W., Haranya, C., Pongwapee, S., 2004. Activation of rift oblique and rift parallel pre-existing fabrics during exension and their effect on deformation style: examples from the rifts of Thailand. J. Struct. Geol. 26, 1803–1829.

Morley, C.K., Gabdi, S., Seusutthiya, K., 2007. Fault superimposition and linkage resulting from stress changes during rifting: Examples from 3D seismic data, Phitsanulok Basin, Thailand. J. Struct. Geol. 29 (4), 646–663.

Morley, C.K., Charusiri, P. and Watkinson, I., 2011. Chapter 11. Structural Geology of Thailand During the Cenozoic. Geology of Thailand. In: Ridd, M.F., Barber, A.J., and Crow, M.J., Geology of Thailand. Geological Society of London, 273-334.

Needham, T., Yielding, T., Fox, R., 1996. Fault population description and prediction using examples from offshore U.K. J. Struct. Geol. 18, 155–167.

Nottevedt, A., Gabrielsen, R., Steel, R., 1995. Tectonostratigraphy and sedimentary architecture of rift basins with reference to the northern North Sea. Marine and Petroleum Geology, 12, 881-901.

Oil and Gas Journal (anonymous), 2011. Thailand: Bua Ban fault block as oil in three zones. Oil and Gas Journal, 04/07/2011, 1pp.

Olsen, P. E., 1990. Tectonic, climatic, and biotic modulation of lacustrine ecosystems—examples from the Newark Supergroup of eastern North America. In Katz, B.J., ed., Lacustrine Exploration: Case Studies and Modern Analogues. American Association of Petroleum Geologists Memoir, 50, 209-224.

Partyka, G., Gridley, J., Lopez, J., 1999. Interpretational Applications of Spectral Decomposition in Reservoir Characterization. The Leading Edge, 18, 353-360.

Peacock, D.C.P., Sanderson, D.J., 1991. Displacements, segment linkage and relay ramps in normal fault zones. Journal of Structural Geology, 13 (6), 721-733.

Peyton, L., Bottjer, R., Partyka G., 1998. Interpretation of incised valleys using new 3-D seismic techniques: A case history using spectral decomposition and coherency. The Leading Edge,17, 1294–1298.

Pigott, J.D., Sattayarak, N., 1993. Aspects of sedimentary basin evolution assessed through tectonic subsidence analysis. Example: northern Gulf of Thailand. SE Asian Earth Sci. 8, 407–420.

Polachan, S., Sattayarak N., 1989. Strike-slip tectonics and the development of Tertiary basins in Thailand. In: International Symposium on Intermontane Basins: Geology and Resources Chiang Mai, Thailand, 243–253.

Phoosongsee, J., Morley, C.K., 2018. Evolution of a major extensional boundary fault system during multi-phase rifting in the Songkhla Basin, Gulf of Thailand, Journal of Asian Earth Sciences, https://doi.org/10.1016/j.jseaes.2018.08.028.

Praidee, A., 2013. Control on reservoir geometry and distribution, Tantawan Field, Gulf of Thailand. BEST, 6, 2, 1-10.

Prosser, S., 1993. Rift-related linked depositional systems and their seismic expression. In Williams, G. D., and Dobb, A., eds., Tectonics and seismic sequence stratigraphy. Geological Society, London. Special Publication, 71, 117-144.

Racey, A., 2011. Chapter 13, Petroleum geology. In: Ridd, M.F., Barber, A.J., Crow, M.J. (eds.), Geology of Thailand. Geological Society of London, 352–392.

Ridd, M. F., Barber, A. J., Crow M. J., 2011. Introduction to the geology of Thailand. In: Ridd, M.F., Barber, A.J., Crow, M.J., (eds.). The Geology of Thailand. Geological Society of London. 1-17.

Rivas, S., Grimmer, J.O.W., Alaminos, A., Navarro, J., 2016. Basin Modelling at the Songkhla Basin (GOT). AAPG/SEG International Conference and Exhibition, Barcelona, Spain, April 3-6, 2016

Roberts, A.M., Kusznir, N.J., Corfield, R.I., Thompson, M., Woodfine, R., 2013. Integrated tectonic basin modelling as an aid to understanding deep-water rifted continental margin structure and location. Petroleum Geosceine, 19, 65-88.

Sautter, B., Pubellier, M., Jousselin, P., Dattilo, P., Kerdraon, Y., Choong, C.M., Menier, D., 2017. Late Paleogene rifting along the Malay Peninsula thickened crust. Tectonophysics 710–711, 205–224.

Scherer, C.M.S., Goldberg, K., Bardola, T., 2015. Facies architecture and sequence stratigraphy of an early post-rift fluvial succession, Aptian Barbalha Formation, Araripe Basin, northeastern Brazil. Sedimentary Geology, 322, 43-62.

Scholz, C.H., Cowie, P.A., 1990. Determination of total strain from faulting using slip measurements. Nature 346, 837–839.

Schumm, S.A. and Khan, H.R., 1972. Experimental study of Channel Patterns. Geological Society of American Bulletin, 83, 1755-1770.

Searle, M. P., Morley, C.K., 2011. Tectonic and Thermal Evolution of Thailand in the regional context of SE Asia. In: Ridd, M. F., Barber, A. J. & Crow, M. J., The Geology of Thailand. Geological Society of London, 539-571.

Sinha, S., Routh P. S., Anno P. D., Castagna J. P., 2005. Spectral decomposition of seismic data with continuous-wavelet transform. Geophysics, 70, 6, P19–P25.

Tapponnier, P., Peltzer, G., Armijo, R., 1986. On the mechanism of collision between India and Asia. In: Coward, M.P., Ries, A.C. (eds.), Collision Tectonics. Geological Society, London, Special Publications, 19, 115–157.

Tingay, M., Morley, C.K., Hillis, R., Meyer, J., 2010. Present-day stress orientation in Thailand's basins. J. Struct. Geol. 32, 235–248.

Trevena, A. S. C., R. A., 1986. Diagenesis of Sandstone Reservoirs of Pattani Basin, Gulf of Thailand. American Association of Petroleum Geologists, 70, 299–308.

Tri Tran, O., 2013. Quantitative Seismic Geomorphology of Early Miocene to Pleistocene Fluvial System of Northern Songkhla, Gulf of Thailand. BEST, 6, 2, 80-88.

Walsh, J.J., Nicol, A., Childs, C., 2002. An alternative model for the growth of faults. J. Struct. Geol. 24, 1669–1675.

Walsh, J.J., Watterson, J., 1988. Analysis of the relationship between the displacements and dimensions of faults. J. Struct. Geol. 10, 239–247.

Walsh, J.J., Watterson, J., 1991. Geometric and kinematic coherence and scale effects in normal fault systems. In: Roberts, A.M., Yielding, G., Freeman, B. (Eds.), The Geometry of Normal Faults. Geological Society, London, Special Publication, 56, 193–203.

Watcharanantakul, R., Morley, C.K., 2000. Syn-rift and post-rift modeling of the Pattani Basin, Thailand, evidence for a ramp-flat detachment. Mar. Pet. Geol. 17, 937–958.

Williams, G. D., Dobb, A. (eds), 1993. Tectonics and seismic sequence stratigraphy: an introduction. Geological Society, Special Publication, 28 (7), 1-13.

Withjack, M. O., Schlische, R.W., Olsen, P.E., 2002. Rift-basin structure and its influence on sedimentary system. Society for Sedimentary Geology, SEPM Special Publication, 73, 57-81.

Young, M.J., Gawthorpe, R.L., Hardy, S., 2001. Growth and linkage of a segmented normal fault zone; the Late Jurassic Murchison-Statfjord North Fault, northern North Sea. J. Struct. Geol. 23, 1933–1952.

Zachariah, A.J., Gawthorpe, R., Dreyer, T., Cornfield, S., 2009. Controls on early post-rift physiography and stratigraphy, lower to mid-Cretaceous, North Viking Graben, Norwegian North Sea. Basin Research, 21, 189-208.

Zachos, J. C., Pagini, M., Sloan, L., Thomas, E., Billups, K., 2001. Trends, rhythms and aberrations in global climate 65 Ma to Present. Science, 292, 686-93.

APPENDIX A:

TIME STRUCTURAL MAPS
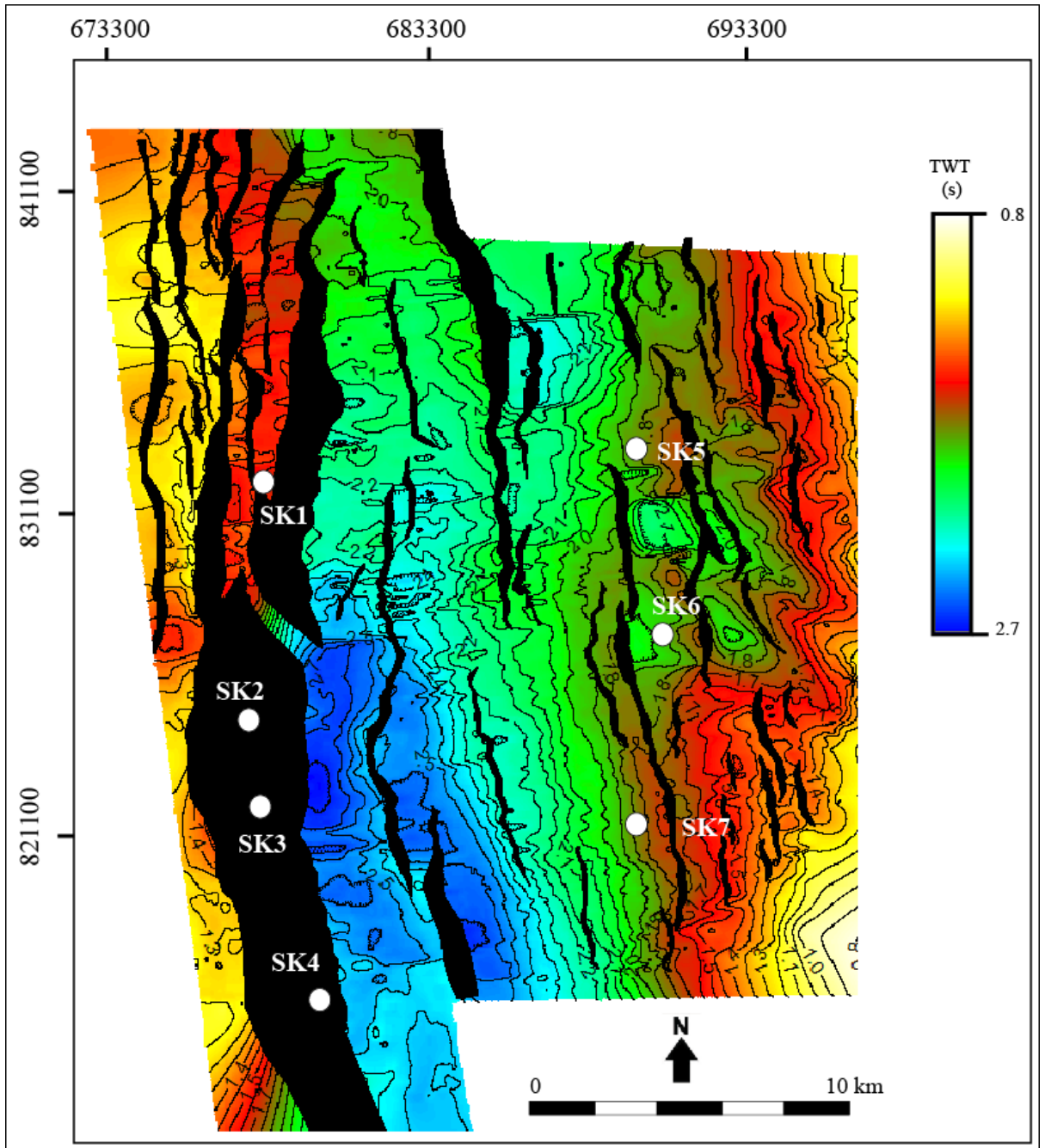
Base Eocene time structural map
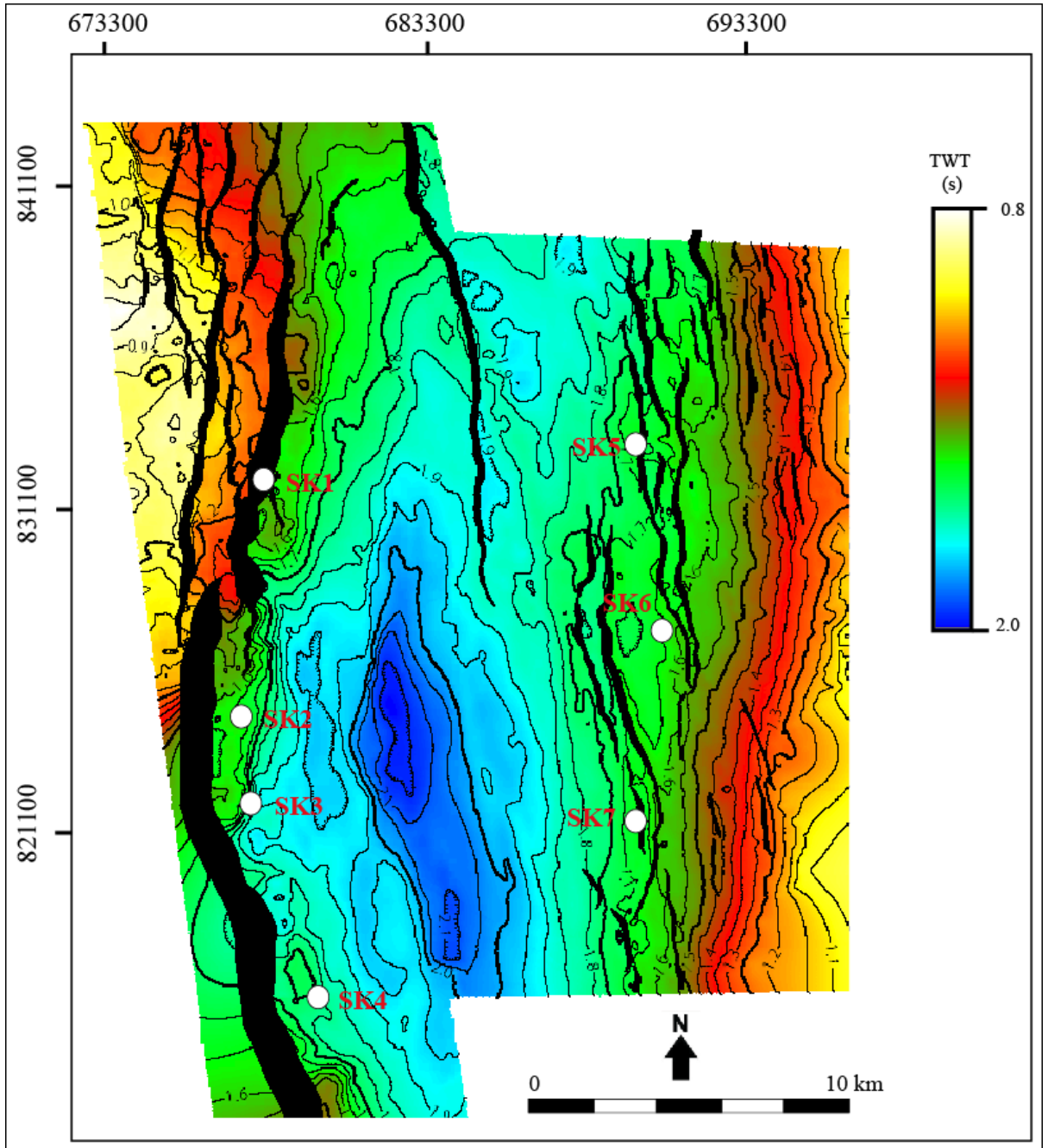
Lower Oligocene time structural map
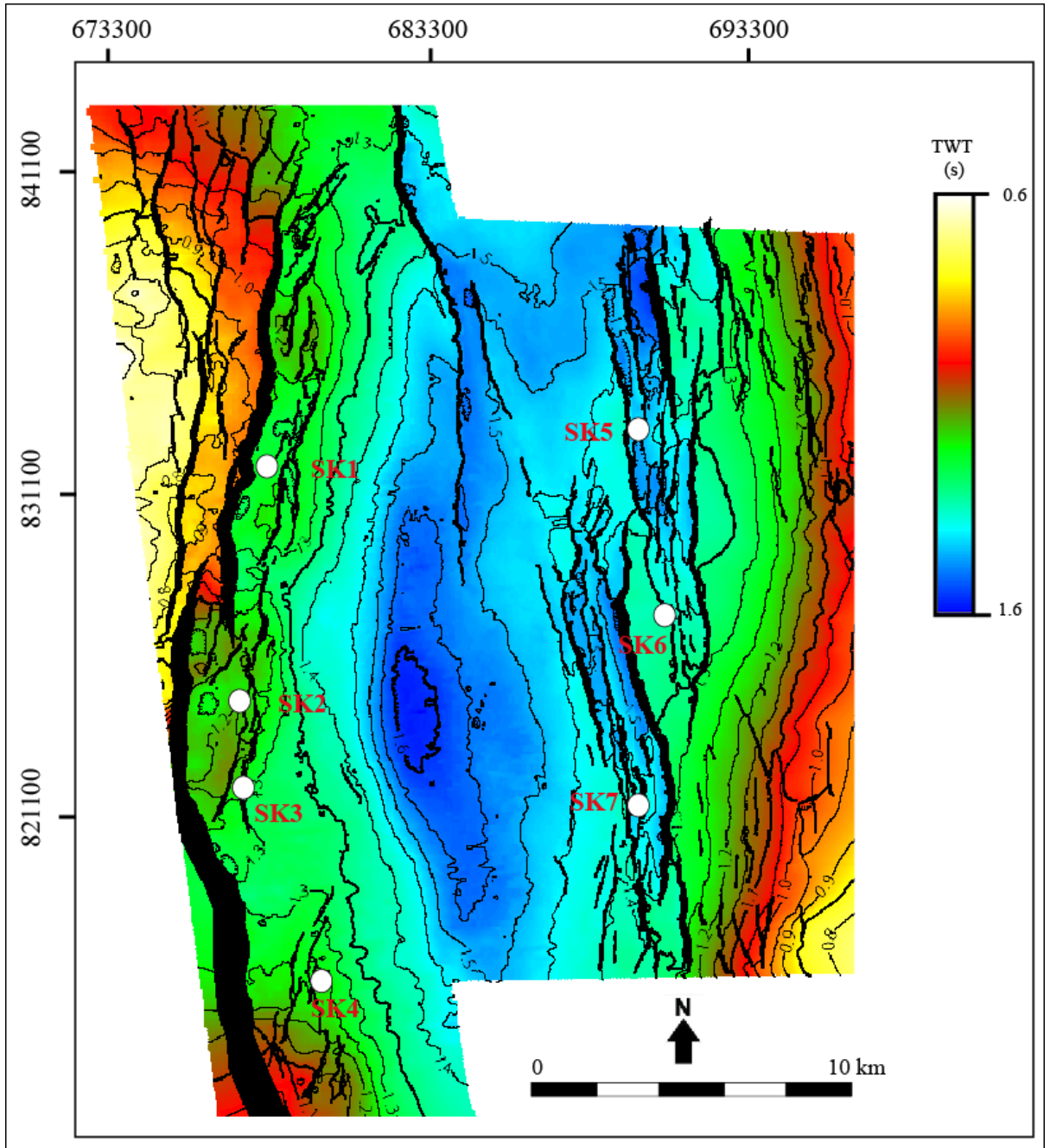
Top Oligocene time structural map
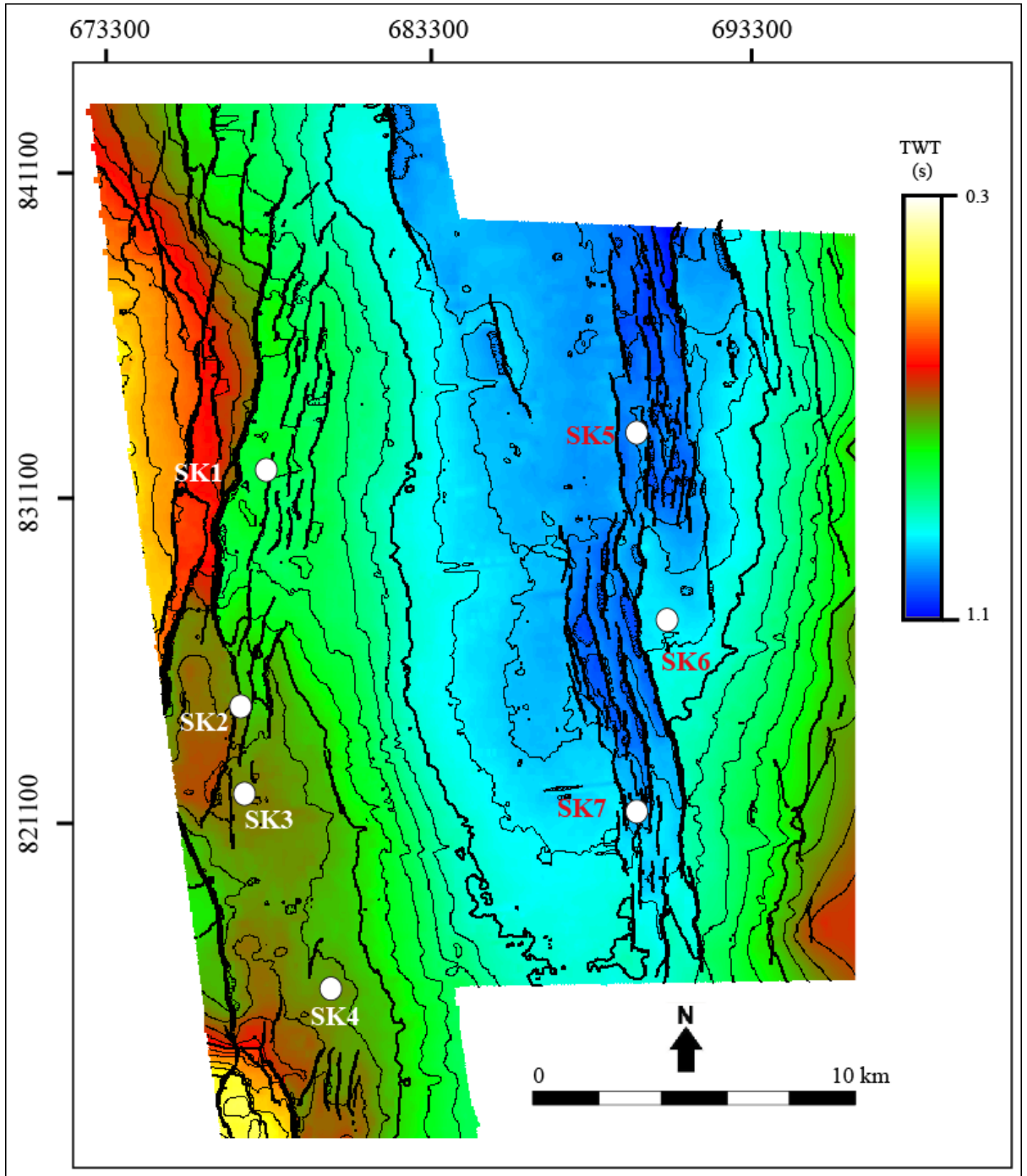
Top Early Miocene time structural map

APPENDIX B:
WELL LOG CORRELATION
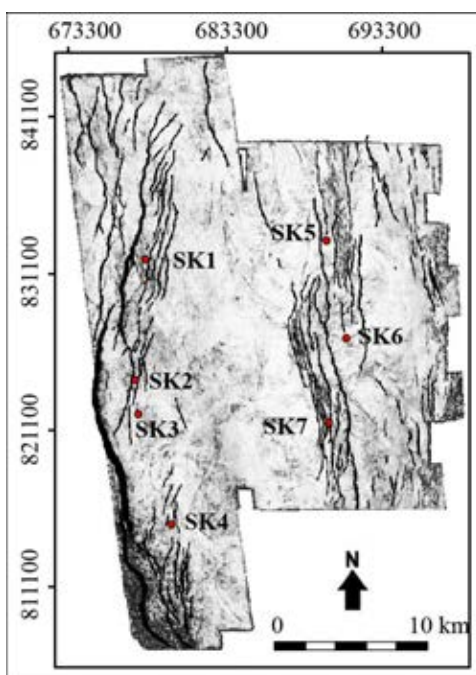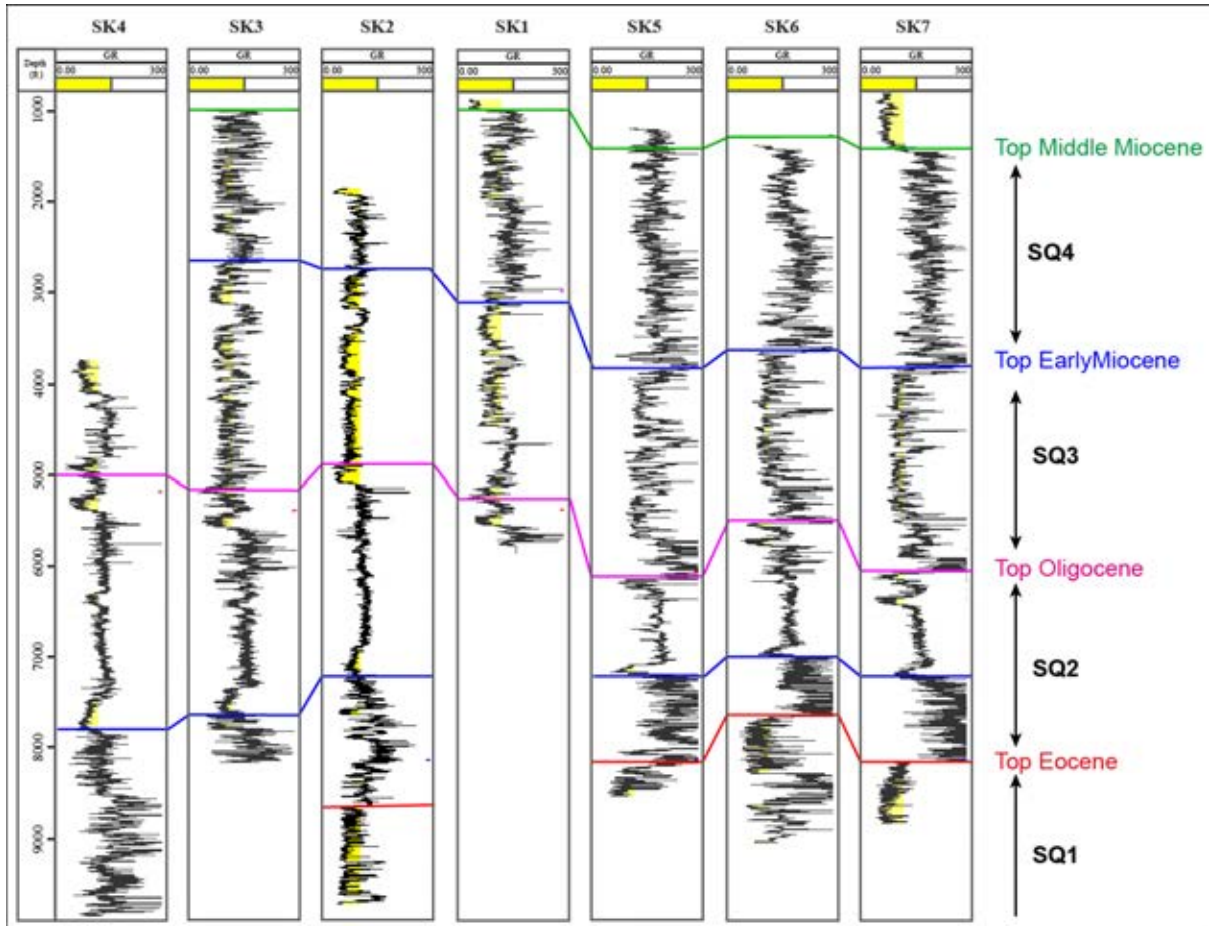
APPENDIX C:

THROW – LENGTH MEASUREMENT

Fault F1

Seismic lines	Distance (km)	Top Early Miocene			Upper Oligocene		
		FW (ms)	HW (ms)	Throw (ms)	FW (ms)	HW (ms)	Throw (ms)
2D 892-838				0			0
2D 87-28	1.17						
2D 87-27	2.19	458	751	293	789	1134	345
2D 892-837	3.18	465	796	331	754	1245	491
2D 87-26	4.20	472	777	305	728	1284	556
2D 87-25	5.25	509	808	299	785	1297	512
2D 87-24	8.12	518	780	262	775	1328	553
2D 87-23	8.64	511	784	273	794	1315	521
2D 892-836	9.14	512	793	281	832	1279	447
2D 87-22	10.39	458	769	311	740	1239	499
2D 87-21	11.19	463	740	277	736	1229	493
2D 87-20	12.01	484	757	273	795	1219	424
2D 87-19	12.87	480	792	312	796	1186	390
2D 892-835	13.52	468	758	290	807	1214	407
2D 87-18 (2335)	14.32	488	788	300	852	1208	356
2D 87-17	14.52	500	757	257	857	1178	321
2435	15.06	593	775	182	825	1197	372
2455	15.30	594	775	181	819	1212	393
2475/2D 87-16	15.56	601	775	174	830	1228	398
2495	15.87	601	778	177	863	1205	342
2515	16.12	617	765	148	866	1172	306
2535	16.38	623	764	141	855	1140	285
2555/2D 87-15	16.71	625	745	120	860	1131	271
2575	16.95	638	752	114	882	1085	203
2595	17.27	628	741	113	863	1086	223
2615	17.57	637	721	84	913	1061	148
2635	17.86	644	707	63	879	1042	163
2655	18.15	667	695	28	919	995	76
2675	18.43	664	671	7	924	971	47

Seismic lines	Distance (km)	Lower Oligocene			Eocene		
		FW (ms)	HW (ms)	Throw (ms)	FW (ms)	HW (ms)	Throw (ms)
2D 892-838				0			0
2D 87-28	1.17						
2D 87-27	2.19	988	1685	697	1470	2586	1116
2D 892-837	3.18	988	1714	726	1421	2655	1234
2D 87-26	4.20	974	1745	771	1410	2697	1287
2D 87-25	5.25	1034	1830	796	1421	2716	1295
2D 87-24	8.12	1123	1840	717	1466	2661	1195
2D 87-23	8.64	1161	1793	632	1501	2608	1107
2D 892-836	9.14	1197	1788	591	1606	2620	1014
2D 87-22	10.39	1171	1841	670	1596	2628	1032
2D 87-21	11.19	1112	1646	534	1476	2672	1196
2D 87-20	12.01	1151	1637	486	1380	2790	1410
2D 87-19	12.87	1088	1715	627	1302	2794	1492
2D 892-835	13.52	1097	1663	566	1375	2669	1294
2D 87-18 (2335)	14.32	1105	1674	569	1392	2754	1362
2D 87-17	14.52	1167	1552	385	1384	2711	1327
2435	15.06	1151	1555	404	1313	2678	1365
2455	15.30	1156	1570	414	1323	2674	1351
2475/2D 87-16	15.56	1142	1574	432	1316	2646	1330
2495	15.87	1134	1540	406	1318	2530	1212
2515	16.12	1139	1535	396	1490	2445	955
2535	16.38	1143	1531	388	1516	2452	936
2555/2D 87-15	16.71	1126	1528	402	1486	1930	444
2575	16.95	1121	1516	395	1674	1918	244
2595	17.27	1138	1450	312	1662	1848	186
2615	17.57	1169	1424	255	1692	1788	96
2635	17.86	1213	1400	187	1693	1742	49
2655	18.15	1280	1387	107	1670	1703	33
2675	18.43	1340	1340	0	1501	1501	0

Fault F2

Seismic lines	Distance (km)	Top Early Miocene			Upper Oligocene		
		FW (ms)	HW (ms)	Throw (ms)	FW (ms)	HW (ms)	Throw (ms)
	0.00			0			0
2895	0.25	716	731	15	928	960	32
2875	0.50	705	736	31	927	965	38
2855	0.75	698	732	34	920	967	47
2835	1.00	702	751	49	910	983	73
2815	1.25	681	836	155	943	1316	373
2795	1.50	678	849	171	917	1325	408
2775	1.75	682	865	183	933	1309	376
2755	2.00	699	868	169	970	1303	333
2735	2.25	667	860	193	938	1288	350
2715	2.50	670	872	202	943	1262	319
2695	2.75	677	881	204	985	1273	288
2675	3.00	681	884	203	995	1300	305
2655	3.25	686	850	164	970	1320	350
2635	3.50	703	858	155	993	1290	297
2615	3.75	711	856	145	1019	1326	307
2595	4.00	705	852	147	1036	1261	225
2575	4.25	709	850	141	1050	1268	218
2555	4.50	748	864	116	1081	1266	185
2535	4.75	747	837	90	1115	1235	120
2515	5.00	753	821	68	1205	1247	42
2495	5.25	756	817	61	1192	1235	43
2475	5.50	757	816	59	1182	1207	25
2455		754	804	50			

Fault F2

Seismic lines	Distance (km)	Lower Oligocene			Eocene		
		FW (ms)	HW (ms)	Throw (ms)	FW (ms)	HW (ms)	Throw (ms)
2895	0.25	1249	1267	18	1608	1608	0
2875	0.50	1239	1304	65	1515	1648	133
2855	0.75	1207	1296	89	1523	1673	150
2835	1.00	1231	1542	311	1558	2280	722
2815	1.25	1240	1609	369	1525	2272	747
2795	1.50	1287	1641	354	1561	2254	693
2775	1.75	1283	1645	362	1587	2259	672
2755	2.00	1294	1607	313	1583	2189	606
2735	2.25	1282	1612	330	1599	2233	634
2715	2.50	1292	1597	305	1588	2236	648
2695	2.75	1305	1672	367	1617	2238	621
2675	3.00	1331	1723	392	1635	2308	673
2655	3.25	1359	1783	424	1705	2328	623
2635	3.50	1357	1790	433	1721	2330	609
2615	3.75	1369	1779	410	1782	2373	591
2595	4.00	1399	1704	305	1919	2415	496
2575	4.25	1425	1633	208	2016	2426	410
2555	4.50	1577	1727	150	2066	2430	364
2535	4.75	1488	1590	102	2137	2466	329
2515	5.00	1513	1579	66	2313	2481	168
2495	5.25	1560	1585	25			0
2475	5.50			0			0

Fault F3

Seismic lines	Distance (km)	Top Early Miocene			Upper Oligocene		
		FW (ms)	HW (ms)	Throw (ms)	FW (ms)	HW (ms)	Throw (ms)
3615	0.25	910	910	0	1238	1263	25
3595	0.50	889	905	16	1219	1255	36
3575	0.75	885	903	18	1183	1247	64
3555	1.00	881	908	27	1172	1255	83
3535	1.25	868	901	33	1145	1250	105
3515	1.50	869	898	29	1129	1238	109
3495	1.75	848	908	60	1093	1212	119
3475	2.00	855	903	48	1063	1246	183
3455	2.25	832	903	71	1066	1256	190
3435	2.50	820	904	84	1053	1248	195

Seismic lines	Distance (km)	Top Early Miocene			Upper Oligocene		
		FW (ms)	HW (ms)	Throw (ms)	FW (ms)	HW (ms)	Throw (ms)
3615	0.25	910	910	0	1238	1263	25
3415	2.75	824	895	71	1056	1291	235
3395	3.00	819	883	64	1039	1294	255
3375	3.25	803	887	84	1053	1267	214
3355	3.50	799	866	67	1030	1278	248
3335	3.75	792	848	56	1023	1272	249
3315	4.00	769	840	71	1005	1245	240
3295	4.25	771	844	73	996	1240	244
3275	4.50	766	848	82	987	1225	238
3255	4.75	756	837	81	982	1233	251
3235	5.00	755	830	75	983	1233	250
3215	5.25	752	826	74	992	1244	252
3195	5.50	747	845	98	988	1234	246
3175	5.75	740	834	94	1007	1223	216
3155	6.00	740	855	115	993	1230	237
3135	6.25	738	863	125	988	1245	257
3115	6.50	733	863	130	970	1263	293
3095	6.75	737	844	107	963	1274	311
3075	7.00	743	863	120	978	1242	264
3055	7.25	751	863	112	965	1245	280
3035	7.50	746	865	119	970	1291	321
3015	7.75	741	863	122	958	1289	331
2995	8.00	734	865	131	969	1298	329
2975	8.25	727	846	119	960	1272	312
2955	8.50	738	853	115	954	1281	327
2935	8.75	716	856	140	949	1298	349
2915	9.00	738	847	109	953	1289	336
2895	9.25	742	857	115	964	1266	302
2875	9.50	740	872	132	952	1299	347
2855	9.75	747	833	86	955	1264	309
2835	10.00	760	833	73	944	1266	322

Seismic lines	Distance (km)	Lower Oligocene			Eocene		
		FW (ms)	HW (ms)	Throw (ms)	FW (ms)	HW (ms)	Throw (ms)
	0.00			0			0
3615	0.25	1563	1588	25	1747	2011	264
3595	0.50	1553	1574	21	1715	2021	306
3575	0.75	1528	1581	53	1728	2020	292
3555	1.00	1556	1580	24	1748	1985	237

Seismic lines	Distance (km)	Top Early Miocene			Upper Oligocene		
		FW (ms)	HW (ms)	Throw (ms)	FW (ms)	HW (ms)	Throw (ms)
3615	0.25	910	910	0	1238	1263	25
3535	1.25	1500	1541	41	1750	1953	203
3515	1.50	1471	1551	80	1718	1913	195
3495	1.75	1445	1540	95	1708	1886	178
3475	2.00	1428	1519	91	1651	1891	240
3455	2.25	1415	1546	131	1614	1859	245
3435	2.50	1424	1513	89	1656	1884	228
3415	2.75	1397	1480	83	1629	1921	292
3395	3.00	1401	1518	117	1638	1934	296
3375	3.25	1367	1497	130	1678	1963	285
3355	3.50	1348	1511	163	1648	1955	307
3335	3.75	1329	1553	224	1636	1985	349
3315	4.00	1296	1564	268	1657	1977	320
3295	4.25	1283	1500	217	1645	1956	311
3275	4.50	1277	1516	239	1636	1974	338
3255	4.75	1282	1530	248	1625	1994	369
3235	5.00	1271	1480	209	1562	2050	488
3215	5.25	1264	1483	219	1591	2039	448
3195	5.50	1258	1469	211	1545	2053	508
3175	5.75	1258	1458	200	1535	2036	501
3155	6.00	1252	1493	241	1536	2101	565
3135	6.25	1244	1533	289	1515	2164	649
3115	6.50	1263	1531	268	1542	2173	631
3095	6.75	1267	1557	290	1518	2194	676
3075	7.00	1264	1588	324	1545	2275	730
3055	7.25	1243	1559	316	1529	2163	634
3035	7.50	1246	1572	326	1522	2197	675
3015	7.75	1236	1608	372	1545	2241	696
2995	8.00	1253	1593	340	1584	2255	671
2975	8.25	1261	1645	384	1553	2330	777
2955	8.50	1252	1650	398	1536	2159	623
2935	8.75	1245	1629	384	1609	2195	586
2915	9.00	1272	1611	339	1638	2223	585
2895	9.25	1280	1625	345	1634	2252	618
2875	9.50	1287	1637	350	1658	2273	615
2855	9.75	1280	1610	330	1666	2270	604
2835	10.00	1383	1565	182	0	0	0

Fault F4

Seismic lines	Distance (km)	Top Early Miocene			Upper Oligocene		
		FW (ms)	HW (ms)	Throw (ms)	FW (ms)	HW (ms)	Throw (ms)
3255				0			0
3235	0.25	631	631	0	820	841	21
3215	0.53	658	658	0	836	865	29
3195	0.78	627	646	19	822	855	33
3175	1.04	631	661	30	800	875	75
3155	1.30	628	660	32	786	881	95
3135	1.54	622	674	52	774	874	100
3115	1.79	624	674	50	801	913	112
3095	2.07	623	665	42	804	893	89
3075	2.33	624	674	50	802	890	88
3055	2.60	626	667	41	785	871	86
3035	2.90	627	669	42	779	873	94
3015	3.16	616	678	62	787	879	92
2995	3.43	606	668	62	797	889	92
2975	3.66	610	671	61	795	893	98
2955	3.94	602	661	59	776	904	128
2935	4.25	592	663	71	790	921	131
2915	4.51	596	673	77	804	922	118
2895	4.79	590	655	65	808	893	85
2875	5.09	582	651	69	805	894	89
2855	5.38	581	670	89	782	879	97
2835	5.63	584	650	66	802	904	102
2815	5.88	586	638	52	812	900	88
2795	6.14	586	634	48	816	874	58
2775	6.39	585	638	53	806	887	81
2755	6.64	585	633	48	803	876	73
2735	6.90	581	636	55	797	868	71
2715	7.16	574	662	88	792	921	129
2695	7.43	574	657	83	810	931	121
2675	7.70	566	653	87	803	925	122
2655	7.95	561	653	92	808	908	100
2635	8.20	557	648	91	817	901	84
2615	8.46	561	636	75	832	894	62
2595	8.74	551	625	74	813	883	70
2575	9.02	554	624	70	812	868	56
2555	9.29	547	612	65	816	844	28
2535	9.54	541	612	71	815	862	47
2515	9.81			0			0

Seismic lines	Distance (km)	Lower Oligocene			Eocene		
		FW (ms)	HW (ms)	Throw (ms)	FW (ms)	HW (ms)	Throw (ms)
3255				0			0
3235	0.25	926	941	15	1189	1189	0
3215	0.53	937	954	17	1183	1217	34
3195	0.78	960	986	26	1169	1254	85
3175	1.04	945	993	48	1195	1366	171
3155	1.30	934	1006	72	1235	1389	154
3135	1.54	922	1015	93	1219	1364	145
3115	1.79	924	1160	236	1257	1364	107
3095	2.07	916	1131	215	1255	1402	147
3075	2.33	914	1119	205	1238	1419	181
3055	2.60	905	1142	237	1233	1412	179
3035	2.90	904	1104	200	1211	1461	250
3015	3.16	911	1106	195	1201	1467	266
2995	3.43	967	1126	159	1213	1494	281
2975	3.66	919	1121	202	1183	1524	341
2955	3.94	930	1168	238	1175	1547	372
2935	4.25	927	1174	247	1185	1587	402
2915	4.51	928	1186	258	1189	1618	429
2895	4.79	914	1186	272	1177	1624	447
2875	5.09	922	1167	245	1205	1635	430
2855	5.38	919	1136	217	1215	1614	399
2835	5.63	939	1130	191	1247	1616	369
2815	5.88	939	1167	228	1230	1597	367
2795	6.14	944	1241	297	1213	1624	411
2775	6.39	941	1182	241	1230	1666	436
2755	6.64	977	1207	230	1234	1633	399
2735	6.90	973	1211	238	1228	1639	411
2715	7.16	983	1222	239	1225	1650	425
2695	7.43	1001	1258	257	1221	1631	410
2675	7.70	1020	1247	227	1189	1702	513
2655	7.95	1028	1224	196	1266	1713	447
2635	8.20	1034	1203	169	1318	1687	369
2615	8.46	1044	1168	124	1335	1696	361
2595	8.74	1076	1164	88	1387	1658	271
2575	9.02	1097	1145	48	1499	1706	207
2555	9.29	1108	1158	50	1501	1666	165
2535	9.54	1116	1154	38			0
2515	9.81			0			0

Fault F5

Seismic lines	Distance (km)	Top Early Miocene			Upper Oligocene		
		FW (ms)	HW (ms)	Throw (ms)	FW (ms)	HW (ms)	Throw (ms)
3795	0						0
3775	0.30				1058	1082	24
3755	0.55				1044	1080	36
3735	0.81				1038	1089	51
3715	1.09				1029	1096	67
3695	1.38				1009	1079	70
3675	1.68				995	1050	55
3655	1.95				975	1028	53
3635	2.25			0	946	1022	76
3615	2.52	717	724	7	921	1017	96
3595	2.78	694	718	24	898	978	80
3575	3.07	680	702	22	887	957	70
3555	3.34	677	684	7	866	939	73
3535	3.58	676	676	0	842	947	105
3515	3.83	667	679	12	839	901	62
3495	4.11	681	689	8	834	920	86
3475	4.36				815	898	83
3455	4.61				798	887	89
3435	4.86	630	644	14	790	845	55
3415	5.12	623	645	22	809	859	50
3395	5.37	610	636	26	751	840	89
3375	5.64	609	636	27	750	813	63
3355	5.90	605	634	29	764	809	45
3335	6.16	604	622	18	765	804	39
3315	6.46	626	636	10	781	816	35
3295	7.02	621	634	13	801	826	25
3275	7.39	621	630	9	811	827	16
3255	7.64				807	815	8
3235	7.91				799	815	16
3215	8.18	623	640	17	800	818	18
3195	8.44			0	798	812	14
3175	8.70				778	798	20
3155	9.08				770	791	21
3135	9.38						0

Seismic lines	Distance (km)	Lower Oligocene			Eocene		
		FW (ms)	HW (ms)	Throw (ms)	FW (ms)	HW (ms)	Throw (ms)
3795	0			0			0
3775	0.30	1277	1306	29	1430	1470	40
3755	0.55	1253	1294	41	1436	1486	50
3735	0.81	1252	1303	51	1403	1462	59
3715	1.09	1234	1306	72	1374	1470	96
3695	1.38	1230	1313	83	1379	1486	107
3675	1.68	1172	1257	85	1420	1516	96
3655	1.95	1170	1282	112	1434	1510	76
3635	2.25	1145	1274	129	1305	1401	96
3615	2.52	1099	1231	132	1265	1414	149
3595	2.78	1087	1222	135	1235	1397	162
3575	3.07	1061	1199	138	1219	1384	165
3555	3.34	1069	1154	85	1227	1385	158
3535	3.58	1019	1121	102	1211	1332	121
3515	3.83	998	1094	96	1182	1290	108
3495	4.11	995	1074	79	1183	1264	81
3475	4.36	1021	1071	50	1193	1263	70
3455	4.61	951	1033	82	1156	1299	143
3435	4.86	966	1007	41	1163	1290	127
3415	5.12	903	986	83	1183	1271	88
3395	5.37	897	975	78	1178	1246	68
3375	5.64	880	938	58	1122	1194	72
3355	5.90	886	936	50	1119	1179	60
3335	6.16	896	945	49	1145	1196	51
3315	6.46	910	963	53	1117	1206	89
3295	7.02	922	992	70	1134	1202	68
3275	7.39	944	972	28	1140	1200	60
3255	7.64	939	952	13	1184	1220	36
3235	7.91	916	926	10	1175	1205	30
3215	8.18	925	941	16	1168	1185	17
3195	8.44	937	967	30	1088	1116	28
3175	8.70	935	958	23	1095	1113	18
3155	9.08	920	939	19	1106	1106	0
3135	9.38			0			0

APPENDIX D:

CHANNEL DIMENSION MEASUREMENT

Time	Horizon	Channels	Channel width (m)	channel thickness (m)	width/depth Ratio	Meander belt width (km)	Channel length (m) (CL)	Meander wavelength (m) (ML)	Sinuosity Index (SI=CL/ML)	Type of channel
Early Miocene	S1	River 1	150	31	5	2	7.0	5.9	1.18	sinuous channel
			210	34	6					
			360	24	15					
			410	30	14					
		River 2	460	23	20					
			470	18	26					
		River 3	470	34	14					
			370	20	19					
	S2	River 4	210	25	8	2.5	5.5	3.0	1.85	meandering
			300	23	13					
			580	39	15					
			500	24	21					
			600	28	31					
			470	31	15					
Middle Miocene	S4	River 5	165	20	8	0.7	3.6	3.3	1.07	sinuous channel
			153	23	7					
		River 6	160	26	6	0.95	4.2	3.9	1.06	
			200	24	8					
			150	17	9					
			170	21	8					
			155	20	8					
		River 7	210	23	9					
		River 8	110	19	6					
		River 9	340	25	14					
			220	22	10					
		River 10	290	26	11					
			340	19	18					
			300	27	11					
			150	25	6					
			200	19	11					
		River 11	260	15	17					
			350	19	18					
	S7	River 12	260	19	14	1.1	5.9	5.3	1.13	sinuous channel
			190	20	10					
			260	22	12					
			230	20	12					
			230	18	13					
		River 13	270	31	9		4.2	3.9	1.06	sinuous channel
			260	24	11					

SI =   channel length (CL)
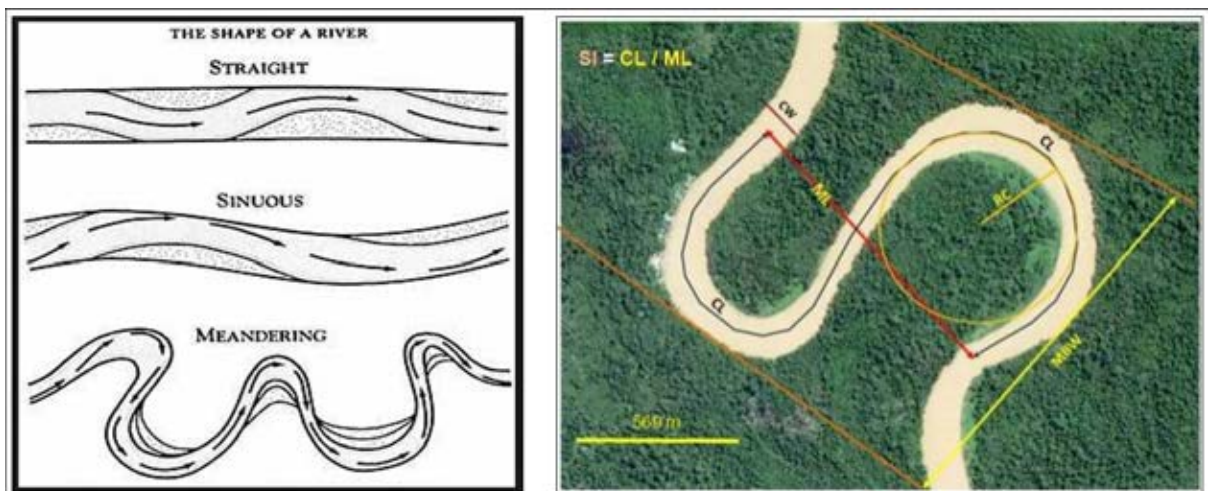   meander wavelength (ML)
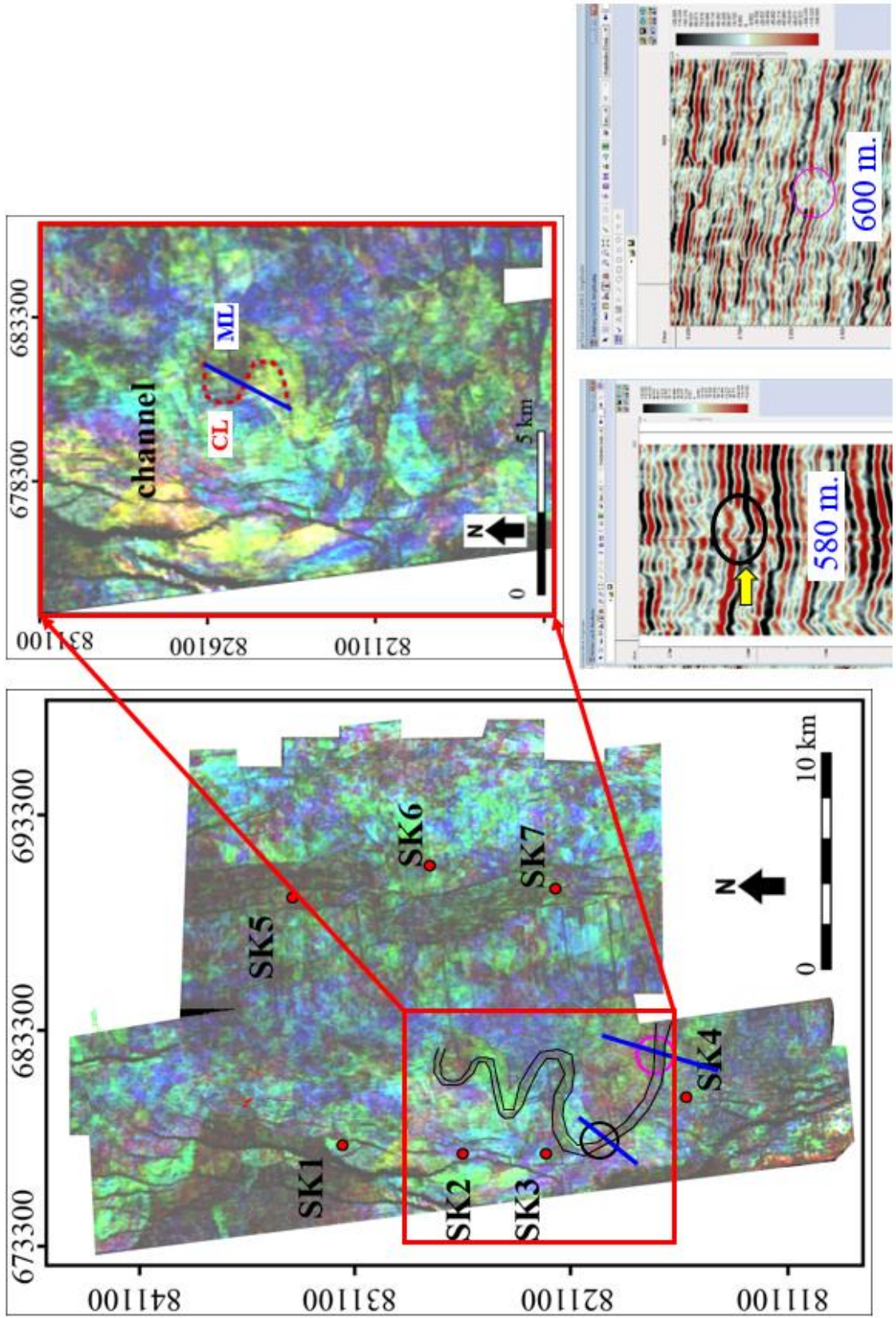
SI = sinuousity index

CL = channel length

ML = meandering wavelength

The sinuousity index has been used to separate channel rivers into three general classes:
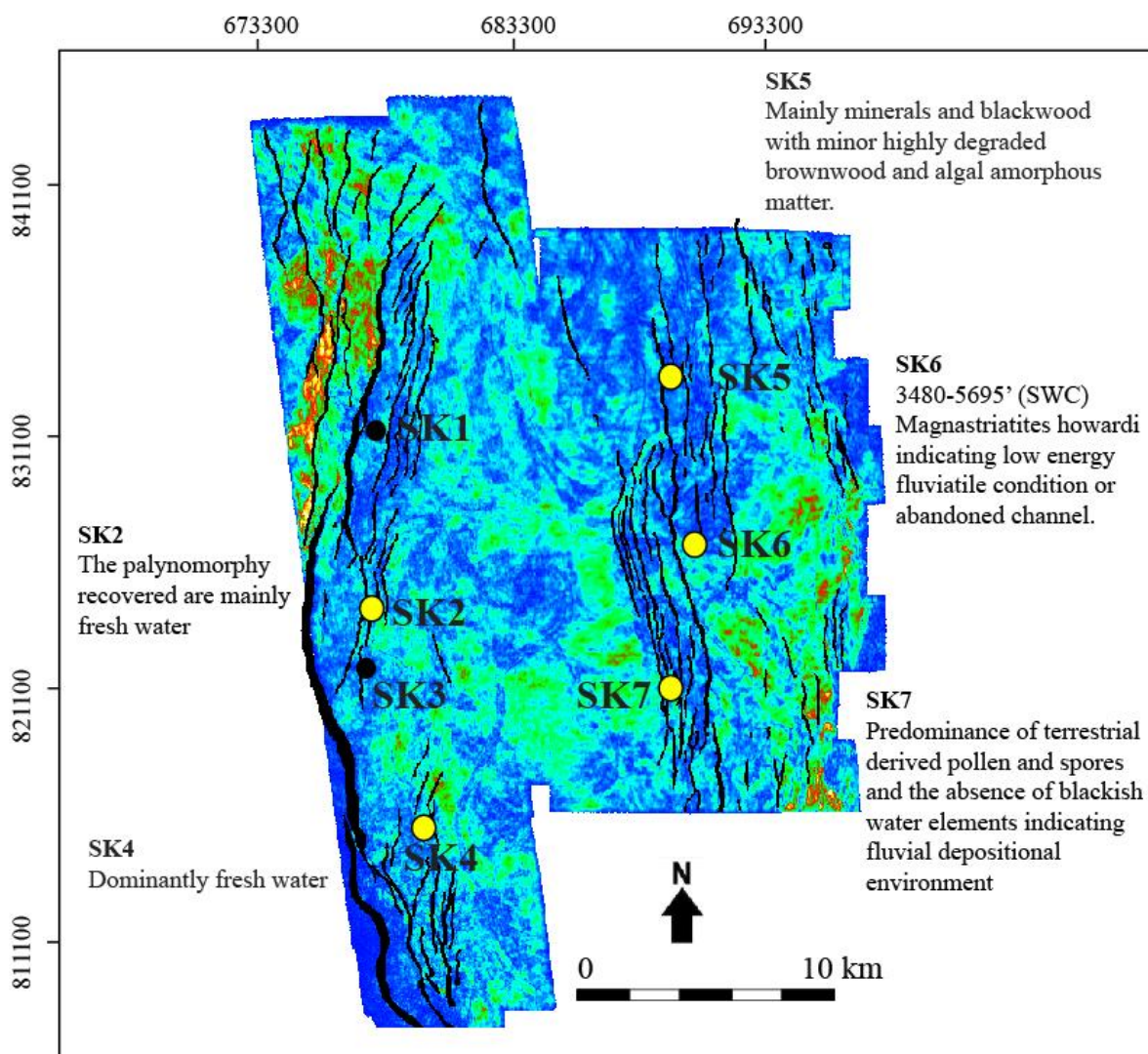
1. Straight (SI < 1.05)

2. Sinuous (1.05 < SI < 1.5)

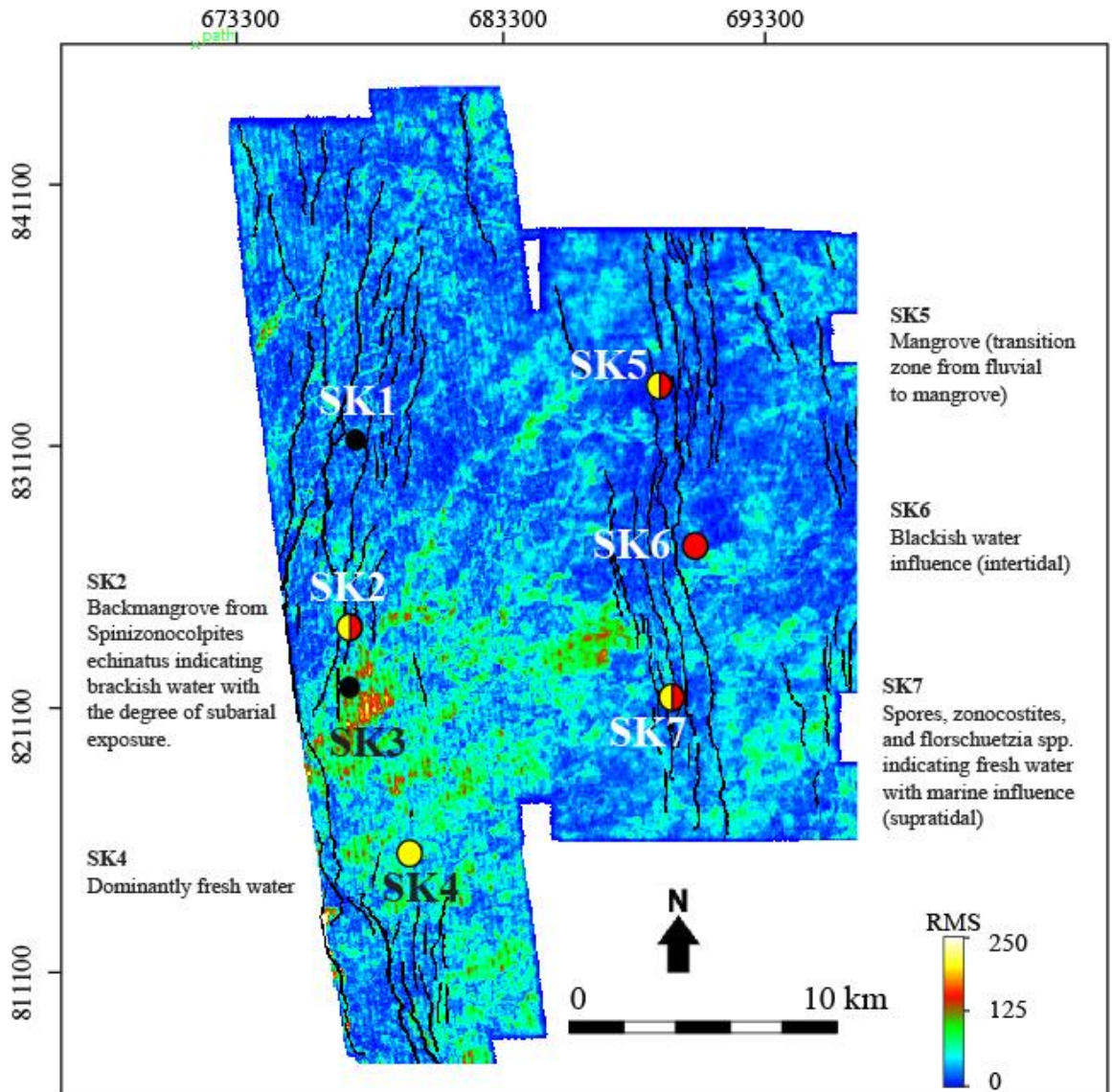3. Meandering (SI > 1.5)

Example of channel measurement on S2 horizon

APPENDIX E:

BIOSTRATIGRAPHIC DATA

Biostratigraphic data on S1

Biostratigraphic data on S4 (lower post-rift I)
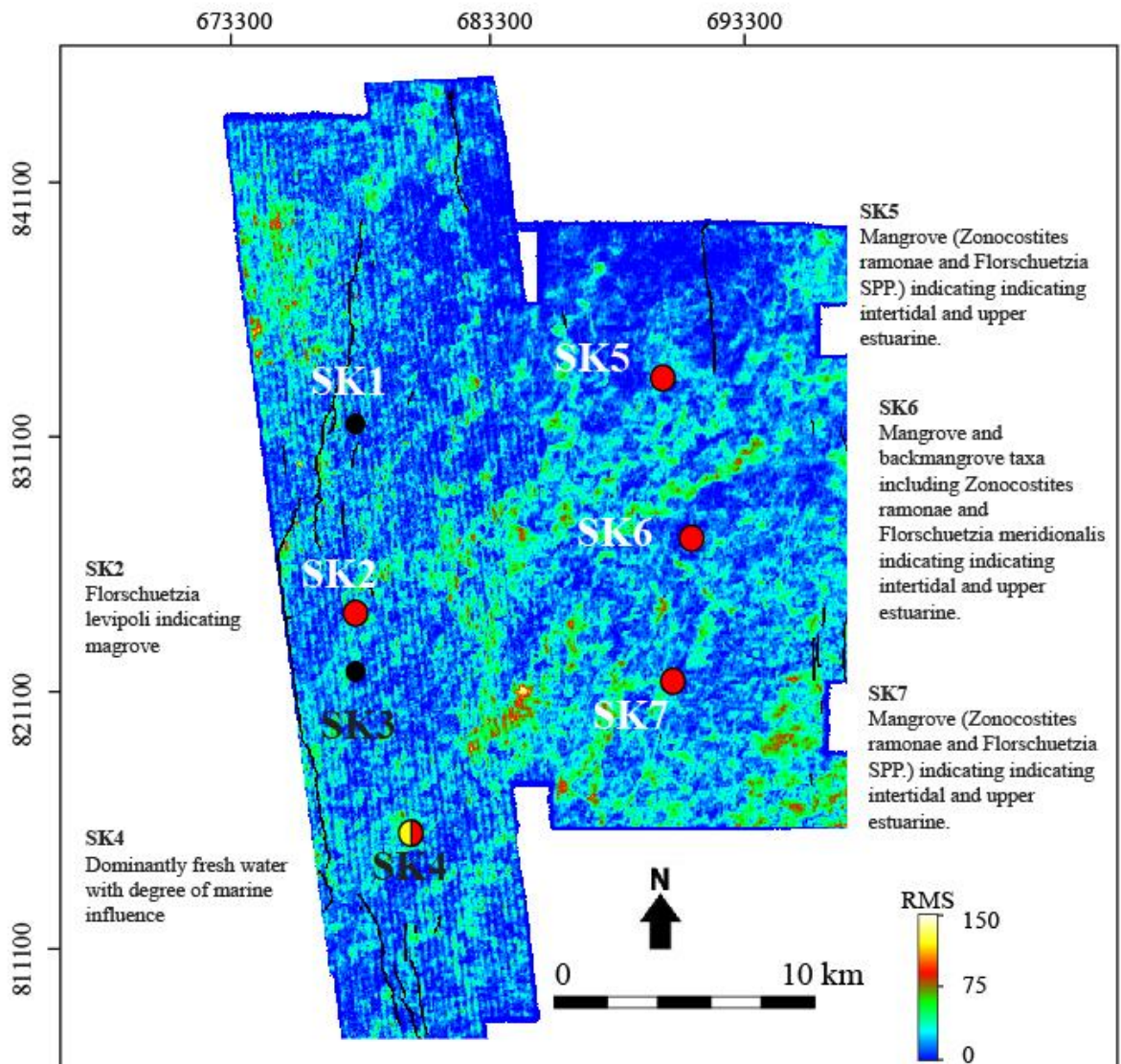
Biostratigraphic data on S7 (top of post-rift I)

VITA

NAME	Jidapa Phoosongsee
DATE OF BIRTH	3 July 1973
PLACE OF BIRTH	Khon Kaen, Thailand
HOME ADDRESS	250/99 Supalai Park Ratchayothin
	Ratchadapisek Road, Ladyao, Chatuchak,
	Bangkok, Thailand 10900